Measuring degradation in cable insulation material under realistic operation conditions

Douglas Jutsell Nilsson

Measuring degradation in cable insulation material under realistic operation conditions

DOUGLAS JUTSELL NILSSON

Göteborg, Sweden 2020

Abstract

One of the challenges in laboratory investigation of degradation and ageing of HVDC cable insulation is related to securing, or in other words, imitating the real service environment of the material specimens. So far, the published data refer to experiments conducted in thermo-oxidative conditions, which is not the case during normal cable operation. In reality the cable insulation is protected by a metallic barrier that blocks the transfer of any substances in and out of the construction. By-products from the cross-linking reactions cannot diffuse out and any foreign substances, such as oxygen and water, are blocked from entering into the insulation. Thus, in order to generate results that are practically valid, these conditions must be replicated in laboratory experiments.

This contribution presents a measuring system developed for performing ageing experiments in a hermetically sealed environment. The material degradation is evaluated through measurements of changes in the electrical tree inception voltage and test object capacitance over time. Securing the environmental isolation is primarily accomplished with an isolation system consisting of a glass enclosure with attached metallic electrodes. Indium is used to create a glass-to-metal seal between the glass and the electrodes. The electrode geometry is of needle-plane type and the needle injection process is largely automated to secure a large degree of repeatability in specimen preparation.

Initial measurements utilising four synchronized but independent data streams show that the electrical tree inception voltage can be accurately detected using the developed specimen capsule. The impedance change of the specimen during the test shows to be a particularly useful measure.

In order to further validate the methodology as well as contribute knowledge on the material's resistance to degradation caused by its exposure to enhanced electrical stress, 40 specimens were prepared and used in an experiment that explores whether multiple joint failures along an HVDC-cable may have any effect on the condition of the cable's the insulation material. The results indicate that the impact seen in the electrical tree inception voltage is minor and that the insulation has withstood the enhanced stress with negligible consequences.

i

Acknowledgements

Table of Contents

1. Introduction

Understanding the effects on HVDC cable insulation caused by long-term exposure to in-service stresses is key to evaluating current and emerging materials. Experiments which yield such results can be carried out in a number of different ways, for example, by conducting full scale experiments using actual or model cables, by using cables that have already been in-service or by carrying out laboratory experiments on miniature specimens with artificial defects.

Full scale experiments, and to a certain extent, model cables, are costly endeavours. Miniature specimens, of a size such that they fit in the palm of a hand, taken from an already produced cable can carry significant advantages. The voltage required for experimentation on this scale is typically in the lower range of tens of kilovolts, as opposed to the hundreds of kilovolts that is required for full scale tests. Since the voltage required is much less, the equipment and space requirements are manageable, miniature specimens with artificial defects present a tempting economical alternative. Further, a specimen from an already produced cable ensures that there are no differences between the examined material and the insulation in-service. The downside arises when trying to relate the stress level introduced by the defect to that of the stresses found in an actual cable.

There are two weakly connected issues that complicate the effort of ageing HVDC cable insulation. Currently, cross-linked polyethylene is the prevailing material used for these applications. The first matter which is of importance is the possible injection and transport of charge carriers which influences the field distribution. The second relates to the metallic sheath that surrounds a typical cable in-service. The cross-linking process leaves residual by-products in the insulation which has a large effect on the electrical properties. Since an actual cable is surrounded by a metallic sheath, these stay inside the insulation. The metallic sheath also serves to block any foreign matter from entering the insulation. A substantial amount of research exists showing the debilitating results in the material when oxygen is available, degradation that intensifies with increasing temperature. In a cable with a metallic sheath, these conditions are simply not present, instead the oxygen content is found to decrease with time due to the presence of antioxidants. For ageing experiments to be valid, the environmental conditions that an actual cable experiences must be replicated.

The thesis has two main parts. The first covers the development and results of a repeatable manufacture of a specimen, encapsulated in a hermetically sealed environment, with an artificial defect in the form of an injected needle. Such a capsule enables studies of the insulation under serviceable conditions. The capsule is accompanied by a cell, a metallic structure which provides mechanical support and electric field control. The capsule and the cell are instrumented with a measurement system elaborated to accurately detect the inception of an electrical tree when exposed to a ramped sinusoidal excitation voltage while simultaneously tracking changes in the impedance of the specimen. The data recorded from the experiments is used to calculate the impedance of the specimen during the experiments, attempting to exclude the influence of discharge activity. The change of the specimen capacitance is shown to be an effective indicator of the electrical tree inception voltage.

The second part of the thesis builds upon the experience from the first part and describes the work carried out to understand whether the voltage waveforms from multiple joint failures along an HVDC-cable has had any effect on the insulation material of the cable. Specimens from an unused HVDC-cable are used and the parameters of the experiment are decided by data from actual cable service or engineering approximations thereof.

The measurement setup consists of 40 concurrent specimens divided into two groups. The system is instrumented to detect whether change in the specimens can be detected due to exposure to a damped oscillation in the kilohertz range. The experiment has two stages. In the first, the setup exposes all the specimens to a constant DC-voltage while simultaneously subjecting half of them to a defined number of oscillatory waveforms. The evaluation parameters in this stage is change in capacitance and PD-activity during the waveform exposures. The second stage of the experiment consists of exposing the specimens to a ramped sinusoidal voltage in order to force the inception of an electrical tree. The results from the latter indicates whether a change in the insulation material has occurred.

2

1.1   Outline of thesis

This thesis begins by a literature review where a brief overview of how polymers react to electrical and thermal stresses is presented. Chapter three describes the development and results of the encapsulation of the specimen as well as the measurement system built to instrument it. Chapter four details the work of scaling up the methodologies in chapter three to investigate the effects of the joint failure waveform on the insulation material. Finally, concluding remarks and suggestions for future work are given in chapter five.

1.2   List of publications

D.J. Nilsson and S.M Gubanski, *"Electrical detection of degradation in specimens of HVDC cable insulation"*, Proc. Nordic Insulation Symposium NORD-IS19, Tampere, Finland, 2019, pp. 43-46.

D.J. Nilsson, S.M Gubanski and Y.V Serdyuk, "Electrical Detection of Degradation in Specimens of HVDC Cable Insulation", Energies 2020*, 13, 3963*.

D.J. Nilsson and S.M Gubanski, *"Detecting signs of degradation in HVDC-cable insulation due to joint failure",* IEEE Transactions on Dielectrics and Electrical Insulation, in manuscript.

2. Literature review

This chapter attempts to give a broad overview of how different stresses affects the material of interest, cross-linked polyethylene.

2.1 Cross-linked polyethylene

Currently used HVDC cables are commonly insulated with cross-linked polyethylene, usually referred to as XLPE or PEX. Manufacturing the material entails polymerising ethylene gas into polyethylene and cross-linking by a peroxide. Different additives, such as voltage stabilisers and anti-oxidants, can be added to the polymer matrix in order to enhance its properties in certain regards.

Historically, low-density polyethylene, (LDPE), a branched version of polyethylene, was first used in the 1940s as electrical insulation. However, since it is a thermoplastic material it melts at high temperatures, in the worst-case scenario resulting in the complete failure of the insulation during a fault. In 1955 LDPE was discovered to be cross-linkable by a peroxide, specifically dicumyl peroxide. Cross-linking the polymer raises the maximum operating temperature of the conductor from 70 $^{\circ}$C to 90 $^{\circ}$C, a temperature that insulation can withstand indefinitely, and the short circuit temperature to 250 $^{\circ}$C from 150 $^{\circ}$C, an event that lasts a few seconds. During an overload of the cable, XLPE can withstand a conductor temperature of 105 $^{\circ}$C for up to 36 h. Cross-linking changes how the material behaves at high temperatures, instead of melting, the thermoset now forms a semi-transparent, rubber-like material. Finally, cross-linking the material also improves a number of mechanical aspects, such as deformation resistance at elevated temperatures and tensile strength [1,2].

XLPE is a semi-crystalline polymer which means that it contains both amorphous and crystalline regions. The crystals are thin structures which has the form of lamellae, these grow during the cooling of the melt and form larger crystalline structures referred to as spherulites. These are highly dense regions with small parts of amorphous material wedged inside. A typical spherulite is 10 μm in diameter. Their size depends on the manufacturing parameters of the cable, especially the cooling rate of the melt. A slower rate allows the crystals more time to form and hence allowing them to grow larger, resulting in a higher crystalline amount and a denser polymer. The interfaces between

the amorphous parts and the crystalline parts of the polymer is of special interest as these sites make up the recombination centres for polyethylene. The regions inside the spherulite which contain amorphous parts are the preferred trapping locations of charged species. As such, some degradation in form of free volume generation can take place due to the electrostatic forces involved in charge carrier trapping and recombination. The amorphous regions of the polymer are thought to be where the majority of charge transport takes place [2, 3].

The melting temperature of the crystalline regions of the polymer depends on the amount of cross-linking agent used and lies in the range of 103-109 °C for concentrations of dicumyl peroxide between 1 and 7 %. The material is considered to be completely amorphous at 120 °C [4, 5].

The by-products from the cross-linking reactions, cumyl alcohol, acetophenone, methane and water, dictates the behavior of many of the parameters of the material. They are reduced in concentration by a process referred to as degassing as part of the manufacturing of the cable. Methane needs to be removed due to work hazards, but also due to the consequences of gas build up. Conductivity and space charge formation has a strong dependence on the concentration level. The by-products also influence the electrical tree inception voltage of the material. A higher concentration of by-products requires a higher voltage for a tree to incept during sinusoidal excitation. The breakdown strength of the material is further affected by the concentration of by-products. It has been shown that a higher concentration leads to an increased breakdown voltage under sinusoidal excitation and the opposite during impulse excitation [6, 21, 22].

2.2   Ageing and degradation

Physical ageing has been shown to occur in unused cables by a process known as secondary crystallisation. After the primary crystallisation has concluded, i.e. the melt has been fully cooled, amorphous regions are still present between and to some extent inside the spherulites. Now, nucleation starts to occur and the non-crystallised material crystallises. The rate of secondary crystallisation depends on temperature and can continue for years at ambient conditions. As crystallised material occupy less volume than amorphous and the bulk of the polymer is rigid, voids and discontinuities will be the result. This may also increase the number of interfaces between amorphous and crystalline regions [7].

6

Thermal ageing alone causes acrylate oligomers to diffuse from the semiconductor screens into the insulation with a migration rate and penetration depth that increases with temperature [8]. Thermal cycling during normal service, (from ambient and up to 90 °C), can cause melting of small and imperfect lamellae and subsequent recrystallisation and lamella thickening. As this might cause additional mechanical stress, it may stimulate the production of voids [3].

Even low levels of oxygen have been shown to have a debilitating effect on the additives that are responsible for tree suppression in the insulation. Instead of reacting with free radicals in the high-field region, the additive reacts with oxygen which leads to rapid chain scission and channel growth [19].

Ageing studies with a moisture content has been shown to increase the dissipation factor, decrease the volume resistivity and a loss of dielectric strength [20].

Ageing in thermo-oxidative conditions has effects that initially depend on the amount of anti-oxidants in the polymer. Before they are exhausted, secondary crystallisation dominates the process, once they are exhausted, oxidation of the polymer at the melting temperature of the crystalline regions causes a large degree of change in the molecular dynamics of the amorphous regions, in other words, chain scission. With even higher temperatures, the process leads to decreased lamellae thickness and the destruction of spherulites [9–12].

Electro-thermal ageing of model cables was carried out by the Artemis program [13], a large European initiative aimed at investigating ageing in power cables. The program concluded that the concentration of voids and their internal surface area has a large radial dependency, being much larger close to the inner semiconductor. This may or may not be related to the manufacturing process, but there are theories that links voltage stress to void creation. Another conclusion was that ageing resulted in a minor decrease in void number but an increase in their internal surface area close to the inner semiconductor. This implies that voids grow and coalesce during ageing [14]. The program also found that the concentration of shallow and deep charge carrier traps increased with ageing [15].

Electro-thermal ageing is according to [16] the most severe of the possible stress combinations. The order from most severe to least severe is electro-thermal, thermal and electrical ageing. While

insulation exposed to thermal and electrical stress separately show signs of degradation, the effect is enhanced when they are combined.

Voids in XLPE are typically in the range of 0.01-0.3 µm. Initially, they originate from the manufacturing process of the insulation. Voids form when the volatile decomposition products from the chemical reactions of the cross-linking and antioxidant agents evaporate. They can also be formed by unvented gas left in the material or from impurities and additives that decompose, migrate or outgas from cross-linking sites. The surfaces of voids are generally, and at least initially, smooth. The size distribution of voids is important and generally, the smaller the better. In small voids which translate to the Paschen minima, Townsend discharges can occur, but these have not been identified to cause any major degradation. Larger voids, where the Townsend discharge under favourable conditions can transition into a streamer discharge, are of much greater concern since they are much more energetic. The degradation caused by streamers can be split up into two categories, the first being ion bombardment. In polyethylene, it has been found that each discharge eroded the polymer by a volume roughly equal to a cube with sides equal to 0.1 µm. Degradation due to electron bombardment was found to be marginal. The second degradation effect due to streamers is due to the release of oxygen species that will erode polyethylene [3].

2.3   Electrical tree inception and space charge

The role of space charge in high voltage electrical insulation is formidable and even more so in HVDC applications. The intuitive and well defined Laplacian field distribution that can be found by the applied voltage for AC situations is not what is usually present in HVDC insulation. Hole injection from the anode, electron injection from the cathode and the movement of said charge carriers and any other non-neutral species through the insulation alters the electric field distribution. Charge carriers can also be produced at sites not located at the anode or cathode in the presence of an electric field. Further, the conductivity of XLPE has a substantial dependency on temperature. In an in-service cable, due to the heating of the inner conductor, there is a thermal gradient present across the insulation. This can lead to a field-inversion, where the highest field is found at the outer semiconductor.

Space charge can act as an inhibitor to electrical tree initiation. Measurements in [17] indicate a threshold of between 30-80 µs for space charge build up in polyethylene at 25 °C. If an applied

impulse is shorter, the field in the material is not reduced by injected homocharge close to the electrode, and thus the inception voltage of electrical trees is lessened and vice versa. On the other hand, the build up of space charge is considered to be a degradation factor in polyethylene and can lead to field enhancement during a polarity reversal [18]. In low field environments, the Schottky injection mechanism is usually used to model the phenomenon. As the field strength intensifies, the mechanism of injection changes into Fowler-Nordheim tunnelling [3].

Due to it being a polymer, XLPE is not perfectly ordered and all molecular sites cannot be occupied. Free volume is a measure of how inefficient the molecular packing of the polymer is and can volume-wise be as small as a molecule and upwards. It has implications in terms of space charge and conduction mechanisms, but it is also at the centre of the model for electrical tree initiation from a void. Briefly, the model assumes that the free volume creates a network of nano-meter sized channels in the polymer, interconnecting the voids. An idea which is supported by the fact that polymers are permeable by liquid. As streamers develop in a void, the discharge ejects ionised gas molecules throughout the network into a tree-like structure. The model suggests that there will be a main channel, or trunk, where a large percentage of the ejected molecules will pass, causing damage. Eventually, the channel will be large enough to sustain discharges and a tree has been incepted [3].

Electrical trees typically initiate from a defect in the material where the electric field strength is much larger than the nominal value. They can initiate under most excitations, such as ramped DC-excitation, short circuits, polarity reversals, impulses, and constant AC or DC application. The inception during AC excitation, which is used in this work, is thought to briefly proceed as follows. Once above the critical field for space charge injection charge starts to be injected and penetrate to the recombination centres. The barrier for the injection of negative charge has been shown to be lower than the corresponding one for positive charge. It has been theorized that electrons are capable of reaching kinetic energies of 3 - 4 eV at this stage, which is sufficient for bond breaking in polyethylene, but evidence suggests these alone do not cause the initiation of an electrical tree. The actual inception happens when deeply trapped electrons capable of creating an avalanche start to be extracted during the positive half-cycle, which will happen when the heterocharge left over from the earlier half-cycle has reached a certain magnitude. These electrons will have an energy in excess of 10 eV, generate positive ions and break bonds. Repetitive avalanching will cause a void to form and a tree has been incepted [3].

3.   Specimen development and basic measurements

The specimen is contained by two separate, but closely related devices. The first being the specimen capsule, which includes the specimen, the electrodes and the environmental insulation. The second is the cell, in which the specimen capsule is housed. The cell provides a stable capacitive environment by fixing the cell inside a metallic structure with controlled potentials as well as electric field control for the specimen capsule. In this chapter these two concepts are gradually introduced, beginning with the specimen itself, the capsule and what is required of it, ending with what the cell needs to deliver and how it is realized.

3.1   The material specimens

The specimens are taken from an HVDC cable that has not been in service and that has been stored with its ends sealed. Specimens are taken radially in the form of a square cuboid with most of the inner semiconducting layer kept while the outer semiconducting layer is removed. As the main parameter of the measurement system is changes in resistance to electrical tree inception, a phenomenon which can occur in the material when it is exposed to a high electric field, the specimen capsule should provide a way to generate that. A practical way of producing a high electric field given a relatively low voltage is to introduce an artificial defect in the material by injecting a needle into it. The artificial defect mimics an actual one by providing a small volume of intense electric field enhancement close to the tip. The needle is injected from the opposite side of the inner semiconducting layer and placed 4 mm away from it, forming a needle-plane electrode geometry.

The inner semiconductor is kept in order to allow for the behaviour of charge carriers due to its presence, resulting from any eventual field enhancing protrusions, diffusion of species originating from it or other deviations from nominal conditions. It also serves in its original purpose as the interface between the insulation part of polymer and the electrode. The radial nature of the electrode arrangement ensures that that the electric field from the artificial defect is aligned in the same direction as during normal operation of the cable, with a sign change depending on polarity. This would not matter in an isotropic material, but the material of interest is an extruded cross-linked polymer. As such it might have some inherent polymer alignment as well as crystalline and amorphous regions with characteristics stemming from its manufacturing process.

3.1.1 Expanding on the prerequisites

In order to understand and clarify the requirements of the specimen containment, the specimen, the electrode geometry and the electrical treeing experiments that it is supposed to be exposed to needs to be understood. The requirements can broadly be split up in two areas, mechanical and electrical. Mechanically, the main property of the capsule is to hinder interaction between the specimen and the outside world. Furthermore, it should maintain electrical contact with the semiconductor and the needle as well as permitting optical inspection of the needle tip inside the specimen. Ideally, the specimen would be "vacuum packed" in a fully transparent impermeable dielectric, i.e. there should be no gap between the dielectric and the specimen, while still providing the needed electrical connections for the needle and the semiconducting layer.

Electrically, the goal of the specimen containment is to ensure that the recorded data from the electrical tree inception experiments originates from between the tip of the needle and the semiconducting surface. This translates into being free of breakdowns and any PD-activity in the insulation system that surrounds the specimen during the electrical tree inception experiments.

At this point, a list of specifications covering the design of the specimen containment can be prepared. The overall requirements for the containment of the specimen are as follows:

- the specimen capsule should act as a heavily diffusion limiting environment, preferably as a diffusion barrier against the outside world
- the specimen capsule should cover the whole lifetime of the specimen
- the entire containment should be apt for ageing, capacitance measurements and electrical tree inception experiments

Further, and in more detail:

- The length of the specimen cannot exceed 20 mm due to the geometry of the cable from which the specimens are taken
- The inception voltage for electrical trees should be substantially lower than the breakdown voltage across the surface of the specimen and any other part of the containment
- The inception voltage for partial discharges in the containment should be substantially larger than the inception voltage for electrical trees in the specimen
- The tip of the needle and its surroundings should be optically observable

- It should be possible to control the temperature of the specimen, specifically it should be possible to hold the specimen at $70\,°C$

- Containment methods that involve heat should be used with great care, especially methods that involve applying heat to the needle when the specimen is not completely amorphous

- Chemical compounds are to be avoided due to the risk of contaminating the specimen

- The capacitance of interest is between the tip of the needle and the semiconductor layer. Since it is relatively small, the containment should act to reduce stray capacitance

- As electrical treeing experiments are involved, multiple specimens are required, thus, the design should take care to reduce manufacturing complexity and cost

3.2   Realizing the specimen capsule

The main property of the capsule is its ability to hinder interaction between the specimen and the outside world while still maintaining electrical contact with the semiconductor and the needle. This is accomplished by using an arrangement of glass and brass as shown conceptually in Figure 3.1. The cuboid specimen is seen in the middle. The transparent blueish part indicates the polymer and the black part is the inner semiconductor layer. The specimen is residing inside of a glass tube with a square cross inner section. The use of glass is motivated by the fact that it is one of the few materials that is transparent, has excellent dielectric properties and that any permeation through it should be negligible for this application. A glass-to-metal joint is utilized to seal the capsule hermetically. The seal itself is a multi-step process involving indium, a chemical element that wets and bonds against glass. The element is commonly used when there is a need to join non-metallic materials to other non-metallic materials or metals. The finished result is shown in Figure 3.2.
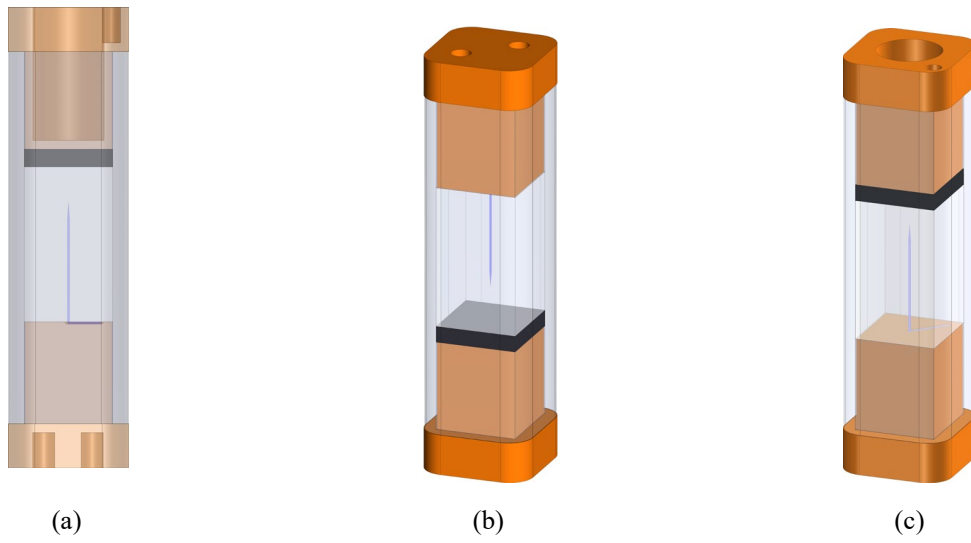
(a)   (b)   (c)

Figure 3.1 The specimen capsule.

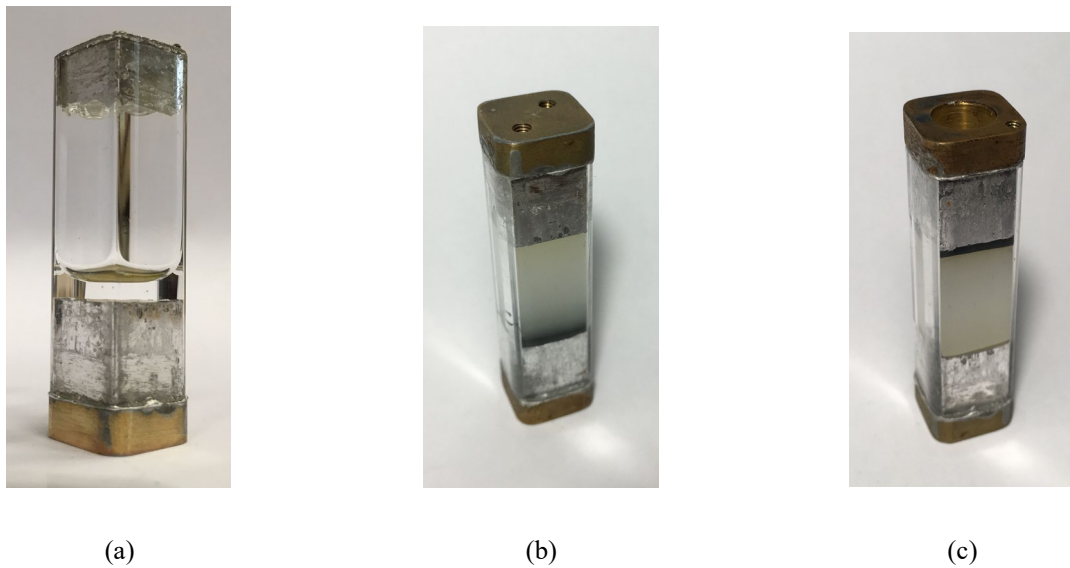(a)   (b)   (c)

Figure 3.2 The finished specimen capsule.

In short, the assembly of the specimen capsule consists of coating the inner sides of the glass and the electrodes with indium, mating one of the electrodes, inserting the specimen and then sealing the capsule by mounting the other electrode. Coating the inner sides of the glass begins by ultrasonic cleaning of the glass in isopropanol followed by rinsing in acetone. The glass tube is then heated uniformly in a hot air stream and the inner electrode contact surfaces are coated by applying indium

and distributing it with a soldering iron at circa 350 °C. The tip of the soldering iron is cleaned similarly to the glass, as well as the indium itself before application. Coating the side which the specimen is inserted from also involves using a facsimile specimen to reduce the thickness of the coating to a minimum. The brass electrodes are coated with the help of flux, they are then in the same way as the glass to remove the flux residue. At this point, the solid needle electrode can be mated to the glass. The result of that process is illustrated in Figure 3.2a, which also shows the testing of the seal. Now, a specimen with a needle already injected, (this process is described in section 3.2.1), can be inserted into the capsule. After the injection process, the needle stands at a right angle in respect to the surface of the specimen. It is now bent down and cut. After bending, it stands at a slight angle with respect to the surface, creating a slight spring. It is then inserted into the capsule, with the specimen aligned such as that the needle fits into the milled slot in the electrode.

Now the critical step is at hand. With the specimen inside the capsule, any heating must be done with care. Especially hazardous is heating the needle without also heating the polymer itself, as the expansion and contraction of the needle will take place in a cold polymer and might result in void creation. The electrode to be inserted needs to be heated to a minimum of 160 °C. The main concern is the time that is needed to achieve a joint. The electrode is inserted, and it melts the pre-coating on its way in. At the same time the air inside of the capsule is evacuated. When fully inserted, the remaining air channel(s) must be closed by letting the melted solder flow and close them. The process should take as little time as possible.

In order to decrease the amount of heat transferred from the electrode to the specimen during mating, the heat capacity of the electrode is reduced. In Figure 3.1a a transparent view of the top electrode is seen, it is evident that it is hollow. Figures 3.1c and 3.2c shows the actual hole. The thickness of the wall that the specimen faces is circa a millimetre. As such, once heat is no longer applied, the electrode will cool quite rapidly. The heat wave that the hot electrode causes in the polymer has to travel approximately 2 mm through the semiconductor and then 4 mm in order to reach the needle.

Gold is used to mechanically coat the semiconductor surface. This is preferable since the surface is not going to be perfectly flat nor is it going to be perfectly parallel to the electrode surface. The gold ensures that even if only a section of the two are in contact, the whole semiconductor surface is at the same potential.

Since a polymer is involved in this arrangement, there is a small inescapable risk of an air gap between the gold coated semiconductor surface and the surface of the electrode once the capsule is assembled. This is mitigated by manufacturing the parts in such a way that the glass is always slightly shorter than its nominal length.

3.2.1 Needle injection and polymer processing

The needle injection process has substantial implications on the repeatability of the experiments. The way it is carried out influences the final geometry of the specimen, the amount of cross-linking by-products in the specimen and the polymeric composition of the final specimen. The injection process involves three steps

- Heating the specimen to a point where the polymer is completely amorphous
- Inserting the needle while the temperature is kept stable
- Cooling the specimen back down to room temperature with the needle residing in it

The implications for repeatability, and a part of the difficulty in this task, comes from the fact that the polymer expands when it is heated and contracts when it is cooled. Furthermore, the final volume of the polymer is determined by the rate of cooling. The longer time it is given to cool, the more time the specimen has to form crystalline regions. These have a higher density than the amorphous ones and thus, takes up less volume. This implies that to ensure that different specimens have the same degree of crystallinity, the temperature curve that the specimens are exposed to during injection of the needle should be similar, with an emphasis on the rate of cooling. The rate of loss of the cross-linking by-products from the specimen also increases with temperature, implying a need for a closed environment when the specimen is heated. An attempt to create a setup that accommodates for the above requirements is shown in Figure 3.3.
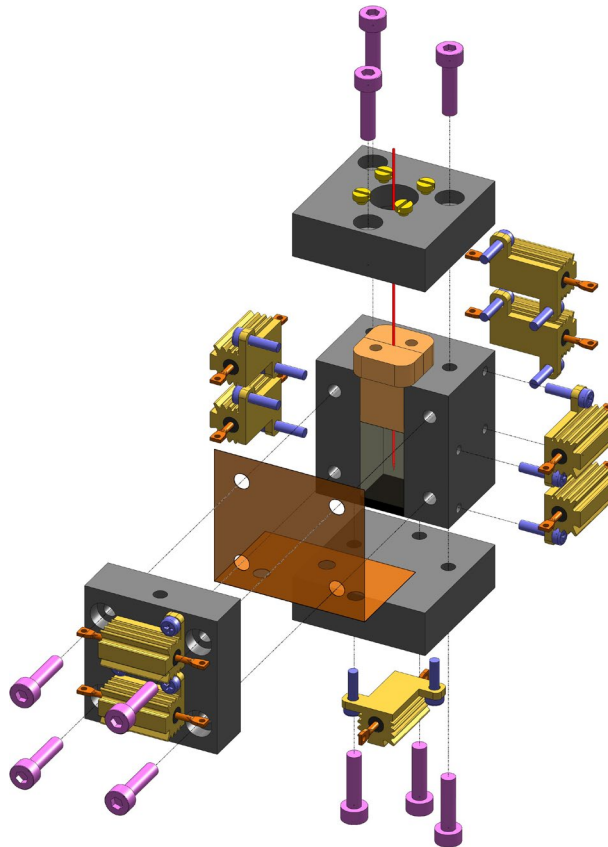
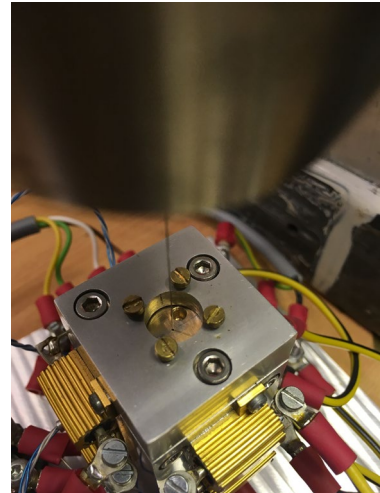Figure 3.3 An exploded model of the injection cell.

The specimen is surrounded on all sides by metal. The piece that sits on top of the specimen is like the electrode used in the capsule, but it is made from two separate pieces. Each one has a groove engraved that is just slightly larger than the needle. The two parts are then merged by soldering. The grooves line up and allows the needle passage through the whole piece. Mechanically, it is held down by four screws, keeping it in place as the specimen tries to expand. The angled orange part in the figure is a thin sheet of a copper that is used in an attempt to try and reduce the leakage from the injection cell. It is meant to deform and seal when pressure is applied. Nine heating elements are screwed to the sides of the specimen to facilitate heating and three RTD temperature sensors provides feedback. A computer running Matlab controls the injection process, it also implements a PI-regulator that controls the temperature of the cell. It has access to the temperature of the device via a bench multimeter that senses the resistance of one of the RTDs using a four-wire connection. The computer communicates with an ARM microcontroller running Linux which commutes the stepper motor and controls the duty cycle applied to the heating elements. The finished injection cell is seen in Figure 3.4.
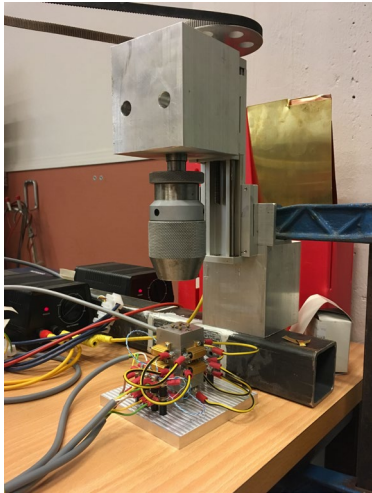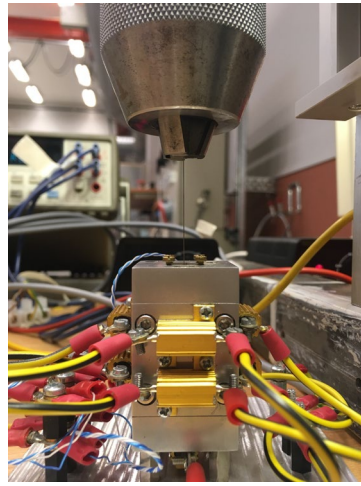
| (a) Overview. | (b) Front view. | (c) Needle passage. |

Figure 3.4 The injection setup.

The temperature cycle that is applied during the injection process is shown in Figure 3.5. The set point arcs for the heating and the beginning of the cooling sections are parametrised circles in order to avoid exposing the PI-regulator to step changes in the set point. The first mark indicates where the needle starts to be lowered, the second when it starts to penetrate the polymer and the third when it has reached its final depth.

The process starts by inserting the needle through the top piece, letting it rest on top of the polymer and tightening the chuck. This point is used to give the software a reference for where the top of the specimen is. It is then raised to a position above the injection cell. When the specimen is heated, it expands a little into the needle channel. If the needle is left at the top of the specimen, it might get bent by the expanding, but not yet completely amorphous, polymer.

The final geometry of the specimen is dependent on the injection procedure. When cutting the specimens from a cross-section of the cable, it is not practical to try to ensure a perfect cuboid, especially since the shape of the specimen inevitably is going to be altered to some degree by going through the injection process later. Using this injection cell with the temperature curve as seen in Figure 3.5 produces specimens which shape is that of the inner dimensions of the injection cell down to the surface texture of the machined metal parts. A small loss of density has thus occurred, but the compromise is a well worth since it enables the production of almost geometrically identical specimens.
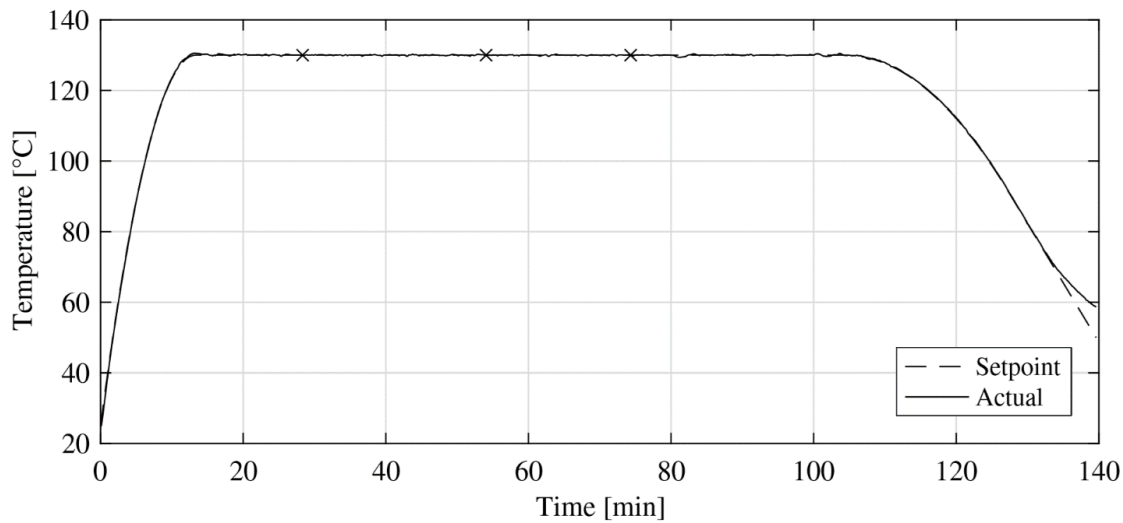
18

Figure 3.5. The injection cell temperature curve, both setpoint and actual.

3.3 The cell

Knowing the details of the specimen capsule, the requirements of the cell can be summarised. The specimen capsule as it is needs electric field control. Both in order to reduce the otherwise high electric fields that would develop around the sharp edges of the electrodes and in order to control the capacitance of the specimen. The measured capacitance of the electrode system should be as small as possible to better resolve small capacitive changes, it is after all the capacitive contribution from the volume in close vicinity of tip of the needle that is of interest. The specimen capsule should also be fixed in place in order to keep it from experiencing any change in its capacitive environment. The cell should support the specimen capsule axially as there is no need to stress the glass-to-metal seal unnecessarily and finally, the needle tip should be optically observable. In Figure 3.6 a cell based on these requirements is presented.

Support. The specimen is held axially as seen in Figure 3.6c and 3.6d. The high voltage brass electrode is screwed to the cell, keeping it in place. On the other side, the low voltage brass electrode is held in place by a stud from the threaded hole in the centre of the lid on the low voltage side. The stud holds the capsule via an insulating disc, shown in white in the Figure 3.6d. While it is not clearly visible in the figure, the bottom of the stud is tapered and enters a hole in the disc. The result is that the specimen capsule can be put under a slight axial compression, effectively keeping it in place and supporting the seals on each end.

Connections. In Figure 3.6c two screws are seen holding the high voltage brass electrode. One of these is also used as the connection point for the high voltage, which is applied using a cable and a cable shoe. In Figure 3.6d a BNC-connector is seen. It connects to the low voltage brass electrode with a wire and is secured by the screw seen in Figure 3.6d. The shield of the BNC-cable is used to carry an actively driven guard to the cell.

Field grading. In Figure 3.6e the guarding of the high voltage electrode is seen. The electrode with its sharp edges is submerged below the surface of the circular disc. By milling the edges of the hole into a radius, ensuring a continuous geometry, the field is effectively controlled. In Figure 3.6e the well of the low voltage brass electrode is seen with the same type of radius as on the high voltage side. Two protrusions are seen in Figure 3.6e. These act to further guard the lower electrode from stray capacitance.

Observing the needle tip. A window, as seen in Figure 3.6e, allows the tip of the needle to be observed. As can be deduced from Figure 3.6b, the observable distance is half the total distance between the needle and the semiconductor. The distance between the tip of the needle and the semiconductor is 4 mm, which makes the observable distance 2 mm. Therefore, care must be taken to ensure that the needle ends up in the correct place. The final height of the needle is decided by the chain of manufacturing, needle injection and assembly processes. First, the depth of high voltage guarding structure, (which the high voltage brass electrode is screwed to), is machined to within a narrow tolerance. Secondly, the total height of the high voltage brass electrode is machined precisely, as it is where the base of the specimen sits. The length of the specimen, which has to be accurate for the overall assembly of the capsule, is not critical at this stage as the reference of the injection process is taken at the non-semiconductor side of the specimen. A precise and repeatable placement of the needle is possible if these steps are carried out successfully.

The finished cell is seen in Figure 3.7. Ultimately, the cell is submerged in an oil bath, shown in Figure 3.8. The oil is used both as a dielectric and as a heat transfer medium. It is necessary since the distance at the narrowest part of the cell between the two polarities is 4 mm. This rules out keeping the cell in air during electrical tree inception experiments. The temperature in the bath is regulated using heating elements inside copper tubing and temperature feedback provided by an RTD sensed in a four-wire configuration. The copper tubing is grounded to reduce electrostatic interference from the heating elements. A PI-controller implemented in Matlab controls the bath temperature.
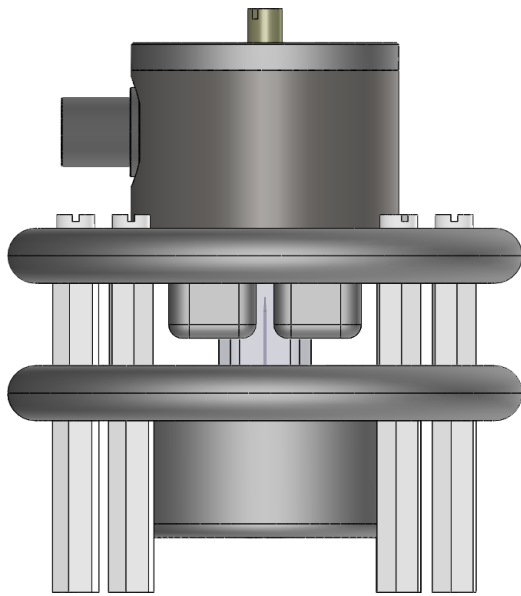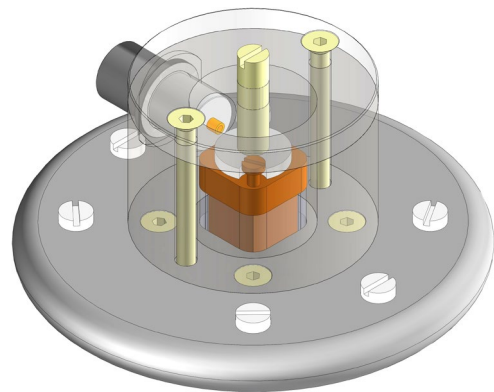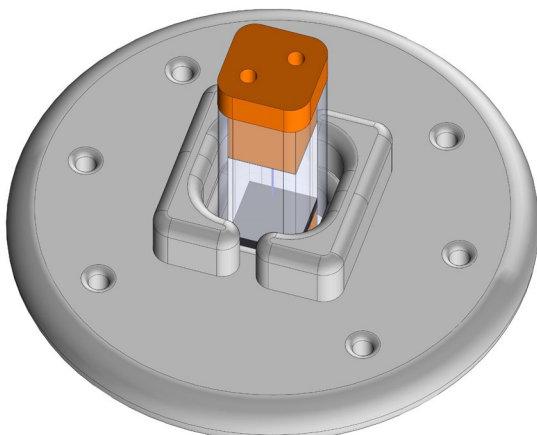
(a) The front of the cell.
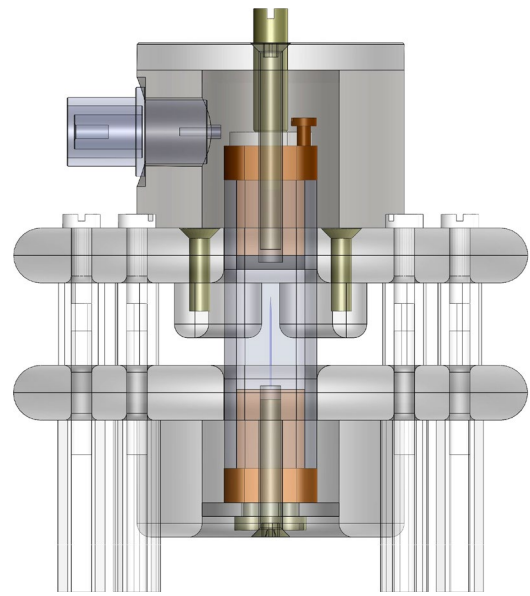
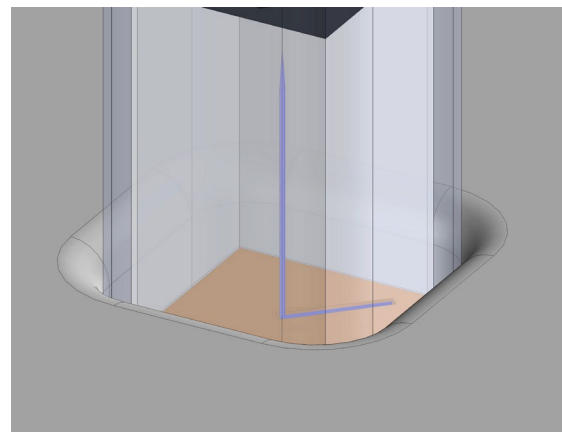(b) The front of the cell, transparent view.
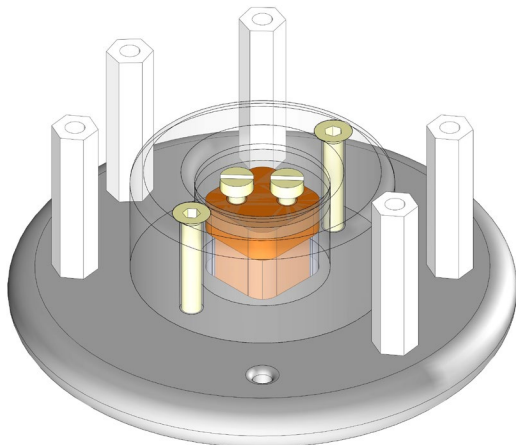
(c) The high voltage side.

d) The low voltage side.

(e) The high voltage well.

(f) The low voltage well.
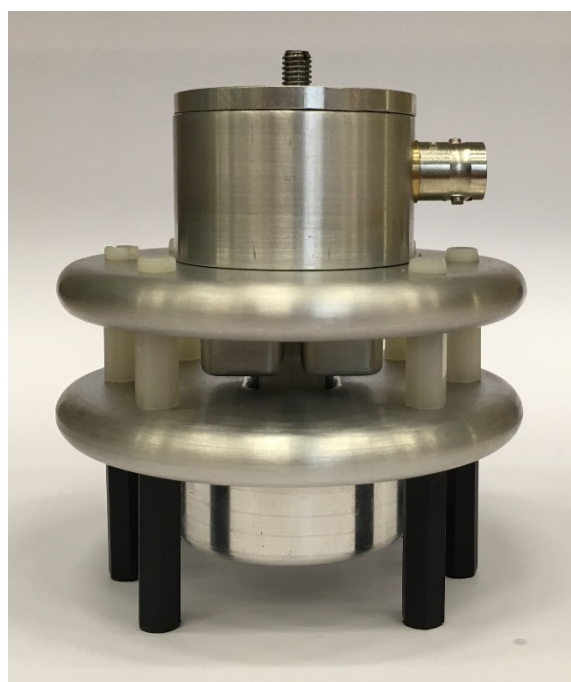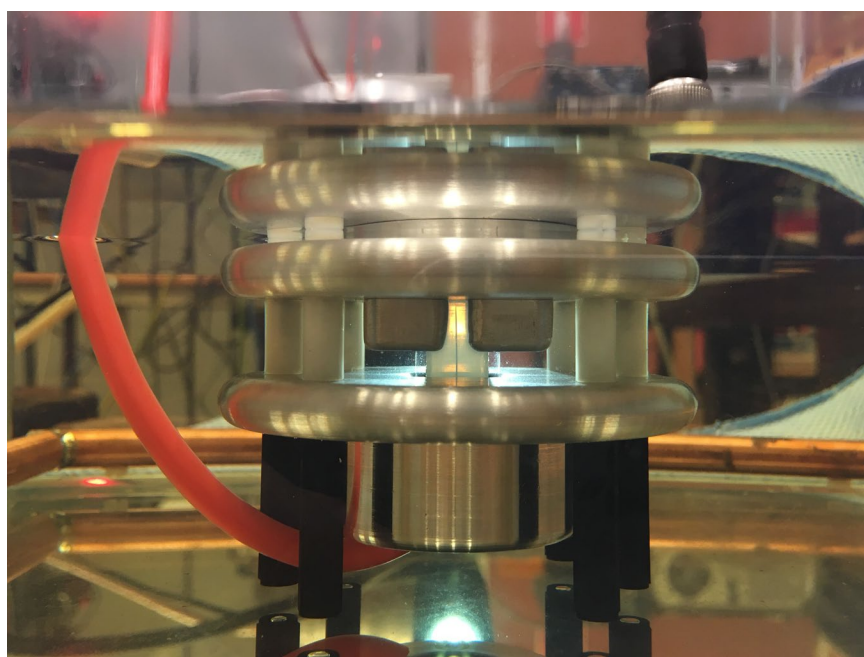
Figure 3.6 The cell

Figure 3.7: The cell.

Figure 3.8: The submerged cell. The illumination shows the needle in the polymer. In the background the copper tubing which houses the heating elements is visible.

3.4   Measurement setup

This part is structured as follows, an overview of how an electrical tree inception voltage experiment conducted with this setup is given first. Secondly, the devices that have been constructed specifically for this setup are described.

Measurements that indicate the inception voltage of electrical trees was carried out using a system as shown in Figure 3.9. Primarily, the system consists of a reference impedance connected in series with the specimen, a voltage divider, the submerged cell as well a conventional PD-measuring circuit: a coupling capacitor and a coupling quadripole. It is supported by computers that are responsible for supervising two temperature control loops, the recording of data from digital acquisition devices (DAQ), the generation of signals using digital-to-analogue converters (DAC) and exercising control of the setup in conjunction with various instruments and devices. The instrumentation list for the setup is summarised in Table 3.1.

As the setup is meant to be used to terminate the ageing process of a specimen by measuring the inception voltage of an electrical tree, an inherently destructive event for the specimen, the generated data point of the inception voltage is quite precious. Its value originates from the time involved ageing, the effort spent preparing the specimen, injecting the needle, sealing the capsule etc. Because of this, the data acquisition systems are configured to record a continuous stream of data from each source and save them for later analysis.

The advantages of this way of doing it, as compared to using a trigger-based recording system, is that it yields the maximum amount of information available and that the risk of a mistake, due to for example a misconfigured trigger, is vastly reduced. The continuous data recording is accomplished by reading a number of samples from the sample buffer of each DAQ-device and writing the received samples to a binary file on disk. If data is read faster or as fast as the device generates it the only limiting factor of the length of the recording is hard drive space. The implementation is carried out in both Matlab and Labview.

Table 3.1: A summary of the principal devices in use.

Device type	Name	Configuration
DAQ	NI-4431	24 bits, ±10 V, f = 102.4 kHz
DAQ	NI-5133	8 bits, ± 4 V, f =10 MHz
DAC	NI-6153	16 bits
PD-calibrator	Haefly type 451	
PD-coupling quadripole	Haefly akv type 568	20 mA, 1 nF, amplifier: on
PD-coupling capacitor	Haefly	1000 pF, 75 kV
Microscope	Olympus SZ61	Camera: Olympus SC30

The system makes four cardinal sources of data available for analysis:

- the voltage applied to the test object, measured by the NI-4431
- the voltage developed over the reference impedance, measured by the NI-4431
- the voltage output from the quadripole, measured by the NI-5133
- the video stream capturing the tip of the needle, recorded by a camera through a microscope

Having access to the entire waveform produced from all data acquisition sources also enables precise analysis of the behaviour of the specimen up to and after the inception of an electrical tree, further elucidating the behaviour of the specimen examined. The disadvantage to this method is that the amount of generated data is quite large.

As there are three different data acquisition units used simultaneously, they need to be synchronised time wise. This is accomplished using two techniques that are closely tied to the beginning of a measurement. An electrical tree inception voltage experiment is started by enabling the video recording followed by the beginning of the execution of the Matlab script that initialises, configures and begins to store data from the NI-4431 device. When the computer has finished configuring the device, it enables an analogue output that energises the circuit responsible for illuminating the cell. The next instruction that it executes is to begin storing data from the device. In the video recording this presents as a step between two frames, i.e. one is dark and the next is fully illuminated. This
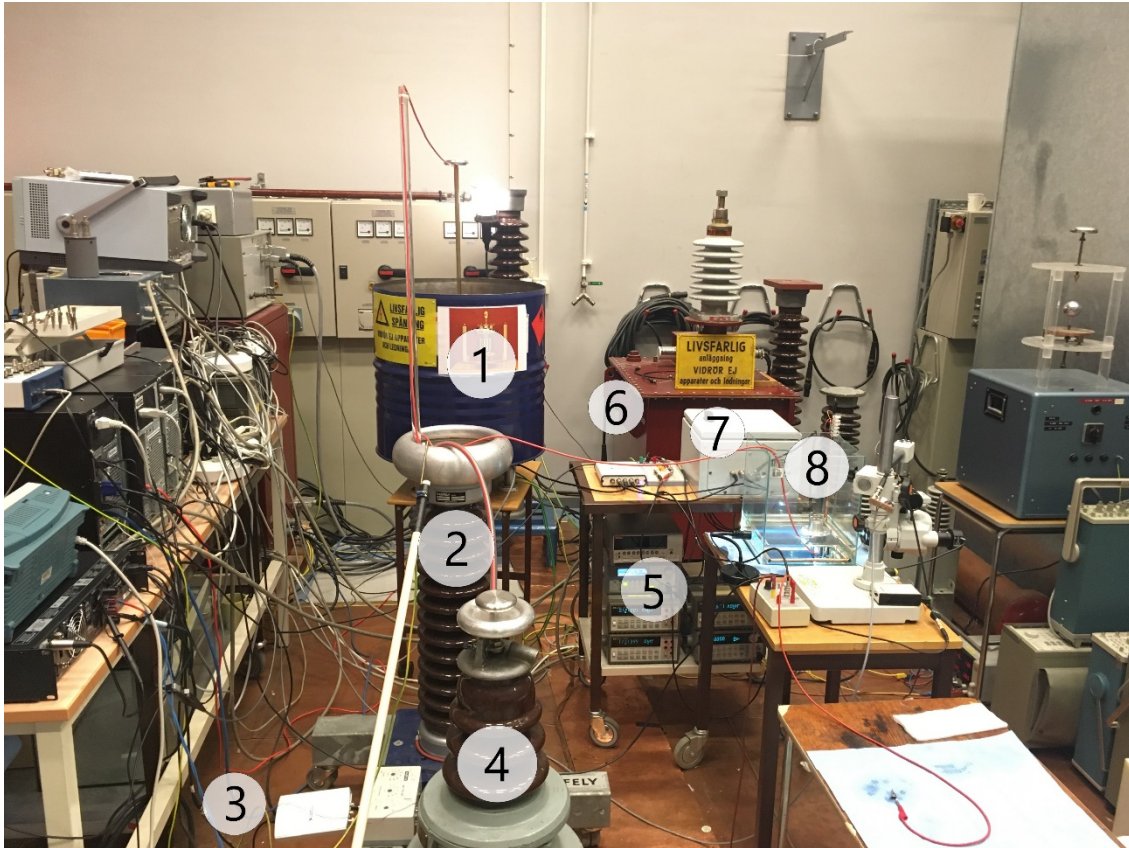
Figure 3.9: The setup which facilitates the electrical tree inception experiments. (1) voltage divider, (2) coupling capacitor, (3) NI-5133, (4) transformer, (5) signal generation and RTD-measurement, (6) NI-4431, (7) reference impedance, (8) test cell submerged in oil.

effectively locks the first illuminated frame to the beginning of the data stream from the NI-4431 device. There is no reason to further complicate this synchronisation as the exposure time of each frame is quite long (~ 50 ms) and the frame rate is one frame per second. At this time the data from NI-5133 begins to be stored and a PD-calibrator is connected across the cell. At the same time the PD-calibrator is connected via logic circuitry to the NI-4431 from the sync output of the calibrator. The logic circuitry outputs a pulse with a duration of half of the time between pulses from the PD-calibrator. This is needed as the PD-calibration waveform is much too short in duration to be reliably captured by the NI-4431. The result is concurrent events present in both the recording of the NI-5133 and the NI-4431 which can be used to synchronise the data streams. The delay introduced by the logic circuitry is $21.25\,\mu s$ and is compensated for. Perfect synchronisation down the sample is not possible due to the finite rise times of the synchronisation signals, but the error should still be in single digits of samples. As the NI-4431 device samples circa 1838 samples per sinusoidal period, the error is negligible. The logic circuitry is then disconnected as it is quite noisy

and the PD- calibrator is used to produce calibration pulses of various magnitudes. The final step before applying voltage is to replace the synchronisation signal from the logic circuitry with the active guard voltage.

By way of a high voltage transformer connected to a class AB amplifier the specimen is then exposed to a ramped sinusoidal excitation. The signal is generated by a DAC-module on the NI-6153 that outputs a sinusoidal period consisting of 1000 discrete points at a rate of 55710.3062 points per second. Each period has its corresponding points multiplied by a number slightly larger than the last which results in a linearly growing sinusoidal wave. The signal is constructed in such a way that it reaches 14.4 kV_{rms} after 20 minutes, in other words, it increases by 12 V_{rms}/s . This signal is first generated in its entirety and then fed consecutively to the DAC-buffer.

3.4.1 Reference impedance

A known impedance connected in series with the test object allows changes in the specimen impedance to be quantified accurately. The impedance consists of a parallel resistive-capacitive arrangement of 1 MΩ ‖ 112 pF. The output voltage, in other words the voltage developed over the impedance, is buffered by an operational amplifier. Present is also an amplifier that actively drives the guard. A simplified schematic is shown in Figure 3.10. The full schematic is available in Figure A.1. The choice of a resistive-capacitive impedance was motivated by two factors:

- The resistive part facilitates usage with both AC and DC voltages
- If there is PD-activity in the specimen, the capacitor will integrate the PD-signal, making the otherwise to fast PD-events visible when measuring at relatively low sampling frequencies

The component values were chosen based on approximations of the specimen impedance. Given that the specimen and the reference impedance forms a voltage divider the values of the components has to be such that the voltage developed over the reference impedance does not exceed the supply voltage of buffering amplifier. Furthermore, the RC-time constant should be appropriate for the sampling frequency.
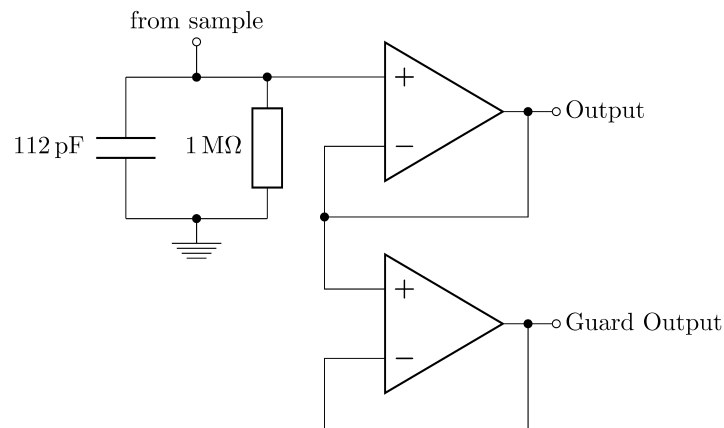
Figure 3.10 Simplified schematic of the reference impedance.

A femtoampere level operational amplifier operating in unity gain mode is used to buffer the signal. The low bias current enables measurements of high impedance specimens without skewing the results. The amplifier also isolates the impedance from any influence

of connected data acquisition systems. The output of the amplifier acts as the input for the guard driver which feeds the guard traces on the PCB. The guard continues in the shield of the cable connecting the reference impedance to the cell, either via the outer shield of a coaxial cable or the inner shield of a triaxial cable. The finished device is shown in Figure 3.11.

Components

The primary buffer amplifier is a LMP7721 while the guard is driven by a LMP7715. The passive components were selected mainly based on their long-term stability. The resistive part is provided by a Vishay VHA516-6 resistor, an oil filled, hermetically sealed secondary standard resistor which bulk metal foil construction gives it low values of parasitic inductance and capacitance. The resistor exhibits a TCR of ± 2 ppm/$^\circ$C and a load life stability of $\pm 0.005\,\%$. The tolerance of the nominal value is $\pm 0.001\,\%$.

AVX M23269J/10-3094, a capacitor which construction consists of a metallic structure embedded in glass and sealed hermetically provides $100\,\mathrm{pF}$ of capacitive part of the impedance, (the remaining 12 pF is contributed by the input capacitance of the LMP7721-amplifier). A consequence of its construction is that, at least according to the manufacturer, it exhibits "zero ageing". The properties of a capacitor with a glass dielectric approaches the of an ideal circuit symbol, in all but one respect.

27

Stability

The downside of the glass capacitor is that it exhibits a TCC of 100 ppm/˚C. Due to this, the reference impedance circuit board is installed in a temperature regulated enclosure, as seen in Figure 3.12. Figure 3.13 shows the temperature during two weeks. It can be seen that the inner temperature is held, with some margin, within 30.3 ˚C and 29.8 ˚C.
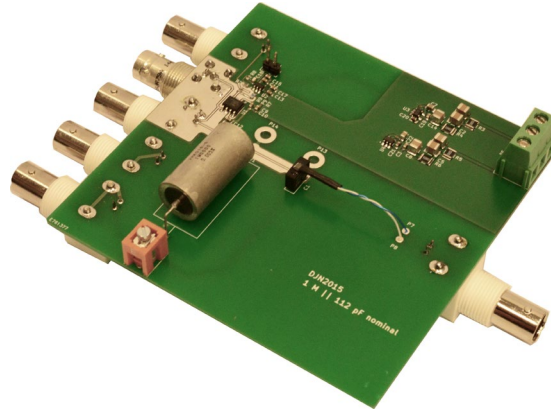

Figure 3.11 The circuit board that houses the reference impedance. The resistor is the large cylindrical grey component and the capacitor is mounted to the right of it. The temperature sensor that is glued to the capacitor was later moved from fears of it influencing the capacitor.

Figure 3.12 Housing of the reference impedance.
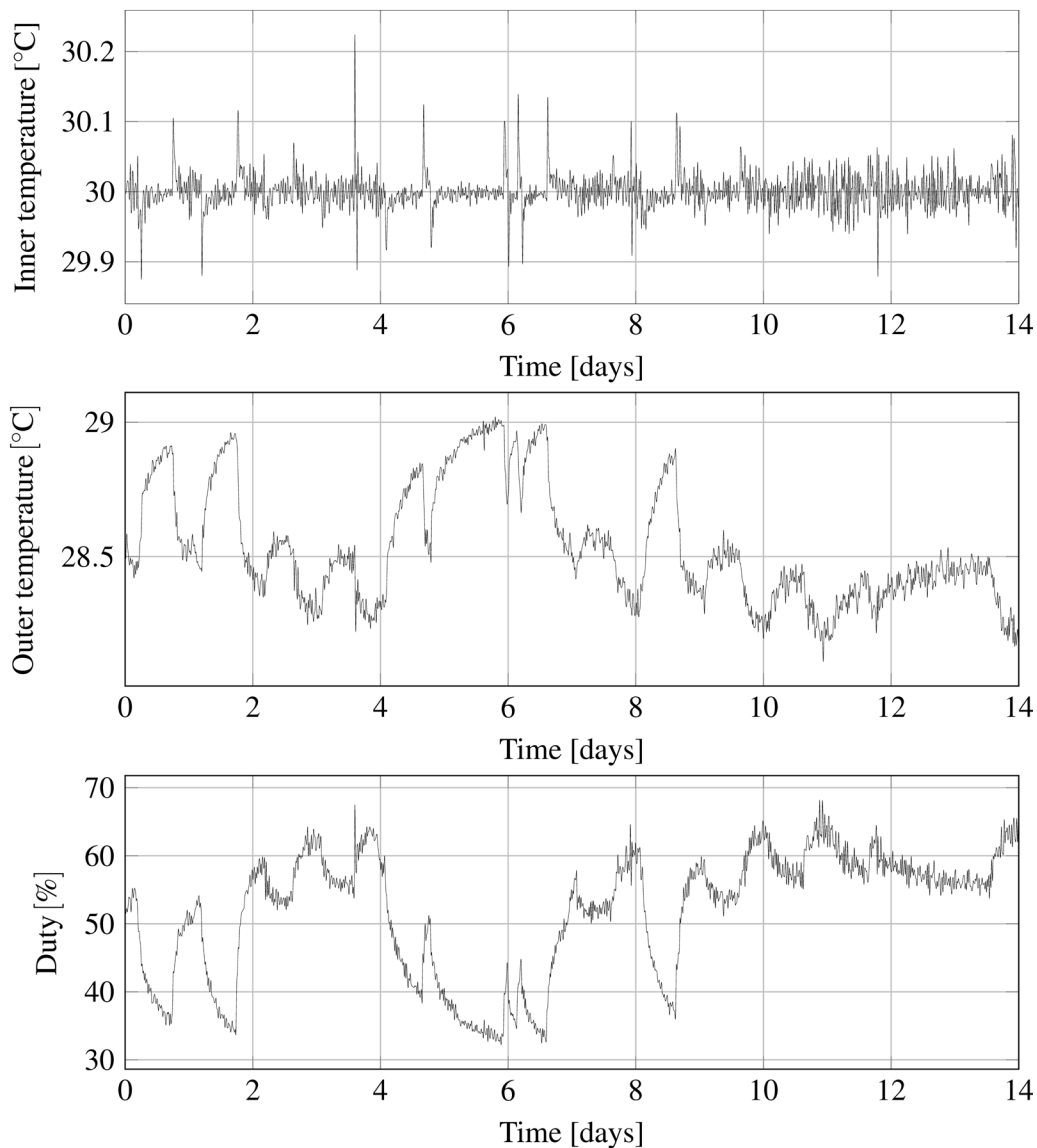
Figure 3.13 Temperature control of the reference impedance.

3.5 Voltage divider

Given the need to measure both AC and DC voltages, a resistive-capacitive topology was chosen for the voltage divider. A basic model of such a device with phasor notation is illustrated in Figure 3.14. An RC-voltage divider has a high and a low voltage part. The high voltage part has a high-ohmic resistive element R_1 and a parallel capacitance C_1 originating from the resistive element itself and from surrounding, connected, metallic structures. The low voltage arm consists of a resistance R_2 which together with the high voltage resistance decides the DC and low frequency ratio of the divider. The frequency response and high frequency ratio of an RC-divider can be easily altered by varying the amount of capacitance C_2 in the low voltage arm.
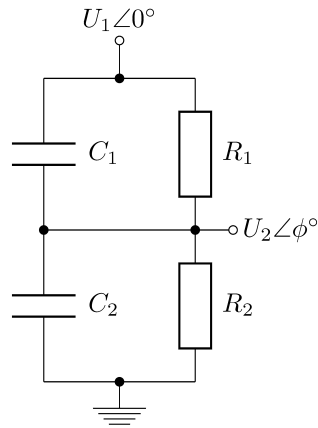
Figure 3.14. A rudimentary model of a resistive capacitive voltage divider.

The design of the voltage divider was heavily influenced by the idea of reducing one of the intrinsic shortfalls of the typical RC-voltage divider. As the high voltage element must withstand almost all of the incoming voltage without breaking down, it is usually made in an elongated fashion. This gives rise to a non-negligible parasitic capacitance emanating from the element to metallic objects in the surroundings where field lines terminate. In Figure 3.15 the resistive part of the voltage divider is shown. The high voltage resistive element is split in two and the entire parasitic capacitance is modelled as connected in between. This is an apparent low pass filter, as the frequency of the applied voltage increases the impedance of the stray capacitance decreases, creating an undesirable connection outside of the transfer function to ground in the middle of the high voltage element.

To counter this, an attempt to control the field using overlapping metallic screens was made. A simplified drawing of the high voltage arm of the divider is shown in Figure 3.16. The figure shows
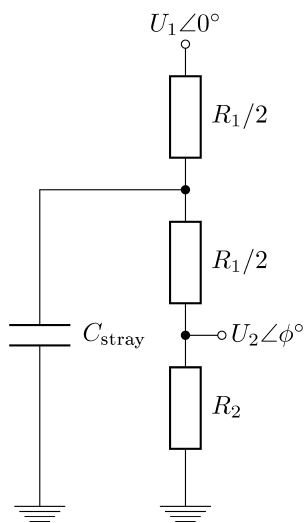
Figure 3.15. A model of the lumped parasitic capacitance.

a cross-section of the device, which is circular. In the middle the vertical high voltage resistor is seen. It is connected to the upper cylindrical screen and toroid, which is the input of the device. At the bottom the resistor is connected to the lower toroid which in turn is connected to the lower cylindrical screen. The entire lower section is also the output of the device. The capacitance that is formed between the metallic parts contributes to C_1 together with the parallel capacitance of the resistor. From the figure it is clear that the field lines emanating from the resistor has a hard time terminating anywhere but on the upper or lower metallic parts. Thus, the parasitic capacitance from the resistor will almost entirely connect to either the input or output of the device with varying amount of series resistance, resulting in a minimal C_{stray}.

The finished high voltage arm can be seen in Figure 3.17. In order prevent heat building up inside the upper cylindrical screen, three holes were drilled in the upper toroid and screen. This is shown in Figure 3.18.
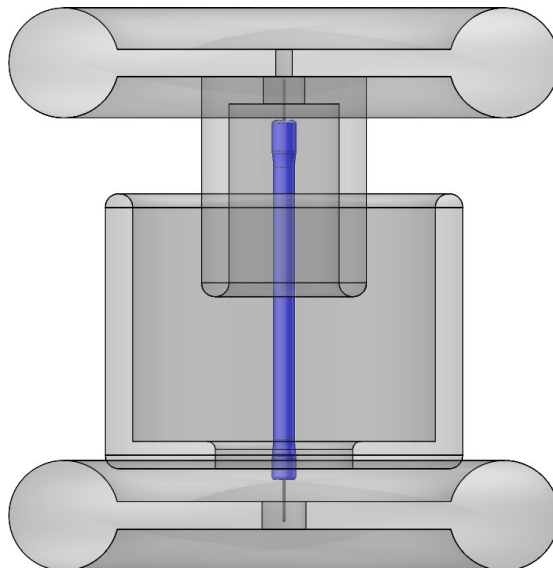
Figure 3.16: The high voltage arm of the voltage divider illustrating the overlapping screens. All fasteners, most holes and connectors have been removed to improve visibility.
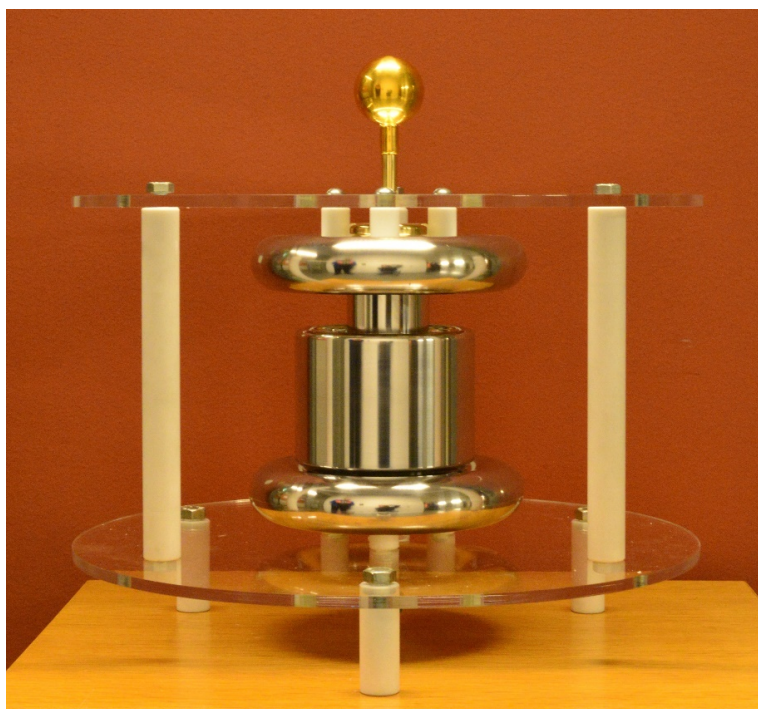
Figure 3.17: A photograph of the high voltage arm of the voltage divider.
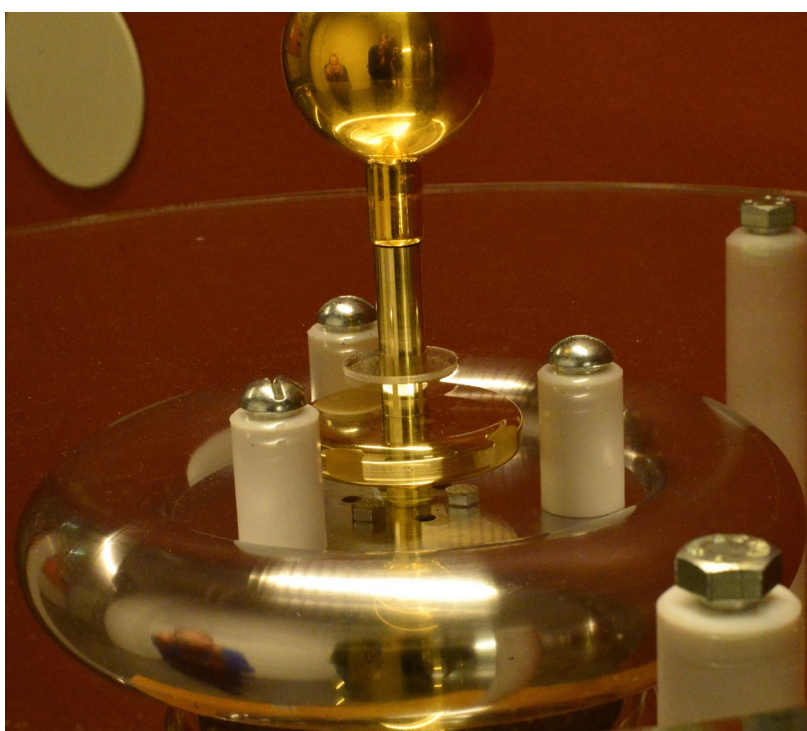

Figure 3.18: The top part of the high voltage arm.

After these pictures was captured, improvements were made to enhance the rigidity of the structure. The lower legs and the supports that separates the upper and lower polycarbonate discs were exchanged from PTFE to aluminium in order to improve the stability of the device. The lower legs and the supports were mounted along the same axis instead of 60 degrees apart. The metallic screws visible in Figure 3.18 were replaced with screws made of nylon.

The low voltage arm of the voltage divider has two components. One that houses the passive components and one that holds operational amplifiers. The resistive part of the passive compensation is made of of two resistors connected in series, totalling 40 kΩ. In parallel with the resistors are capacitors. They can be divided into three parts. Bulk compensation is provided by 13 capacitors, delivering 26 nF. Further, there are three 2 nF, one 1 nF and one 0.5 nF capacitors of the same type that can be manually connected or disconnected via jumpers. Finally, there are three variable air capacitors that each provide between 15-384 pF that are intended for fine tuning of the device. A schematic of the passives in the low voltage arm can be found in Figure A.3. Two operational amplifiers in unity gain configuration provides two impedance isolated measurement outputs. The schematic of this circuit is available in Figure A.2. The enclosures and circuit boards that contains the passive and active components are shown in Figure 3.19.

Figure 3.19: Left: the low voltage arm of the voltage divider, the air capacitors are mounted far side of the PCB. Right: The buffering amplifiers.

Finally, the high voltage arm is mounted inside a metallic cylindrical enclosure to ensure a stable capacitive environment. This ensures that the parasitic capacitances that contribute to C_2 is kept static. It also prevents any disturbance of the electric field between the upper and lower toroids and cylinders, thus keeping C_1 static. The enclosure itself has feet and the low voltage arm is mounted on the bottom of the enclosure. The finished device can be seen in Figure 4.1, the enclosure is the blue drum.

Components

The low voltage resistors are from Vishay's Z-series. They exhibit a TCR of ± 0.2 ppm/$^\circ$C, a tolerance of ± 0.005 % and a load life stability of ± 0.005 %. The inductance of each resistor is $< 0.08\,\mu$H and their voltage coefficient < 3 ppm. The bulk compensation capacitors are from Cornell Dubilier MC22-series. These are mica capacitors and such they have excellent frequency properties. Their TCC are 25 ± 25 ppm/$^\circ$C. The variable air capacitors are of type N50 and manufactured by Oren Elliot Products. The dielectric constant of air varies based on temperature, pressure and humidity and it has influence on both C_1 and the air capacitors. While the effects of changes in pressure and humidity can be considered to be minor in this application, the dielectric constant of air varies by 5 ppm/$^\circ$C. Finally, the high voltage element is a $100\,\text{M}\Omega$ low-inductive resistor. It is rated for 6 W, 50 kV and has a TCR of 25 ppm/$^\circ$C.

Measurements

The voltage divider is able to work up to 25 kVAC. Up to this point no flashovers or detectable partial discharges occurs. The frequency response and phase shift up to 45 kHz of the device is seen in Figure 3.20. In this frequency range, the variation in the scale factor and the phase shift is less than 1 %. The phase shift is calculated with the applied voltage as reference. This measurement was carried out by feeding a sine wave with an amplitude of 9.95 V to both the voltage divider and a 24-bit, 102.4 kHz, ± 10 V, simultaneous sampling DAQ-device, (NI-4431). The output of the voltage divider was connected to the same device. The scale factor was calculated using the ratio of the two RMS-values. The phase shift was found using a DFT. The frequency was increased in discrete steps and each one was measured for 5 seconds, except for the sub-Hertz frequencies that were measured for 20 seconds.

The frequencies measured were:

- Up to and including 1 Hz, measurements of 0.1, 0.5 and 1 Hz
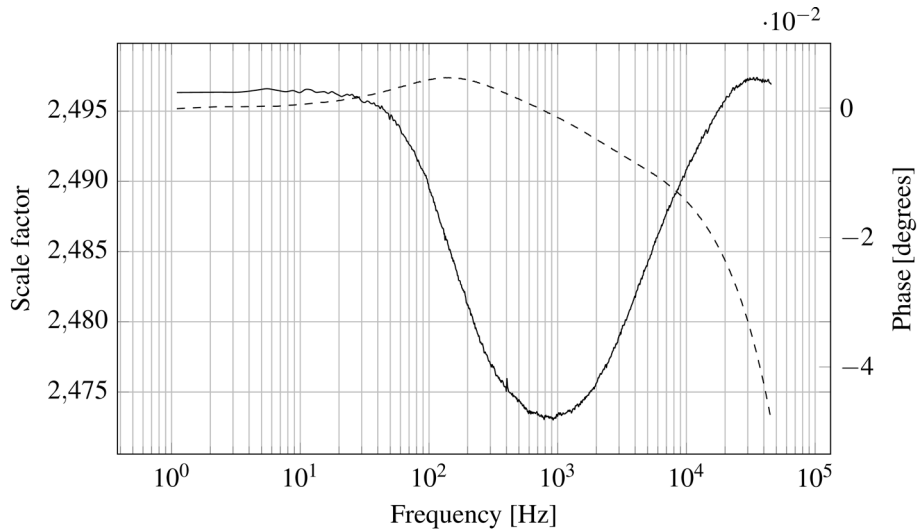- Between 1-2000 Hz, the frequency was increased by a step of 2 Hz

Figure 3.20. Frequency response of the voltage divider

System measurements

An uncalibrated $1.0\,\text{pF}\pm0.1\,\%$ three terminal standard air capacitor, GR Type 1403-K, was used to test the voltage divider together with the reference impedance. The capacitor was connected in series with the reference impedance in the same way as specimen capsule would be connected. The circuit was energized with $115\,\text{V}_{\text{rms}}$. The active guard was utilized and connected to capacitor's the third terminal. Capacitance was calculated per period over 20 minutes. The average value recorded was $1.0034\,\text{pF}$ while the maximum value recorded was $1.0083\,\text{pF}$ and the minimum value recorded was $0.99976\,\text{pF}$.

In order to further evaluate the effect of the actively driven guard, a cell with a specimen capsule but without a specimen was assembled. Without the guard, and with the otherwise driven structure grounded, the measured capacitance was 185.0 fF, with the guard enabled the measured capacitance to drop to 8.5 fF.

3.6 Results

In this part the results of three electrical tree inception experiments are presented. A comparison between the different available detection sources of the inception voltage is presented first. Following that, two different approaches to calculating the specimen's impedance during a measurement are presented and examined. The sought impedance omits the influence of any ongoing discharge activity. The results of the impedance calculations are presented which ends the part concerning the inception voltage.

Finally, a few observations regarding the measurement system in general and some comments about the differences between the individual measurements conclude this part.

3.6.1 The electrical tree inception voltage

The raw output from one measurement of the electrical inception voltage in a specimen is shown in Figure 3.21: Unprocessed results, here, the used data set originates from the first measurement. Figure 3.21a shows the measured excitation voltage that was applied to the needle, Figure 3.21b shows the measured voltage developed over the reference impedance and Figure 3.21c shows the PD-events with a threshold of 5 pC from the external PD-circuit. Figures 3.21d, 3.21e and 3.21f shows the video output one frame before the detection of inception, the frame in which inception is detected and one frame after. The inception voltage is discernible from each of these sources except for the excitation voltage. A comparison between the detected inception voltage levels between these sources is shown in Table 3.2.
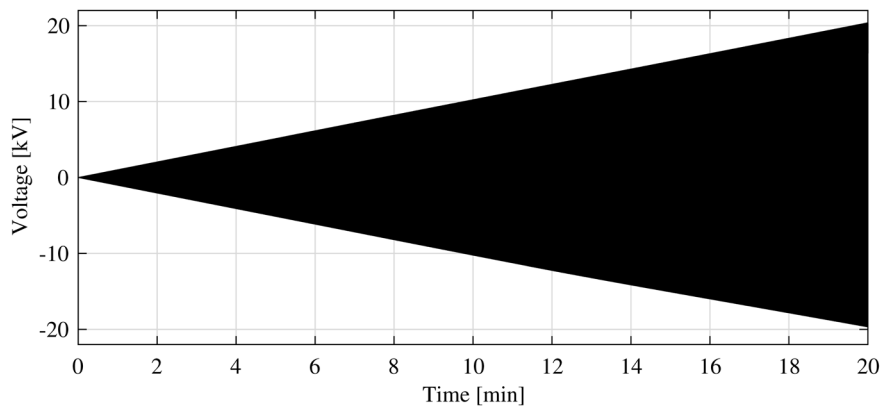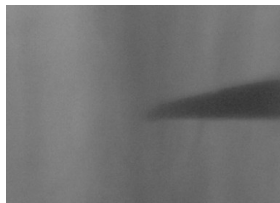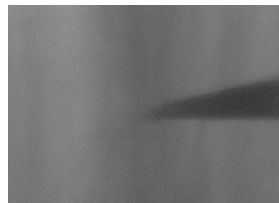
(a) Excitation voltage.
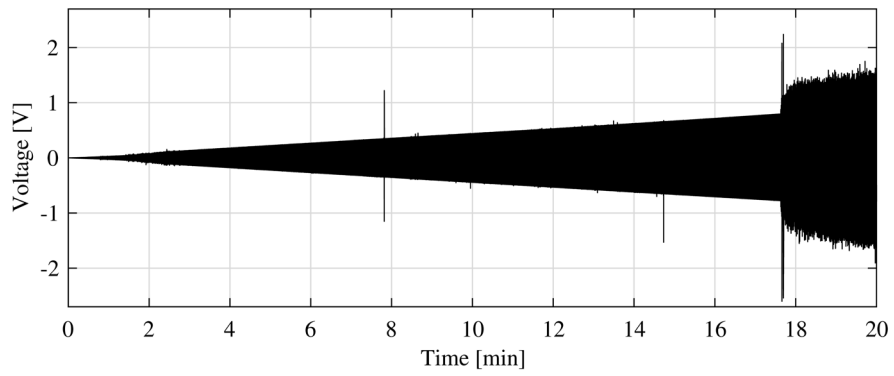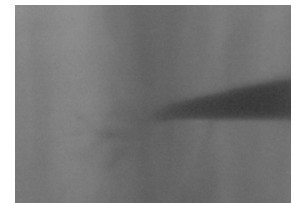

(b) Reference impedance voltage.
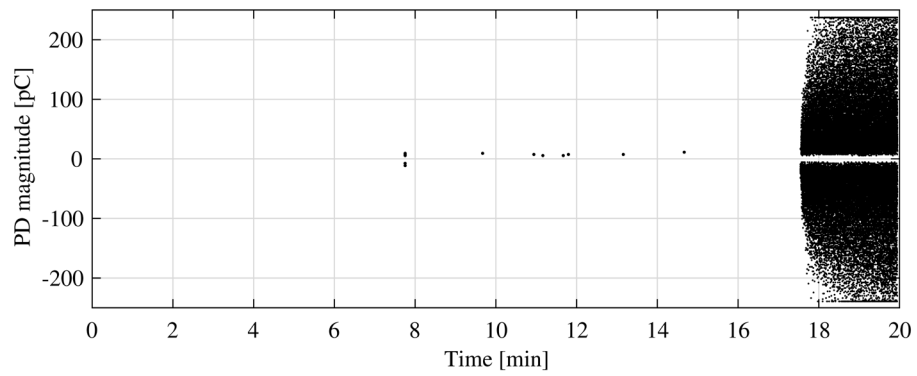
(c) Conventional PD-circuit output.

(d) One frame before inception.

(e) Inception.

(f) One frame after inception.

Figure 3.21: Unprocessed results

Table 3.2: Comparison between the different data sources in terms of their ability to detect the inception of an electrical tree.

Source	Time	Voltage [kV]
$U_{\text{ref imp}}$	17m 37.37s	
PD	17m 37.42s	12.62
Optical	17m 37.28s	

The optical inception time was calculated using

$$\text{Optical inception time} = \left(N_{\text{visible tree}} - N_{\text{light}}\right) \cdot T_{\text{time per frame}} - T_{\text{time to start}} \qquad 3.1$$

where $N_{\text{visible tree}}$ denotes the frame number when the first sign of an electrical tree is visible, the N_{light} is the frame number when the cell is illuminated, (which is triggered when the NI4431 data collection is started), $T_{\text{time per frame}}$ is the time between each frame and $T_{\text{time to start}}$ is the delay between the start of data collection from the NI-4431 and the beginning of the voltage excitation. Since the start of the recording is referenced to a device that samples the excitation voltage, the inception voltage can be found. The exact moment of initiation of the voltage ramp is not specifically known to any of the data acquisition sources, instead it is calculated by a linear fit of the measured excitation voltage. Somewhat simplified, the optical inception time has an error of $\pm\ T_{\text{time per frame}}$. As $T_{\text{time per frame}}$ is typically 1 s, the resulting error is $\pm 12\ \text{V}_{\text{rms}}$.

3.6.2 Post-processing the results

Even though the inception voltage can be accurately detected by any of the sources as is evident by Table 3.2, further understanding of what transpires in a specimen during an electrical treeing experiment can be gained from post-processing the results. This section is structured as follows. The methods for calculating the impedance of the specimen during an experiment are introduced in 3.6.2.1 and 3.6.2.2. Each method takes a different approach, but the end goal is shared: to exclude the influence of electrical discharges in the specimen, such as charge injection, (but not charge build-up), and partial discharge activity. By knowing the underlying impedance of the specimen, as well as the excitation voltage and the component values of the reference impedance, the waveform that a discharge free specimen would give rise to can be found and the discharge activity can be found via subtraction. The results of these calculations are presented in 3.6.2.4.

3.6.2.1 Assuming that the excitation voltage is sinusoidal

Figure 3.22 shows the circuit under consideration. The specimen is modelled as R_1 and C_1, a parallel RC-circuit, R_2 and C_2 represents the known component values of the reference impedance and U_1 and U_2 represents the input and output voltages respectively, both of which are sampled quantities
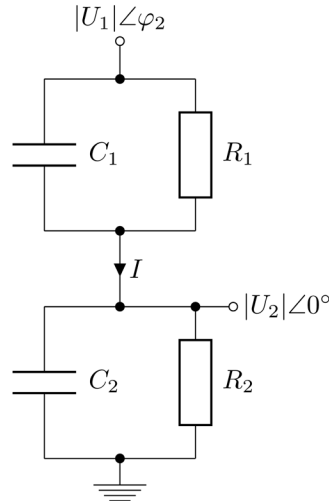

Figure 3.22 Schematic representation of the device under test connected to the reference impedance.

This method relies on that the input voltage U_1 is perfectly sinusoidal and as such can be represented by a phasor. U_2 is chosen as the reference voltage and its angle is thus set to zero. Since R_2 and C_2 are known, the current that flows into the reference impedance I can be calculated by

$$I = \frac{|U_2|\angle 0}{R_2 || \frac{1}{j\omega C_2}} = |I|\angle\varphi_1 \qquad 3.2$$

Using the discrete Fourier transform (DFT), the phase shift between U_1 and U_2 can be calculated by

$$\text{angle} \frac{\text{DFT}\{U_1\}(k)}{\text{DFT}\{U_2\}(k)} = \varphi_2 \qquad 3.3$$

where angle is a Matlab command that returns the four-quadrant inverse tangent. The values of the DFT are taken at bin k which in this case corresponds to the fundamental frequency of U_1 and U_2. Knowing the phase difference allows the input voltage of the circuit to be referenced to U_2 by $U_1 = |U_1|\angle\phi_2$. The current I that flows into the reference impedance must also flow through the unknown impedance. Combined with the fact that the voltage drop over the unknown impedance is known allows for the impedance to be calculated using

$$Z_{\text{DUT}} = \frac{|U_1| \angle \varphi_2 - |U_2| \angle 0}{|I| \angle \varphi_1} \qquad \text{3.4}$$

which yields the series impedance. The equivalent parallel impedance has the expression

$$Z_{\text{DUT}} = R_1 \parallel \frac{1}{j\omega C_1} = \frac{1}{\frac{1}{R_1} + j\omega C_1} \qquad \text{3.5}$$

which has the inverse

$$\frac{1}{Z_{DUT}} = \frac{1}{R_1} + j\omega C_1 \qquad \text{3.6}$$

The resistance and capacitance can then be written as

$$R_1 = \frac{1}{\text{Re}\left(\frac{1}{Z_{\text{DUT}}}\right)} \qquad \text{3.7}$$

$$C_1 = \frac{\text{Im}\left(\frac{1}{Z_{\text{DUT}}}\right)}{\omega} \qquad \text{3.8}$$

A simplification can be made by assuming that the sample is purely capacitive, in which case the capacitance can be expressed as

$$C_1 = \frac{|I|}{\omega |U_1| - |U_2|} \qquad \text{3.9}$$

If the excitation voltage of a circuit containing only discharge free elements is perfectly sinusoidal, it follows that the response of such a circuit will also be perfectly sinusoidal. Thus, trigonometric interpolation can be used to fit a curve based on the sampled output voltage U_2. Specifically, a first order trigonometric Fourier series fit on the form

$$y = a_0 + a_1 \cos(\omega x) + b_1 \sin(\omega x) \qquad \text{3.10}$$

was used. With the help of Matlab's curve fitting toolbox, the curve is fitted in a non-linear least square sense using a Trust-region algorithm, yielding ω, a_0, a_1 and b_1. Given the discharge free waveform, the impedance of the specimen can be found by substituting the sampled U_2 with the fitted U_2.

3.6.2.2 Assuming that the excitation voltage is sinusoidally shaped

If the excitation voltage cannot be expressed analytically, the waveforms needs to be processed using derivatives in the time domain. The circuit under consideration is still the same as shown in Figure 3.22, but with a change in notation as to be clear that these are time-varying signals. The current $i(t)$ can be expressed as

$$i(t) = \frac{u_1(t) - u_2(t)}{R_1} + C_1\frac{d(u_1(t) - u_2(t))}{dt} = \frac{u_2(t)}{R_2} + C_2\frac{du_2(t)}{dt} \qquad 3.11$$

where the left hand side of the equation refers to the current flowing in the upper arm of the circuit and the right hand side refers to the current flowing in the lower arm.

At this point, the current $i(t)$ in the circuit can be calculated point wise using the right hand side of equation 3.11. The derivative of $u_2(t)$ is approximated by the finite difference

$$\frac{du_2(t)}{dt} = \frac{u_2(t + h) - u_2(t - h)}{2h} \qquad 3.12$$

where h is the time between two subsequent samples. This ensures that the derivative is referred to the point t in the sampled waveform. In order to find R_1 and C_1, multiple regression is used. The method fits data that depends on more than one predictor variable. The circuit is modelled by

$$A_1x_1 + A_2x_2 = B \qquad 3.13$$

where $A_1 = u_1(t) - u_2(t)$, $x_1 = 1/R_1$, $A_2 = d(u_1(t) - u_2(t))/dt$, $x_2 = C_2$ and $B = i(t)$. Solving $\mathbf{Ax} = \mathbf{B}$ for $\mathbf{x}$ is carried out by the Matlab command 'mldivide', which uses QR decomposition to find a least-squares solution of the equation system, yielding R_1 and C_1.

With all circuit parameters known, the discharge free u_2 based on the excitation voltage u_1 can be calculated. Since equation 3.11 is an ordinary differential equation, Heun's method is employed to approximate the response. Implementing the method with the same electrical notation as before results in the expression

$$u_2(t + h) = u_2\frac{1}{2}(k_1 + k_2) \qquad 3.14$$

where $k_1 = h \cdot du_2(t)/d$ and $k_2 = h \cdot du_2(t + h)/dt$. k_1 represents the derivative multiplied by the step length h at the time t and k_2 is the derivative of u_2 at $t + h$ multiplied by h. The former is readily calculated by rearranging equation 3.11, shown in equation 3.15. The latter expression is seen in equation 3.16, it uses the Euler method for an approximation of $u_2(t + h) = u_2(t) + k_1 = u_2(t) + h \, du_2(t)/dt$.

$$\frac{du_2(t)}{dt} = \frac{\frac{u_1(t)}{R_1} + C_1 \frac{u_1(t+h) - u_1(t-h)}{2h} - u_2(t)\left(\frac{1}{R_1} + \frac{1}{R_2}\right)}{(C_1 + C_2)} \qquad 3.15$$

$$\frac{du_2(t+h)}{dt} = \frac{\frac{u_1(t+h)}{R_1} + C_1 \frac{u_1(t+2h) - u_1(t)}{2h} - (u_2(t) + k_1)\left(\frac{1}{R_1} + \frac{1}{R_2}\right)}{(C_1 + C_2)} \qquad 3.16$$

The differentiation of the u_1 is kept as a finite difference in order to avoid having a 0.5 sample offset and the step length h is equal to the time between samples.

As this is an initial value problem, a starting value for u_2 must be chosen. One way is to set it to zero and allow for the approximation to settle, but the length of time before that occurs depends on the waveform window. The worst-case scenario, when the window begins with one of the maximum or minimum peaks, requires ~ 60 samples to be processed before the approximation settles. An improvement can be made by using the actual sample of u_2 at the beginning of the window, but this can be catastrophic if there happens to be a PD at that moment in time. The most practical way is to use the already fitted curve resulting from the trigonometric Fourier series fit from 3.6.2.1, as that of course will be devoid of any PD-activity.

This method allows for u_2 to be calculated for any given time window of the waveform, which in turn enables the discharge free current to be calculated using the same expression as before, the right side of equation 3.11, but with the approximated voltage u_2 instead of the sampled u_2.

3.6.2.3 The excitation voltage

Two different amplifiers were used to drive the high voltage transformer. The first measurement used a 600 W amplifier while the second and third used a 2.4 kW amplifier. Both amplifiers use the AB topology. The change of amplifier resulted in two slightly different excitation voltage waveforms. Qualitatively, the difference between them can be thought of as their distance to a pure sinusoidal waveform, where one is further away and one is closer. Henceforth, the waveform that exhibits properties that can be described as being far away from being sinusoidal will be referred to as E1. This was the waveform used during the first measurement. Correspondingly, the second waveform will be referred to as E2, which was the waveform used during the second and third measurements. The change of amplifier also caused an unintentional deviation in the excitation

42

voltage's ramp rate. While E1 has an actual ramp rate of 12.08 V_{rms}/s, which is close to the nominal rate of 12 V_{rms}/s, E2 has a ramp rate of 11.1 V_{rms}/s. While the gain was set equally on both amplifiers, the gain tolerance of the second amplifier was not considered.

Comparing the waveforms quantitatively requires a journey into the frequency domain. In Figure 3.23 a comparative spectrum of the two waveforms are shown. Creating the spectra was done by computing the DFT over a 100-period long window of the waveform, where the amplitude of each waveform was normalized to one. The harmonic components are listed numerically in Table 3.4 and THD of the first nine harmonics is shown in Table 3.3. Including any further harmonics does not alter the THD other than in the far decimals.
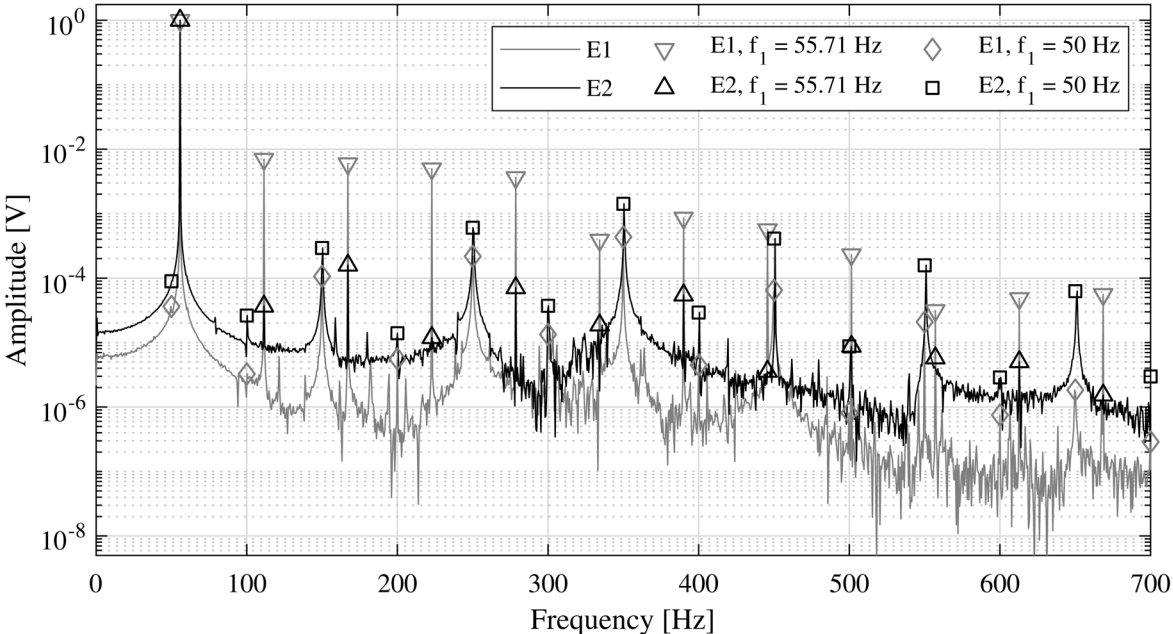
Figure 3.23 Single sided amplitude spectrum of E1 and E2.

Table 3.3: THD of the excitation voltages.

	THD [%]	THD + 50 Hz [%]	THD [dB]	THD + 50 Hz [dB]
E1	1.116	1.117	-39.05	-39.04
E2	0.01874	0.1643	-74.54	-55.68

Table 3.4 Harmonics of the excitation voltages.

Harmonic number [Hz]	55.71 Hz harmonics		Harmonic number [Hz]	50 Hz harmonics	
	E1, ▽	E2, △		E1, ◊	E2, □
	$A_n \times 10^4$			$A_n \times 10^4$	
$f_1 = 55.71$	9958	9950	$f_1 = 50$	0.363	0.893
$f_2 = 111.42$	69.9	0.365	$f_2 = 100$	0.0326	0.262
$f_3 = 167.13$	59.5	1.57	$f_3 = 150$	1.06	2.93
$f_4 = 222.84$	49.6	0.119	$f_4 = 200$	0.0558	0.139
$f_5 = 278.55$	36.3	0.705	$f_5 = 250$	2.17	6.04
$f_6 = 334.26$	3.88	0.186	$f_6 = 300$	0.133	0.372
$f_7 = 389.97$	8.55	0.544	$f_7 = 350$	4.33	14.2
$f_8 = 445.68$	5.62	0.0356	$f_8 = 400$	0.0447	0.292
$f_9 = 501.39$	2.30	0.0872	$f_9 = 450$	0.649	4.10
$f_{10} = 557.10$	0.314	0.0574	$f_{10} = 500$	0.00810	0.0872
$f_{11} = 612.82$	0.482	0.0502	$f_{11} = 550$	0.209	1.57
$f_{12} = 612.82$	0.558	0.0152	$f_{12} = 600$	0.00749	0.0287
$f_{13} = 612.82$	0.325	0.0274	$f_{13} = 650$	0.0183	0.627

3.6.2.4 Comparing the methods

The methods described in 3.6.2.1 and 3.6.2.2 are used to calculate the impedance per period for the entire duration of each experiment. The calculations continually adjust to maintain the same phase as the excitation frequency is not synchronized to the sampling frequency.

Examining the waveforms on a 1.5 period scale, Figure 3.24 shows the results of excitation by the E1 waveform and Figure 3.25 shows the results when the E2 waveform was used. Each sub-figure is windowed identically in time, showing 1.5 periods from the same measurement, but the window obviously differs between the figures. The examples in Figure 3.24 are from the first measurement while the examples in Figure 3.25 are from the third measurement. As the calculations run on a period basis, there is a step present in the waveforms. It is visible at 1085.00125 s in Figure 3.23 and at 590.935 s in Figure 3.24, (zooming in is required to resolve the step).

Each figure contains four subplots. The two first refer to the trigonometric Fourier series fit and the latter refer to the multiple regression fit and Heun's method for approximating u_2.

Figure 3.24a and 3.24b shows the results of the trigonometric Fourier series fit. Both figures include the subtraction between the sampled curve and the fitted one. Figure 3.24a has both the excitation voltage U_1 and its derivative included, both are scaled for visibility, the y-axis refers to the voltage U_2. The figure highlights the deviation in U_2 due to the derivative of U_1. Figure 3.24b shows curve of the fitted waveform. The discrepancy between the waveforms can be most clearly seen at the third zero crossing, at around 1085.0025 seconds.

Figure 3.24c and 3.24d shows the time domain processing of the waveforms. Here, R_1 and C_1 has been found by multiple regression. The circuit parameters, together with Heun's method and the sampled excitation voltage u_1, is used to find u_2. As the discharge free voltage is known, the discharge free current in the circuit can be calculated, as is shown in 3.24d.

Figure 3.25a, 3.25b, 3.25c and 3.25d shows the results of the curve fittings during E2 excitation.

Table 3.5 lists the different values found by each method of calculation. Here, as well as in the figures, 'nofit' indicates that raw data has been used without any attempt to remove the influence of discharge activity. Figure 3.26, 3.27, 3.28, shows the calculated capacitance and resistance during the entire measurements with a rolling average of 43 periods, or approximately 0.77 s. Figure 3.29 shows a view of the capacitance at and after inception alone for all three measurements. The latter figures has the detected inception time of the camera system marked, except for the plot showing the second measurement where the optical data was not definitive.
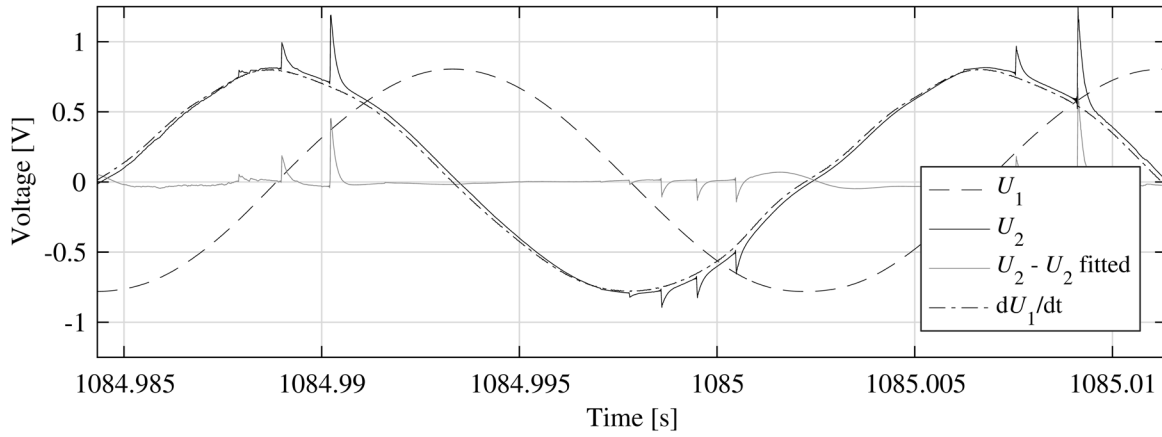
(a) The excitation voltage and its derivative.
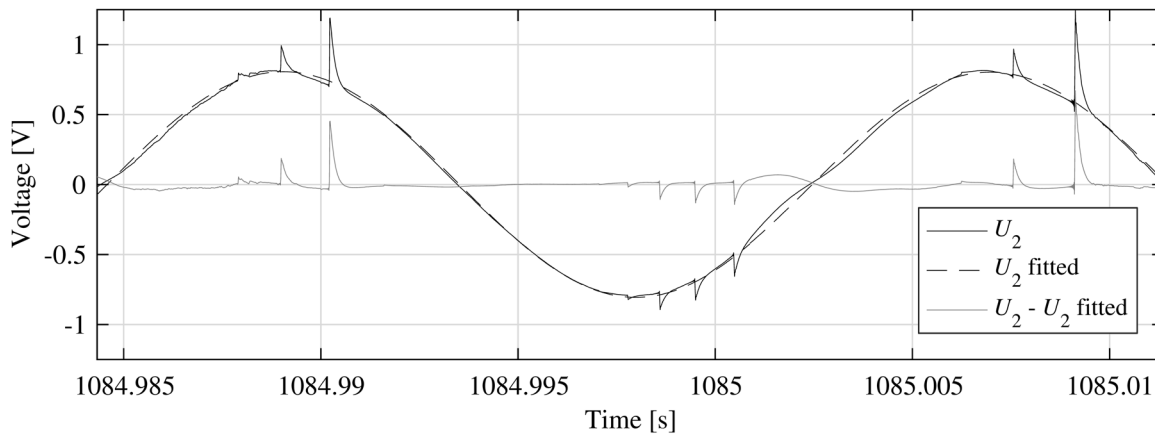
(b) Trigonometric Fourier series fit of U_2.
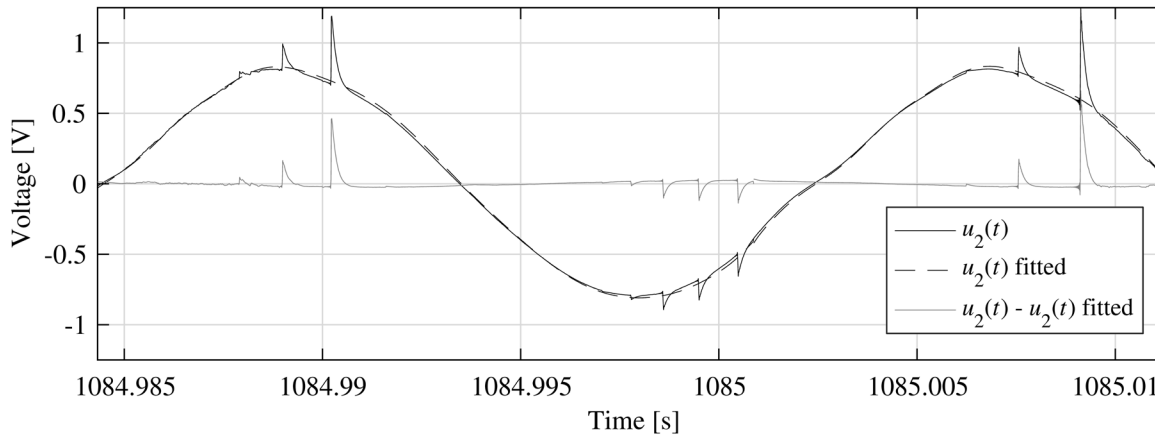
(c) The fit resulting from the regression calculation and Heun's method.

Figure 3.24: E1 excitation.
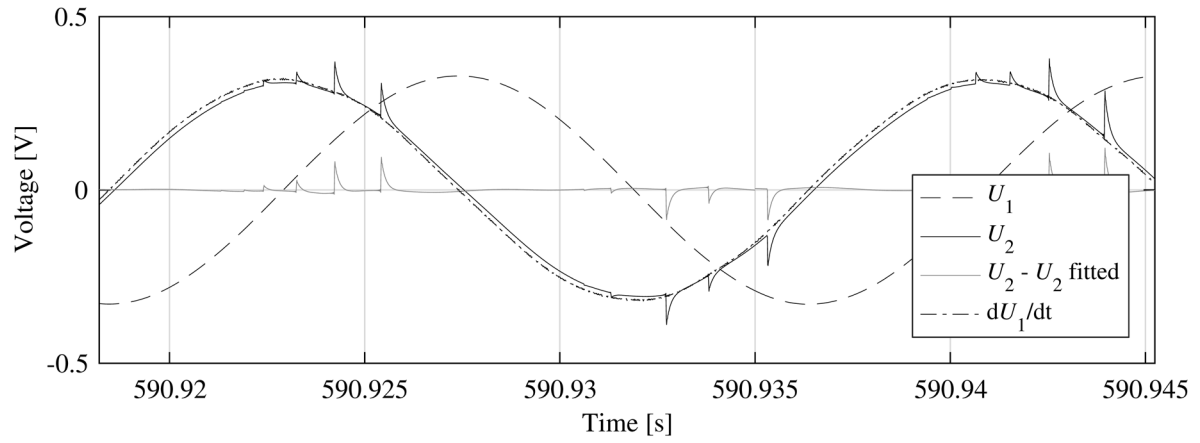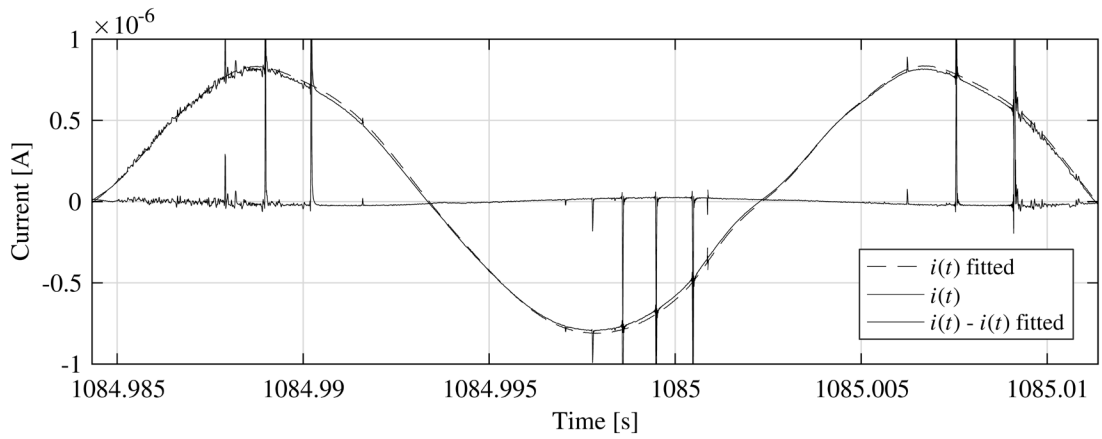
(a) The excitation voltage and its derivative.
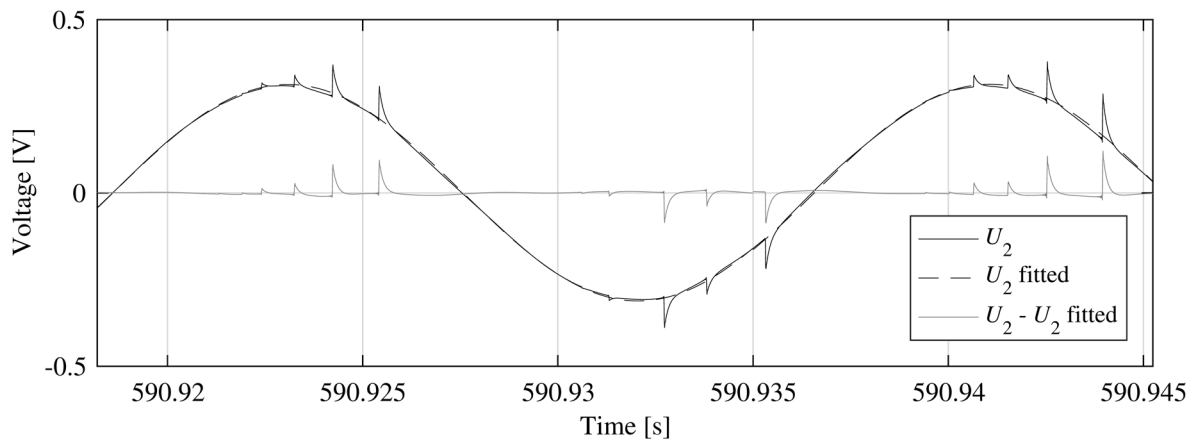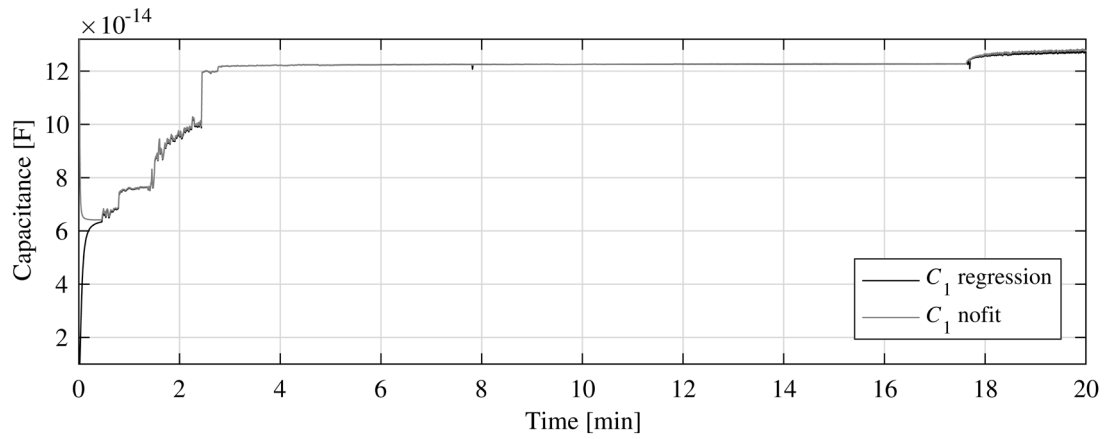

(b) Trigonometric Fourier series fit of U_2.
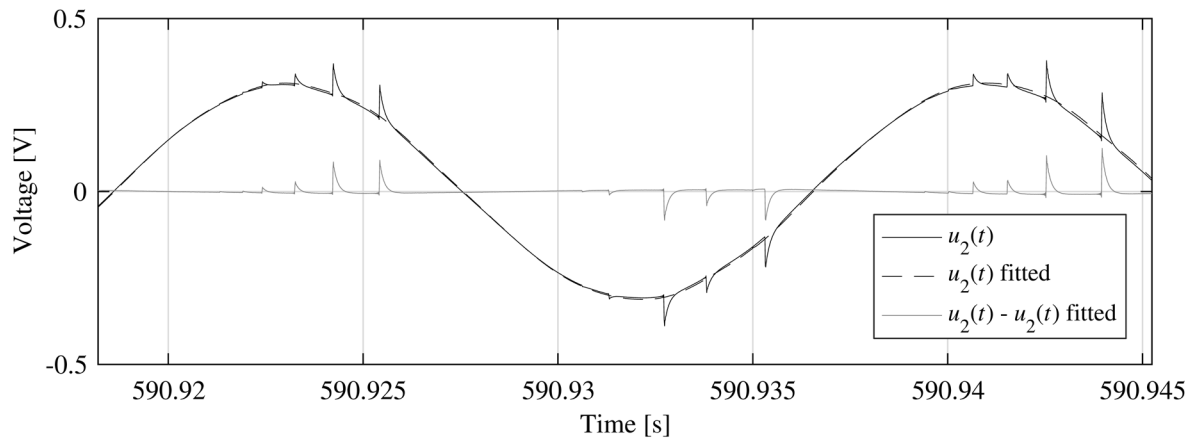
(c) The fit resulting from the regression calculation and Heun's method.
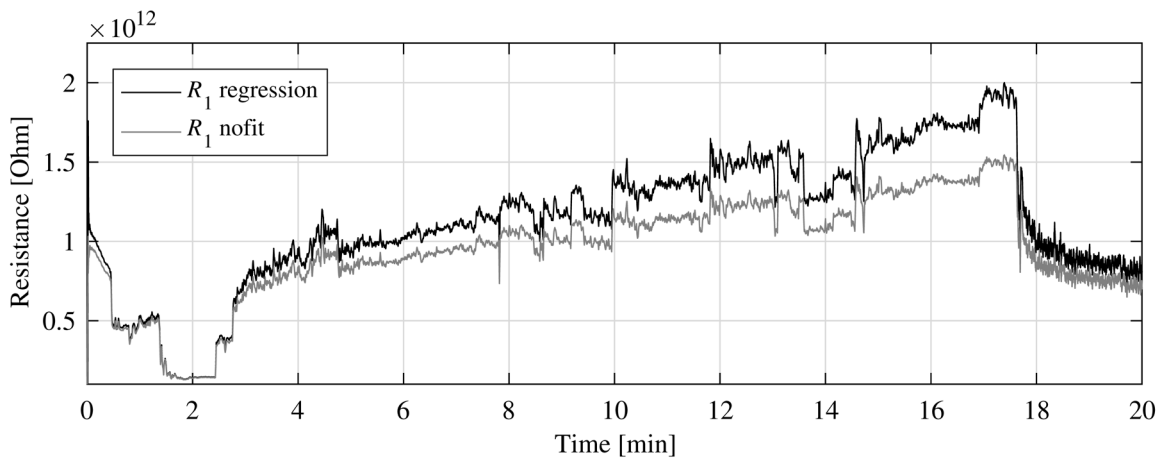
Figure 3.25: E2 excitation.

(d) The actual current as well as the discharge free current from the regression calculation.

Figure 3.24: E1 excitation.

(a) C_1 during the first measurement.

(b) R_1 during the first measurement.
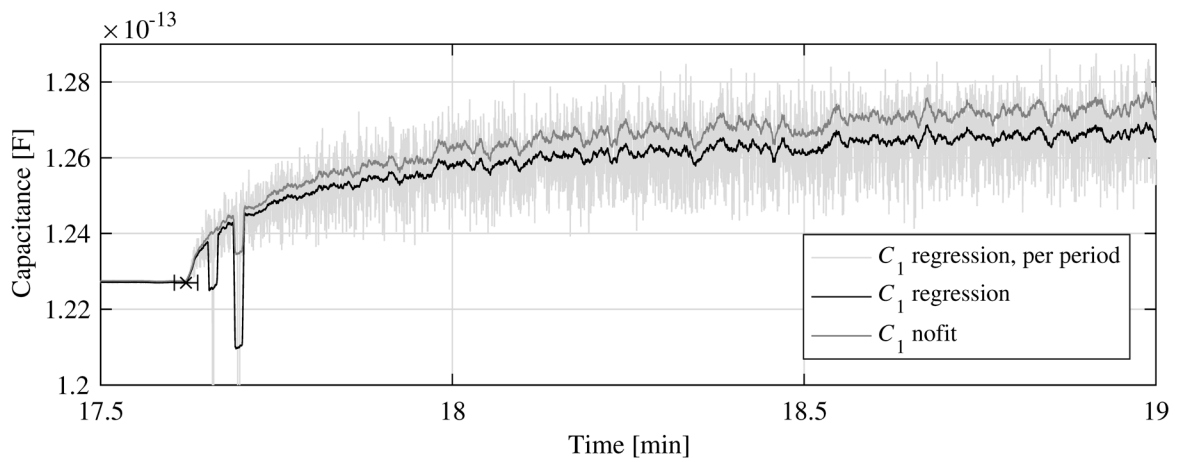
Figure 3.26: C_1 and R_1 during the first measurement.
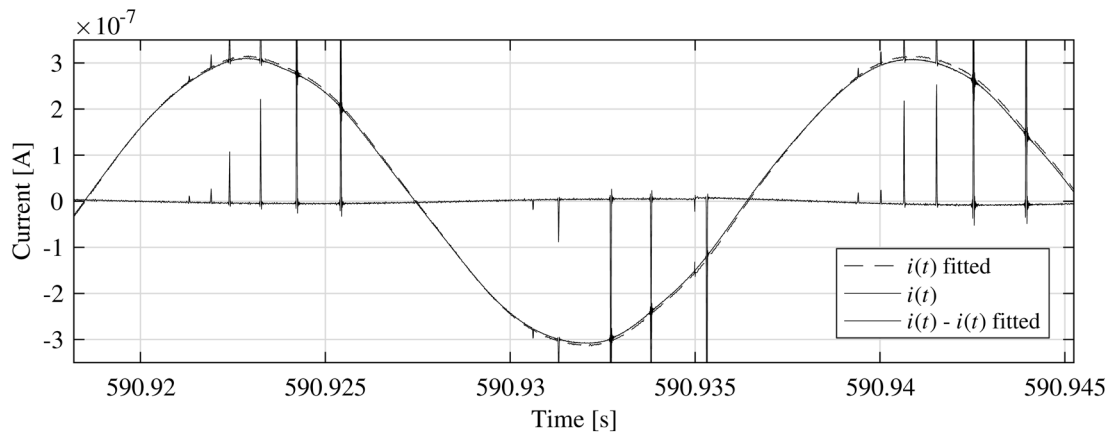
(d) The actual current as well as the discharge free current from the regression calculation.

Figure 3.25: E2 excitation.
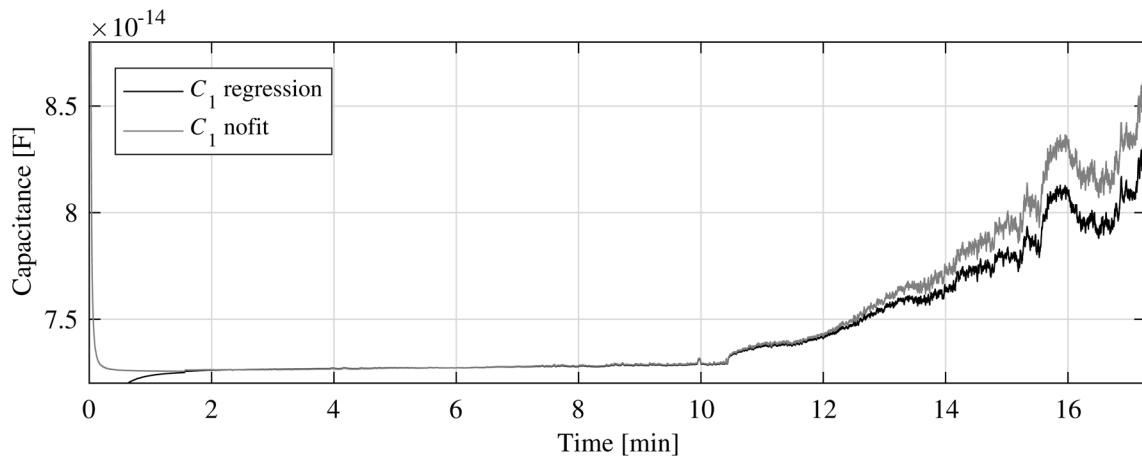
(a) C_1 during the second measurement.
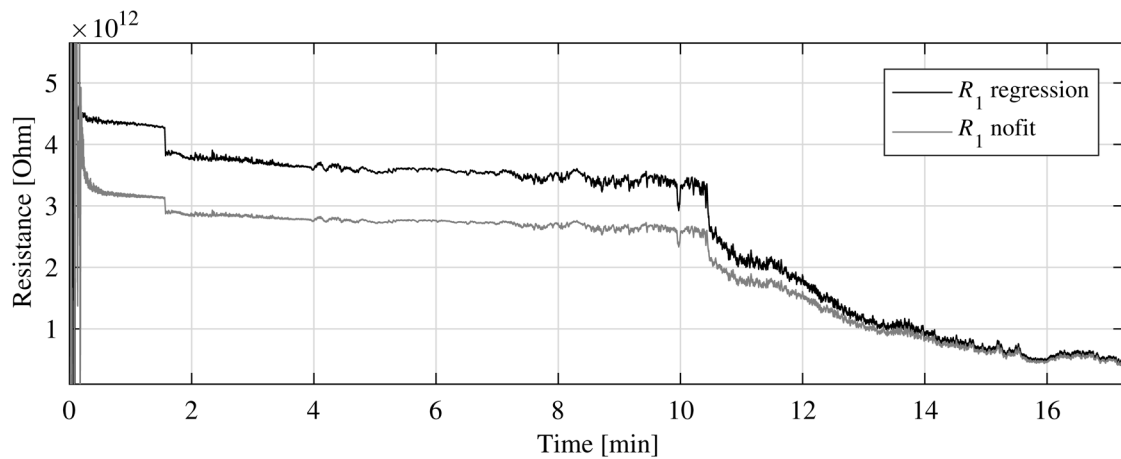
(a) R_1 during the second measurement.

Figure 3.27: C_1 and R_1 during the second measurement.
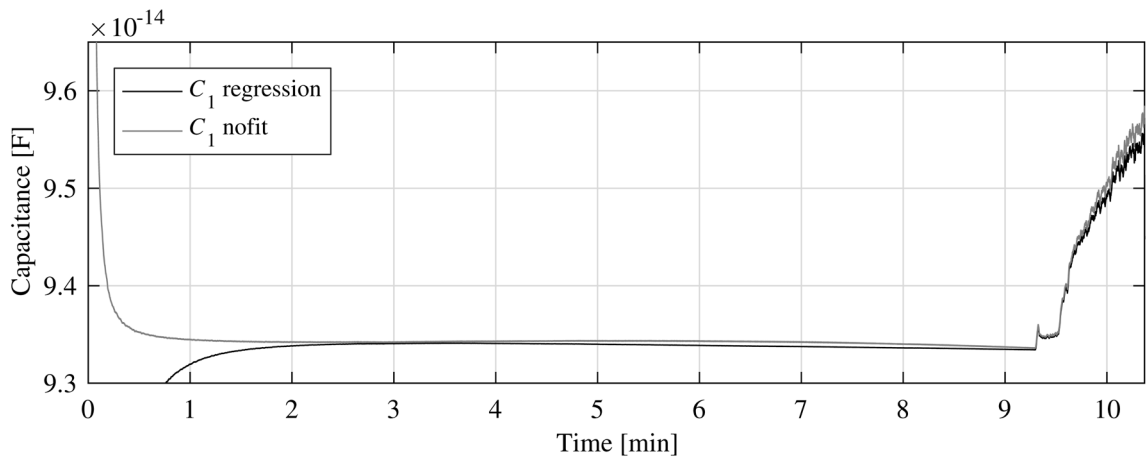
(a) C_1 during the third measurement.
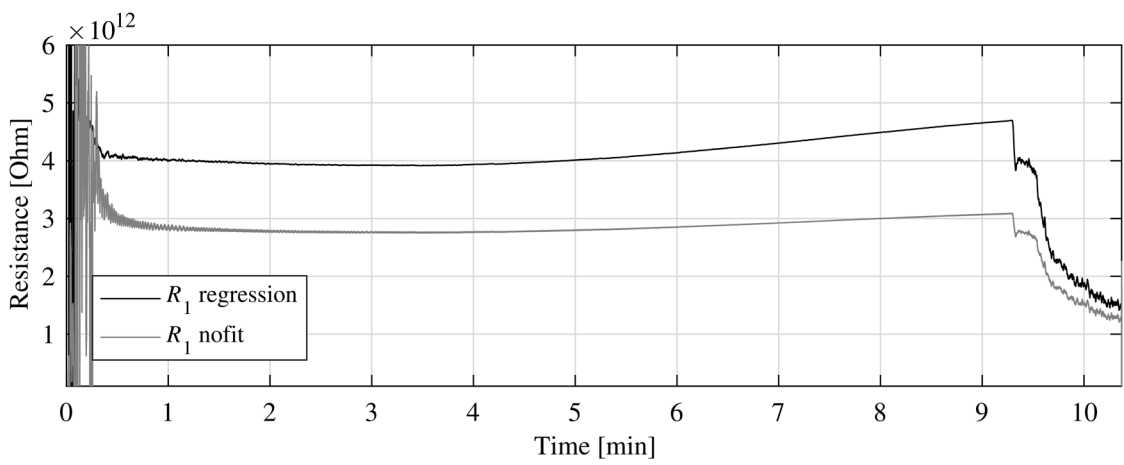
(b) R_1 during the third measurement.
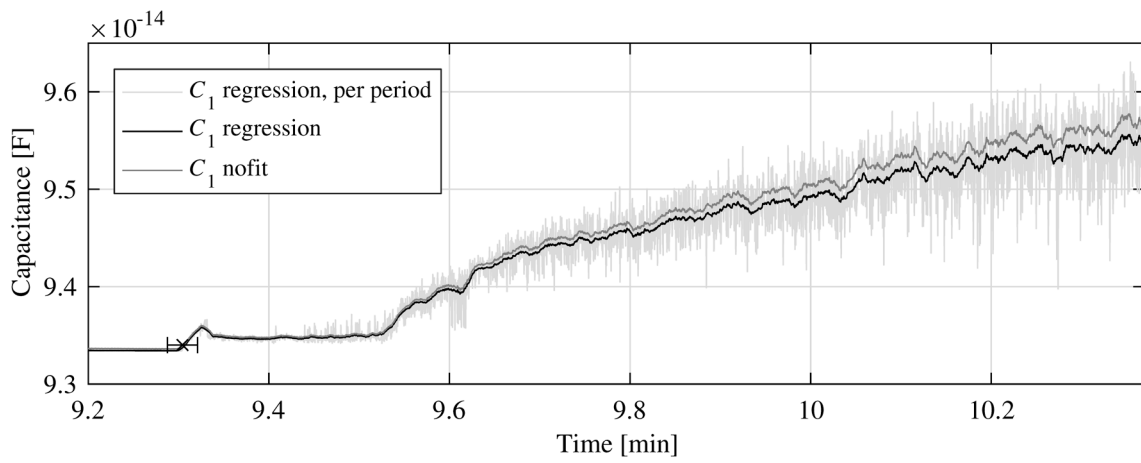
Figure 3.28: C_1 and R_1 during the third measurement.

(a) The change in C_1 during tree growth, first measurement.

Figure 3.29: Capacitance during three growth.
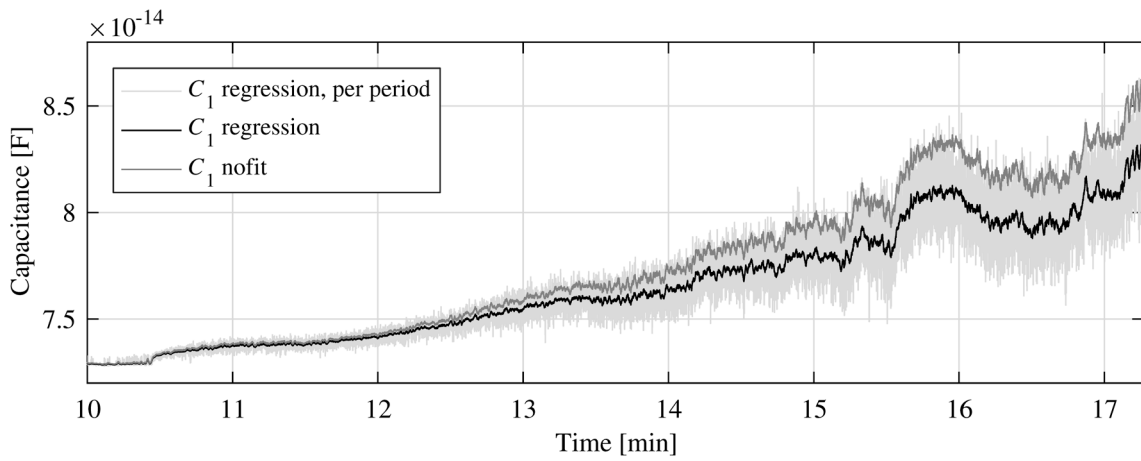
(b) The change in C_1 during tree growth, second measurement.

(c) The change in C_1 during tree growth, third measurement.

Figure 3.29: Capacitance during three growth.

Table 3.5: Different values of R_1 and C_1 based on the method of calculation.

| Method of computation	E1		E2	
	R_1 [GΩ]	C_1 [fF]	R_1 [TΩ]	C_1 [fF]
Nofit, assuming an entirely capacitive specimen	N/A	126.07	N/A	94.776
Nofit	754.43	126.01	1.6363	94.757
Trigonometric Fourier series	756.39	125.54	1.6375	94.665
Multiple regression	764.66	125.48	1.6380	94.711

3.6.3 Measurement system remarks

In Figure 3.30 two sub-figures are seen. 3.23a shows the inception event of the electrical tree in the first measurement and 3.23b shows a window in time during the growth of the same tree. The data used originate from the first measurement. These figures have the PD-quadripole output overlaid on the current waveform. In the beginning of 3.4, the synchronisation in time between the sampling of the reference impedance voltage and the sampling of the output of the quadripole was explained. In theory, the signals should be synchronized down to within a few samples. When examining the recorded waveforms, the opposite was found. A shift in time of approximately half a period was observed and a manual correction was necessary in order to match the waveforms. The on-board clocks of the sampling devices has a specified time base accuracy of ± 100 ppm and ± 50 ppm respectively, resulting in a worst case error after 1000 s of 150 ms, the observed shift in time is thus well within the specified operation conditions of the devices. The figures show the result after the correction has been made.

The PD-signals from the external PD-circuit in the figures show up as mark and a number of tightly spaced vertical lines. The mark represents the location of the major flank of the PD-signal. 100 samples before the major flank and 200 samples after are also plotted. Due the short integration time of the external PD-system in combination with its high sampling frequency, when overlaid on 7.5 periods of the current waveform, the signals appear as vertical events.

The performance of the guard circuit during a period of intensive PD-activity is shown in Figure 3.31. Output is the measured voltage from the reference impedance, or u_2. Guard is the signal that is applied to the PCB, cable and the cell. As the output signal can be considered to be identical to the signal which is the target for the guarding, the circuit can be deemed to be functioning.
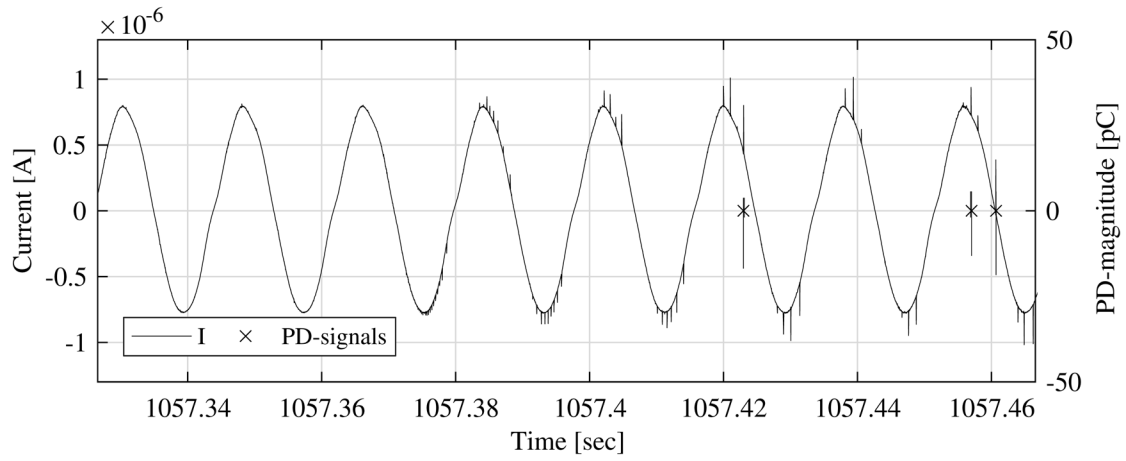
(a) Electrical tree inception of the first measurement showing both the external PD-circuit and the current.
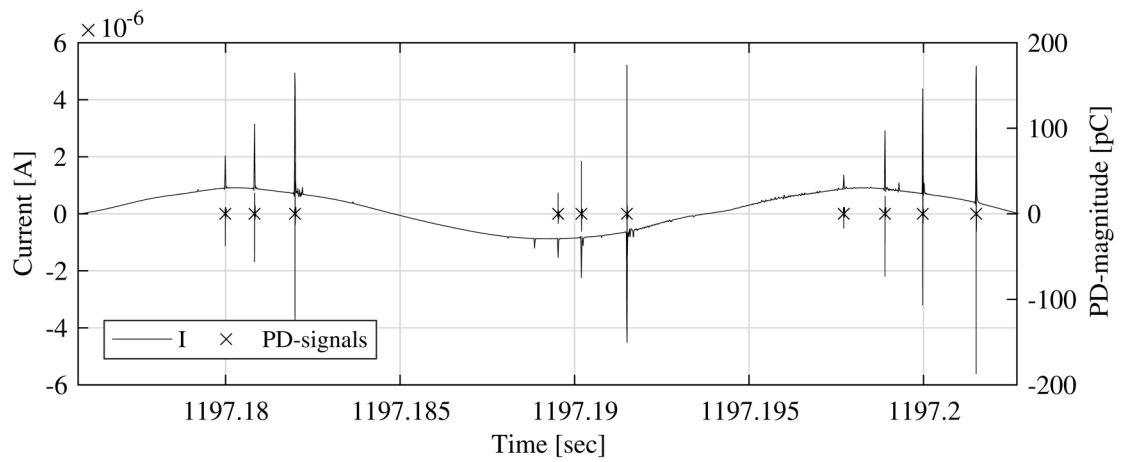
(b) Electrical tree inception of the first measurement showing both the external PD-circuit and the current.

Figure 3.30: Comparing the external quadripole PD-circuit to the current.
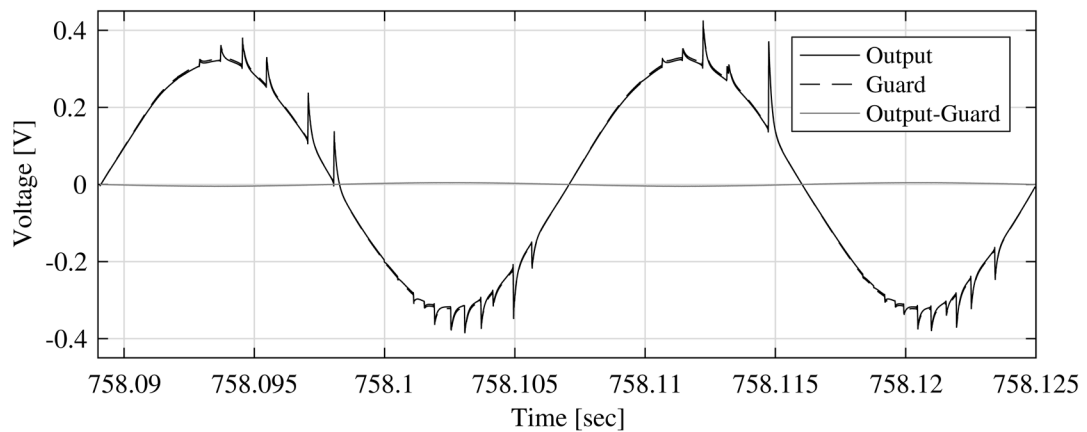

Figure 3.31: Guard performance.

3.6.4 Variations between the measurements

Another way of interpreting the measurements is to look at the waveforms of the currents, as shown in Figure 3.32. Observing the current instead of the voltage is advantageous since a small change in the derivative of the voltage waveform is more significant in the current waveform. The figures clearly suggest that the three measurements did not turn out identically. While a thorough investigation of the differences is outside of the scope of this thesis, a few comments that highlights the difference are deserved:

- The first measurement contains three anomalous events where a few cycles violently dominate the waveform and each event is similar in fashion to the others. The first one appears at the 8 minute mark, the second and third close to the 18 minute mark. The third one is shown inFigure 3.34. A fourth event is visible at a little after 14 minutes but it differs from the others having a length of only half a period.

- The first and second measurements exhibits PD-activity before the inception of an electrical tree. The first measurement has sporadic and difficult to quantify PD-activity starting at 3.8 kV_{rms}. The second measurement has a PD-inception voltage of 1.04 kV_{rms}, 5 s long PD-patterns from the inception moment, (1 m 27 s), and at 5 m and at 9 m are shown in Figure 3.33

- Activity that does not resemble the typical PD-waveform is present in the first measurement. It is barely visible in the voltage waveform, as seen in Figure 3.24b, but it becomes clear in the current waveform, as seen in Figure 3.24d.

- The third measurement shows what might best be categorised as "textbook" behaviour. It is free of any discharge behaviour up to the point of inception.

- Apart from the detailed differences, the electrical tree inception voltage varies between the measurements. While the first measurement showed an inception voltage of 12.62 kV_{rms}, the second measurement showed inception at 6.92 kV_{rms} and the third at 6.19 kV_{rms}.
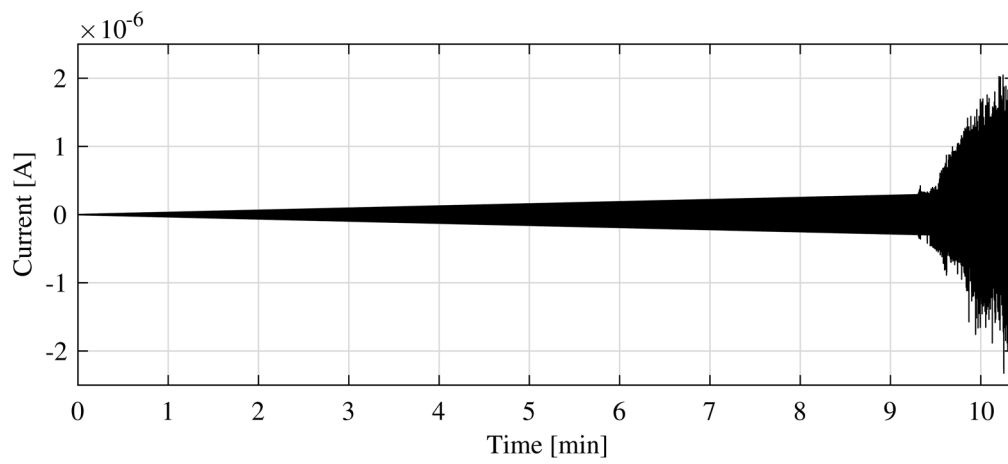
Figure 3.35 shows the PD-patterns from all three measurements during tree growth. Each measurement has three corresponding sub-figures showing 5 s long PD-patterns from the inception moment of the tree, halfway through the recording and at the end of the recording.
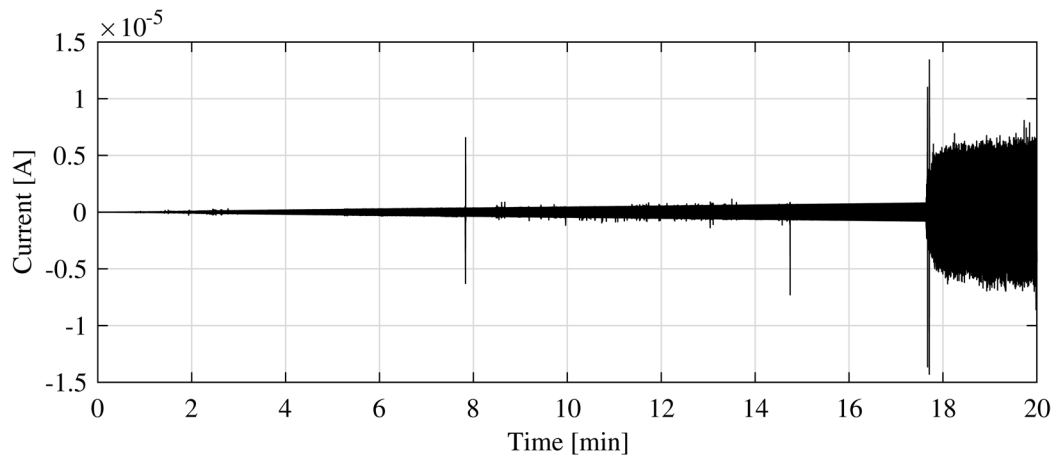
(a) Current during the first measurement.
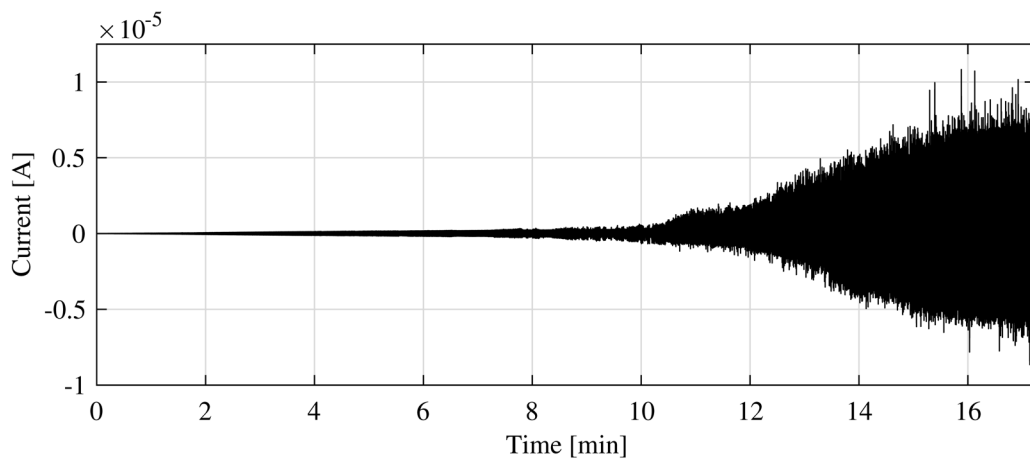
(b) Current during the second measurement.

(c) Current during the third measurement.

Figure 3.32: Current during the measurements.

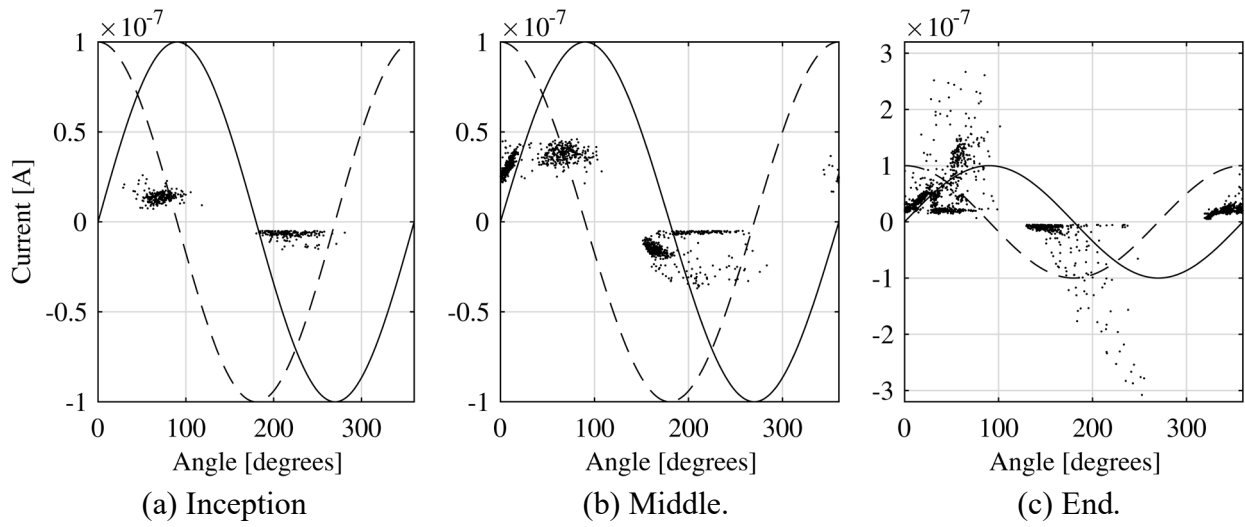(a) Inception   (b) Middle.   (c) End.

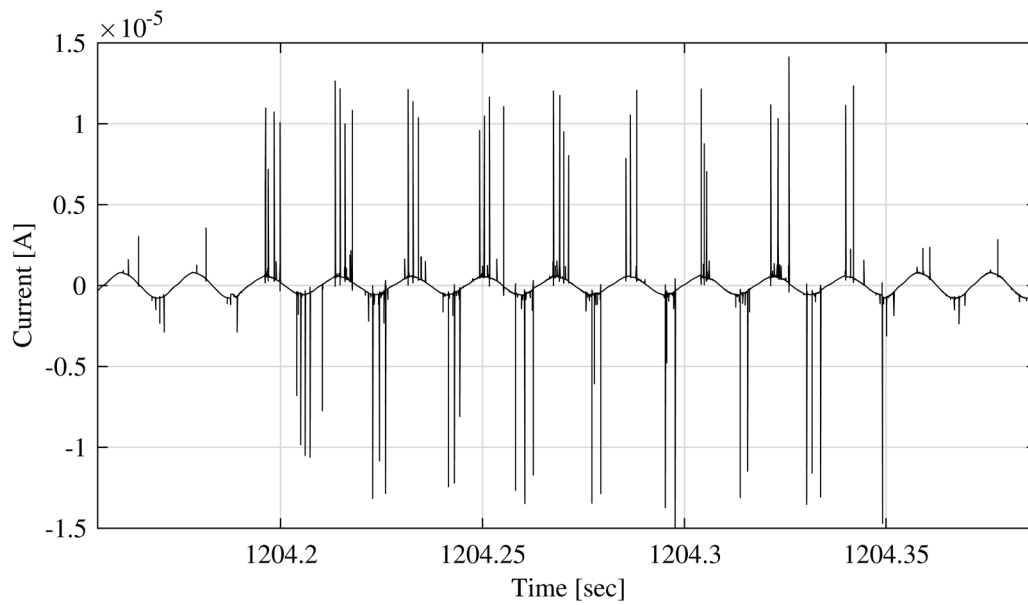Figure 3.33: PD-patterns before inception, measurement two.

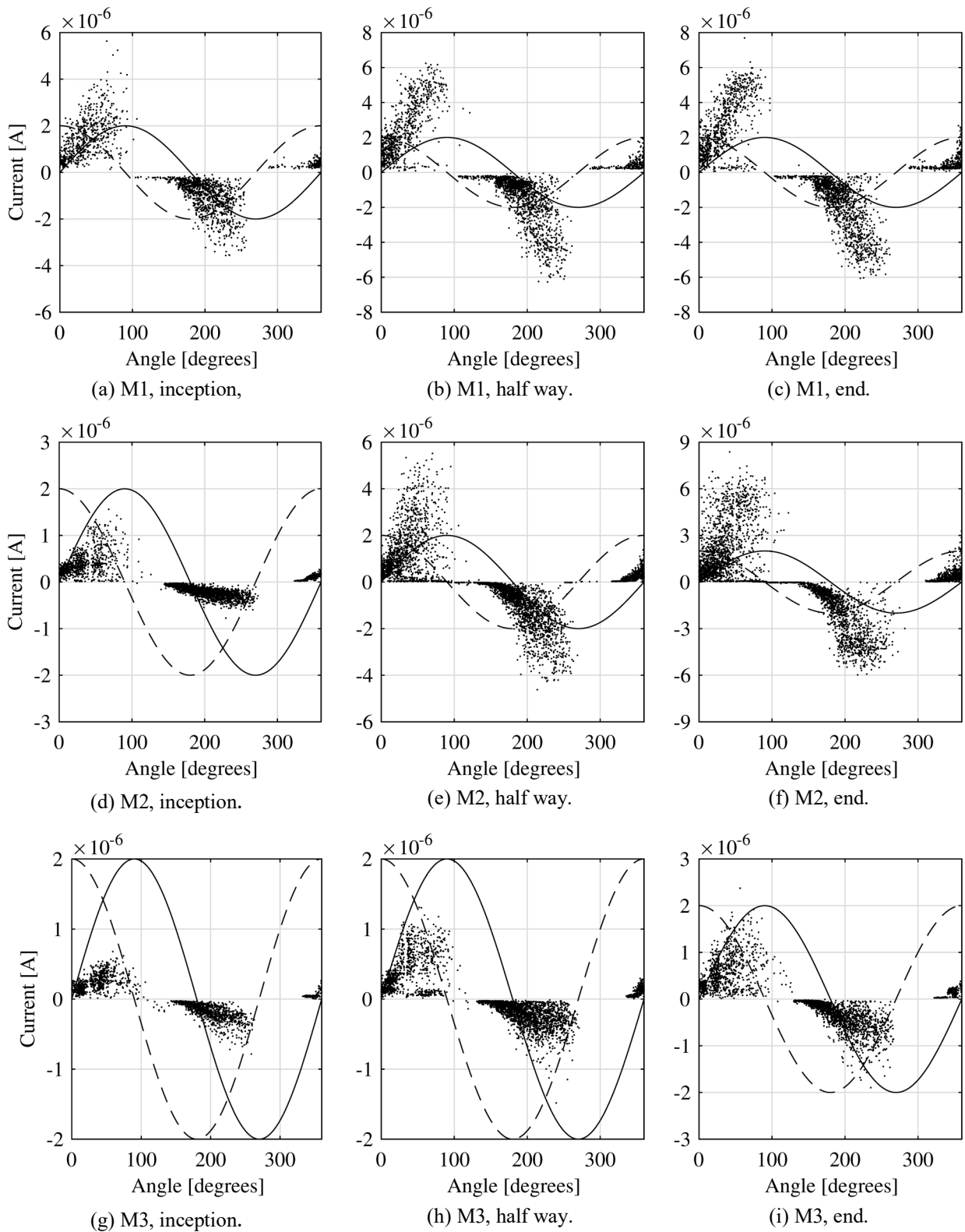Figure 3.34: The third anomalous event in the first measurement.

Figure 3.35: PD-patterns during three growth. The solid line is the voltage reference and the dotted line is the current reference.

4. Large scale validation of the effects of joint failure

4.1 Joint failure waveform

The cable systems of interest are part of two bipolar, ±300 kV, 600 MW HVDC-links. Both have experienced joint failures with one of them being having been subjected to 12 such events The specimens originates from cable samples that were left over from the installation and has thus not been exposed to service or the joint failure waveforms.

When a joint fails, the insulation in the cable is exposed to a voltage waveform which consists of a polarity reversal followed by damped oscillations until the voltage reaches zero.

The experiment is composed of two groups of 20 specimens each. They are enclosed as described in the first part of this work in order to mimic the conditions found in a cable in-service. One of the groups is exposed to a constant DC-level while the other is exposed to the same DC-level as well as a number of fault waveforms.

The fault waveform that is used is a close replication of the voltage shape that was recorded when an actual joint failed. The recording is seen in Figure 4.1. Here, three traces are visible. The voltages on both ends of the cable and a scaled representation of the voltage generated by the setup. The fault occurred relatively close to one end of the line corresponding to the trace End 1. The choice of the constant DC-voltage level in the experiment is critical for the validity of the results. However, it is not a trivial problem. It must relate the stress found in the actual cable insulation, where the geometry is usually thought of as a pair concentric cylinders, to a needle-plane type geometry, taking space-charge injection into account. In this work, it was done using a simplified calculation where the maximum electric field magnitude found at an uncommon defect in the material is matched to the maximum electric field magnitude at the needle tip. The choice of defect was inspired by the worst-case scenario found in the literature.
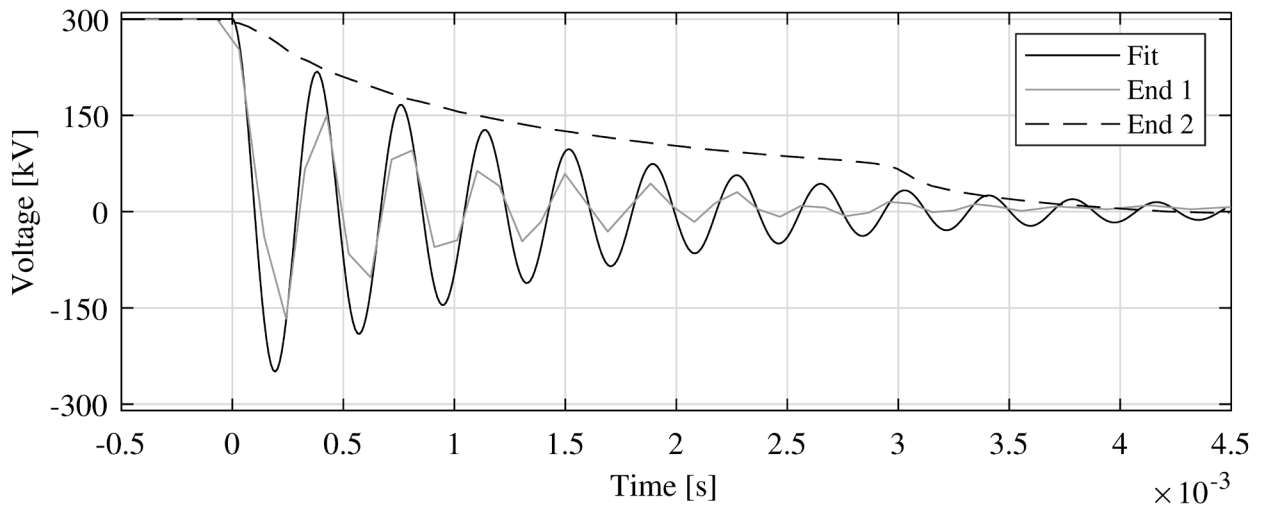
Figure 4.1 The fault waveform. The frequency of the oscillation is 2.6 kHz.

As shown in the first part of this work, a change in the specimen capacitance is an effective way of detecting the inception of an electrical tree and thus, during the experiment, the capacitance of each specimen is measured periodically and more importantly, before and after being exposed to the fault waveform. As exposure to the fault waveform alone is not enough to cause the inception of an electrical tree in the specimens. To determine if the exposure had any effect on the electrical treeing inception voltage, both groups of specimens are subjected to an experiment where a sinusoidal voltage is ramped until an electrical tree is detected. A difference in the inception voltage between the specimen groups may thus indicate whether the insulation have been affected by the exposure.

4.2   Experimental setup

Two setups were used to complete this experiment, one that exposes the specimens to a constant DC-level and the joint failure waveform and one that forces the inception of an electric tree by applying a ramped sinusoidal voltage. Only the former is described here since the latter is already explained in the earlier part of this work. The only difference between the earlier setup described and the one used here is that

- the external PD-circuit was excluded since its contribution is minor when both the optical method of inception detection and the reference impedance connected in series with the specimen is used
- the oil bath was not used, instead, the experiments were carried out with the cell in air.

The setup that exposes the specimens to the DC-level and the joint failure waveform is in principle composed of

- a high voltage part that manages DC-voltage generation, fault waveform generation and the distribution of said voltages, as well as measuring the applied voltage.
- a low voltage part that connects one of the data acquisition units to any cell of interest as well as various signal conditioning devices
- the 40 cells
- three computers that control the temperature of the reference impedance, the low-level control of the setup and the high-level control of the setup.

The entire arrangement is seen in Figure 4.2 and Figure 4.3. Some of the nomenclature introduced in these images is used and explained in subsequent sections.
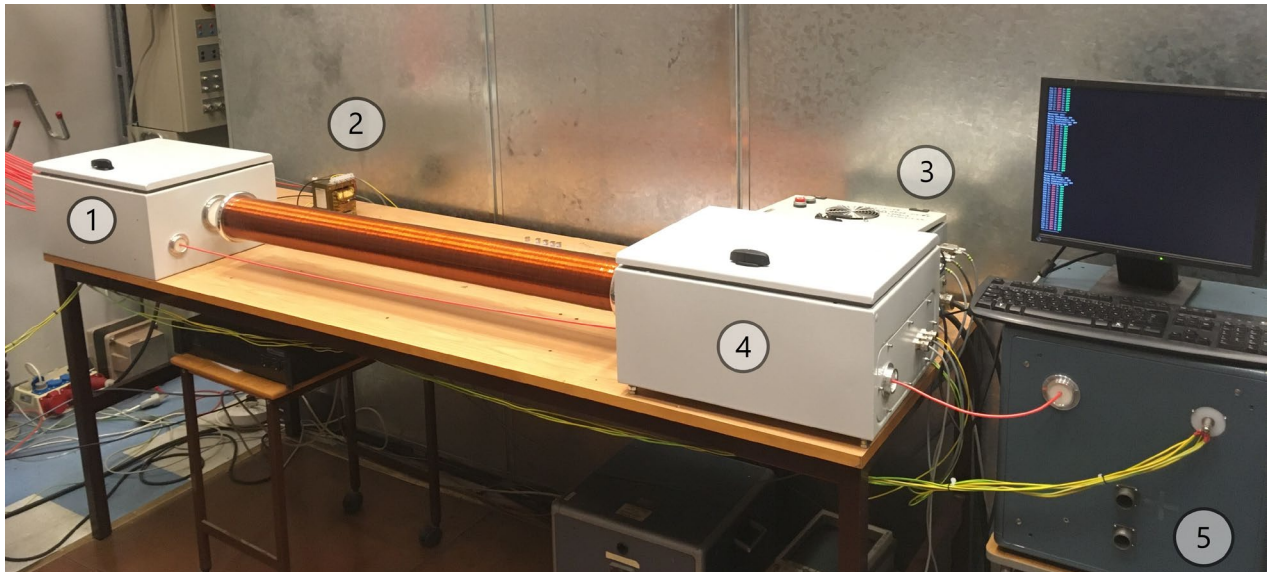
Figure 4.2. The high voltage part of the setup. 1. "Enclosure 2", 2. T_1, 3. low-level control PC, 4, "Enclosure 1", 5, high voltage transformer.
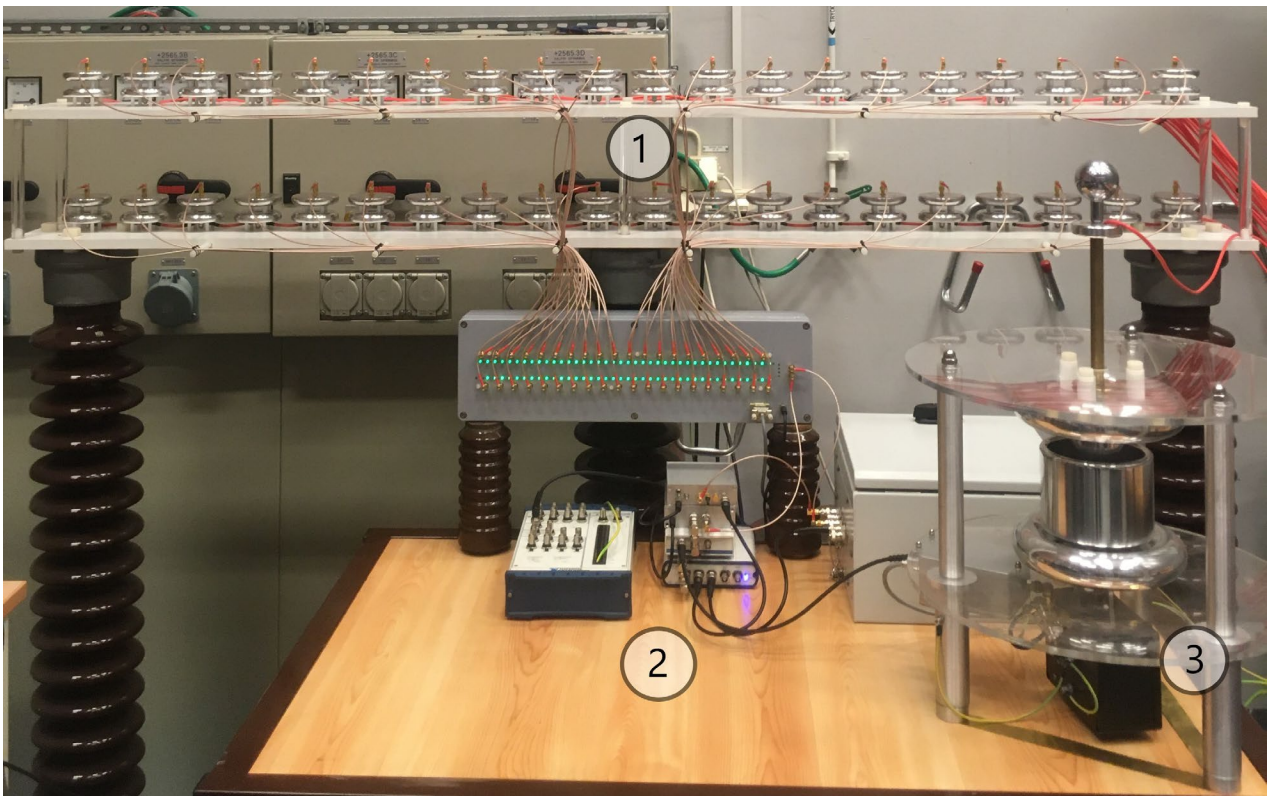

Figure 4.3. The cells (1), the voltage divider (3) and the low voltage part of the setup (2).

4.2.1 The high voltage side

A conceptual schematic of the circuit responsible for the voltage supply is seen in Figure 4.4. The figure is simplified and only shows two specimens. This part of the setup essentially has three duties: to provide a constant DC-level, the fault waveform and the means to switch the specimens between the two. An RLC-oscillator controlled by a solid-state half bridge is used to generate the waveform. In the schematic, the oscillator is represented by L_1 and C_2. The resistance comes from the on-state resistance of the semiconductors as well as the resistance of the inductor.

Time constants for both charging and discharging the circuits are introduced by R_1C_1, R_2C_2, R_3 and R_4+R_5. They work in conjunction to prevent the undefined condition that the specimens would enter following a power outage. Via the transformer T_1 and the coupling capacitor C_5 it is possible to superimpose a sinusoidal voltage on either circuit allowing for capacitance to be measured.

In the schematic, two specimens are visible. One of which is subjected to a constant DC-level and one which is exposed to both a constant DC-level and the fault waveform. The latter is connected to two voltage sources, the first being a constant DC-voltage, the other being the output of the oscillator. High voltage relays, SW3 and SW4 in the schematic, are used to move the specimens between the two circuits.

The relays operate on the make-before-break principle. A specimen that is going to be exposed to the fault waveform is moved from the constant supply to the already energised RLC-circuit, subjecting it to a trivial change in voltage. The capacitance of the specimen is measured, the oscillator is activated and afterwards, the capacitance is measured again and the specimen is brought back up to the constant DC-level via charging of R_2C_2 and moved back to the constant circuit. The waveform of the current during the waveform exposure is recorded and saved.

Control of the high voltage part of the setup is facilitated by a PC that controls the low voltage measurement side, the high voltage control relays, SW1-SW4 in the figure, and high voltage relays responsible for which circuit the specimen is connected to, SW-C-1 and SW-O-1 in the figure. The PC is operating behind a battery backup, maintaining the states of the relays of the setup in case of a power outage. SW4, which all of the specimens connected to the constant circuit is located behind, is there to ensure repeatability in case the battery backup fails.
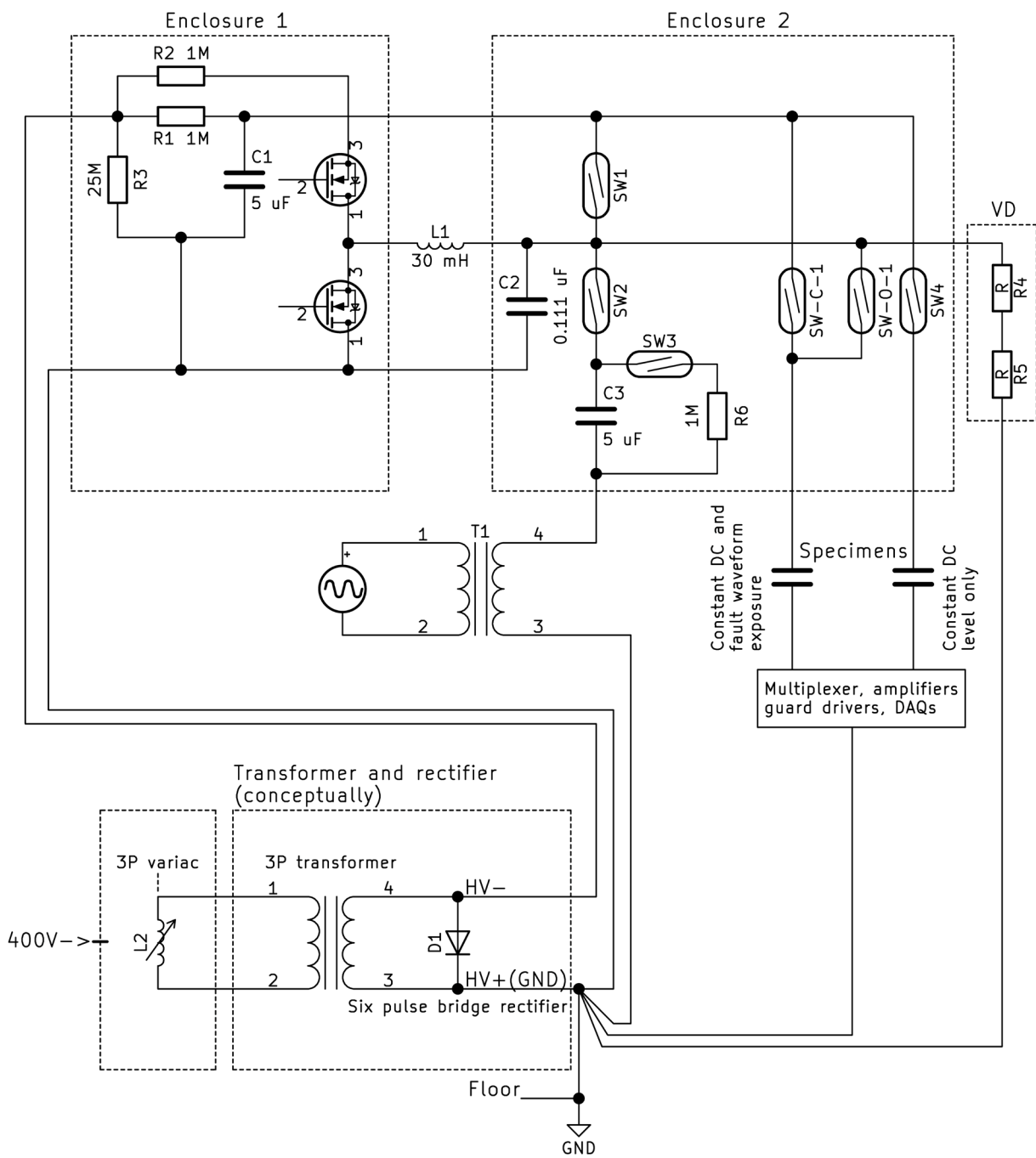
Figure 4.4. Conceptual schematic of the high voltage side of the experimental setup showing two specimens.

4.2.2 The enclosures

The two cabinets referred to as Enclosure 1 and Enclosure 2 contain the equipment for waveform generation and voltage distribution. The inside of the two are shown in Figure 4.6 and Figure 4.7. The former holds the switch, the switch controller and a high voltage module which scehamtic is seen in Figure 4.4. A full schematic of the switch controller is seen in Appendix A.4

The second enclosure houses 40 high voltage relays, separated into four modules. It also contains a module that contains the control relays SW1-SW4 and the rest of the passive components from Figure 4.4 as well as a relay controller. A full schematic of the controller is seen in Appendix A.5 and A.6.

The high voltage modules that the components reside in are made of acrylic glass and potted with the encapsulation compound QSIL-216, a silicon rubber that has a nominal dielectric strength of 20 kV/mm. The components need to be joined and in order to achieve a controllable electric field distribution this was done by soldering and 1 mm copper wire. This is illustrated in Figure 4.5.
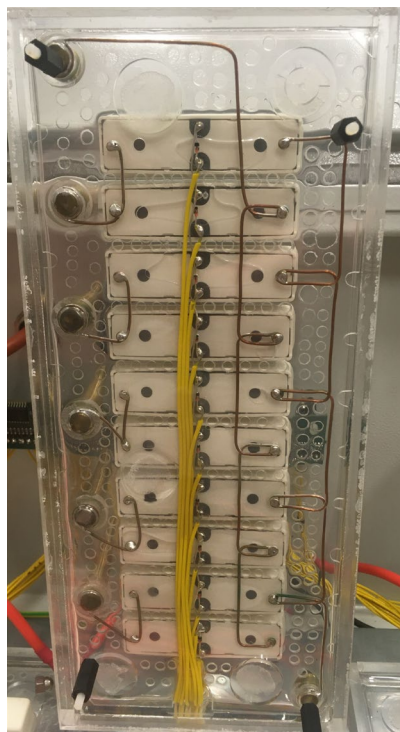

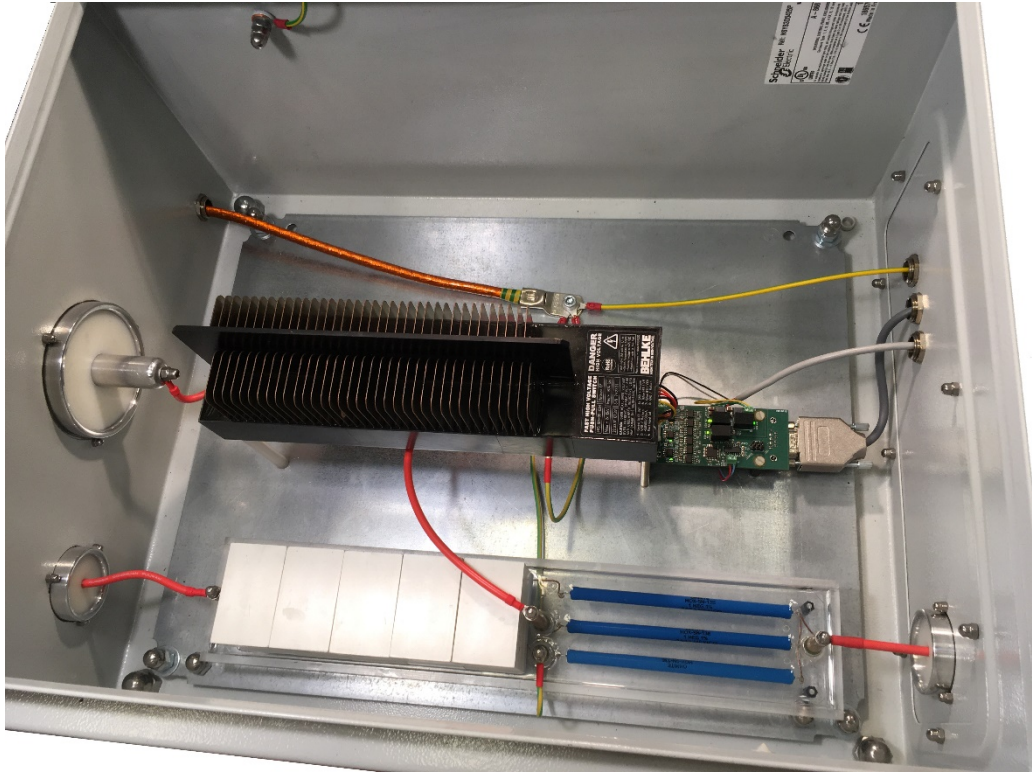Figure 4.5. The wiring of the high voltage modules.

Figure 4.6. Enclosure 1.

Figure 4.7. Enclosure 2.

4.2.3 The low voltage side

The low voltage and measurement side of the setup consists of six different devices. An overview is shown in Figure 4.8. The specimens are connected to a multiplexer that provides each specimen with four relays. These facilitate the control of both the signal and shield of the incoming coaxial cable. The signal part, which is in contact with the semiconductor of the specimen, can be connected to a common measurement signal path which can then be further connected to one of two measurement circuits. One measures the capacitance of the specimen and the other records the current through the specimen during the fault waveform exposure. The multiplexer also connects the guard of the cable and cell to either ground or a common guard signal path. The guard is driven by circuits purposed for either measurement. By intent, only the cell that is undergoing a measurement is driven actively since driving them all simultaneously would introduce a large capacitive load on the driving circuitry.

Both measurements operate on the principle where the voltage over a series connected RC-parallel is measured. In the case with a superimposed sinusoidal voltage, the capacitance is calculated. In the waveform capture case, the voltage waveform developed over the input impedance of the data acquisition card is saved and the current is calculated. It is then inspected for PD-activity.

For the capacitance measurement, the temperature stabilised reference impedance developed earlier is used. Since the voltage developed over it is relatively small in this experiment, it is connected to a linear amplifier before being measured at 102.4 kHz, 24-bits. For the waveform capture, the input impedance of a data the fault waveform exposure, the time constant that is formed by the input impedance in combination with the sampling speed matters. Since the parasitic contribution from the connecting cables, the multiplexer and the cell itself would increase the time constant beyond what is acceptable, an active guard driver is connected at the input of the data acquisition card.

4.2.4 The devices of the low voltage side

The low voltage side in the setup is shown in Figure 4.9 and 4.10 while the conceptual design is seen in Figure 4.8. The multiplexer is essentially 40 instances of an SMA connector connected to four reed relays, type HE3621A0510. Two for the signal and two for the guard, allowing for make-before-break operations. The 160 relays are controlled by IO-expanders operated via SPI from
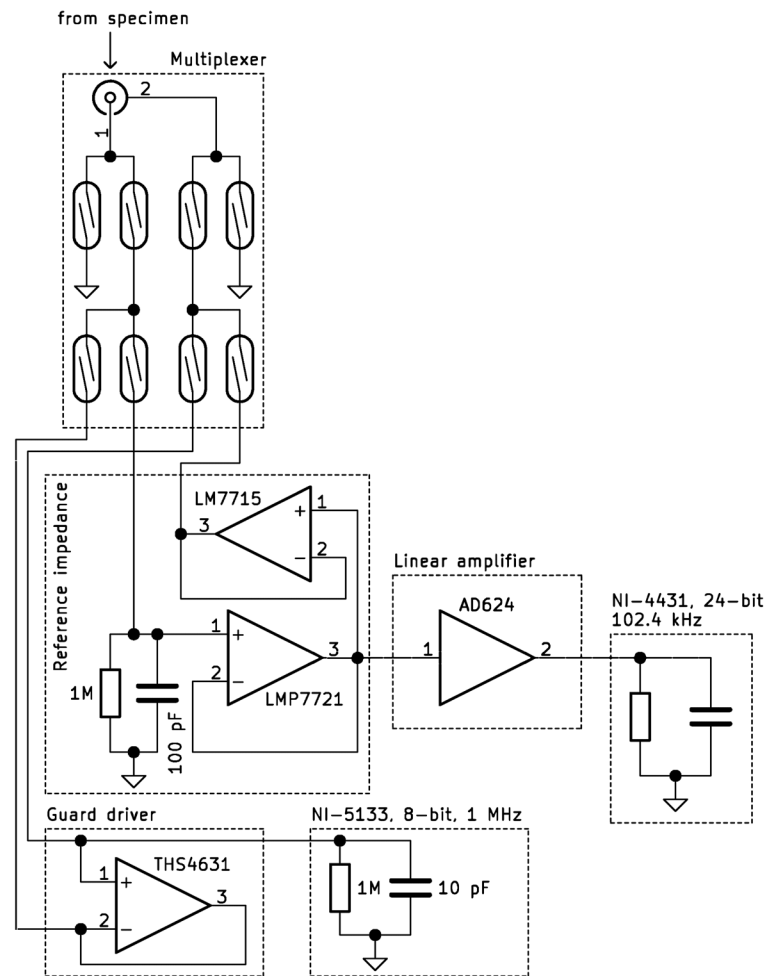
Figure 4.8. The low voltage and measurement side of the experiment.

microcontroller that accepts instructions via a serial interface. A full schematic of the multiplexer is available in Appendix A.7 and A.8.

The amplifier is not temperature controlled. Instead, care was taken during component selection not to introduce any detrimental temperature dependencies. The amplifier is designed around the AD624A, a low noise (~0.2 μV p-p, high gain accuracy (±0.5 % at G500), low gain temperature coefficient (25 ppm/°C), and high linearity (±0.005 % at G500) instrumentation amplifier. The input and output voltage offset dependence on temperature is 2 μV p-p and 50 μV p-p respectively. Both input and offset nulling trimming potentiometers are installed, here the dimensioning factor was temperature stability and a pair of Accutrim 1240 Bulk metal foil trimming potentiometers from Vishay with a temperature coefficient of resistance of ± 10 ppm/°C was fitted. A number of reed
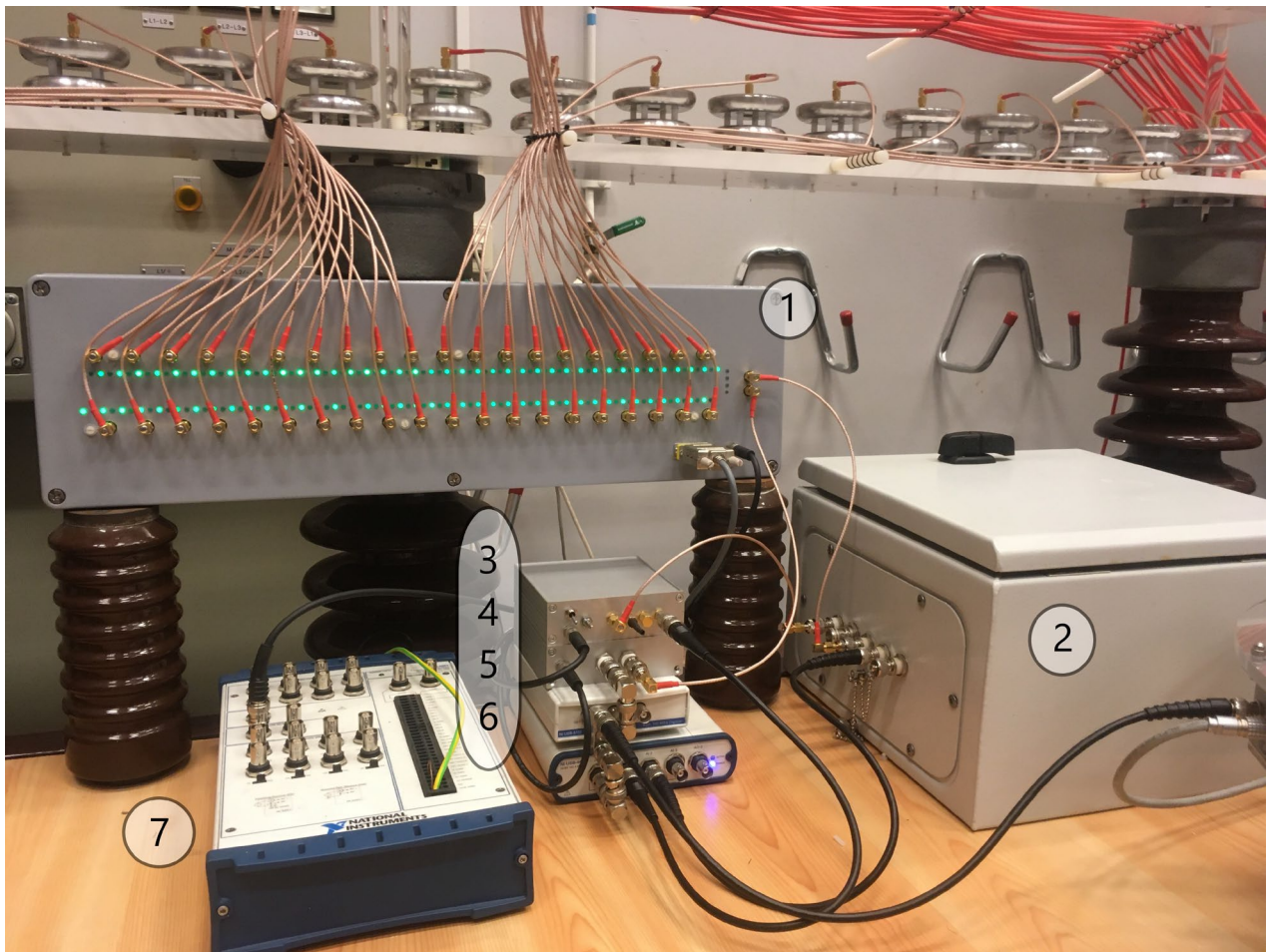
Figure 4.9. The low voltage side of the setup: 1. Multiplexer, 2. Reference impedance, 3. Guard driver, 4. Amplifier, 5. NI-5133, 6. NI-4431, 7. NI-6153
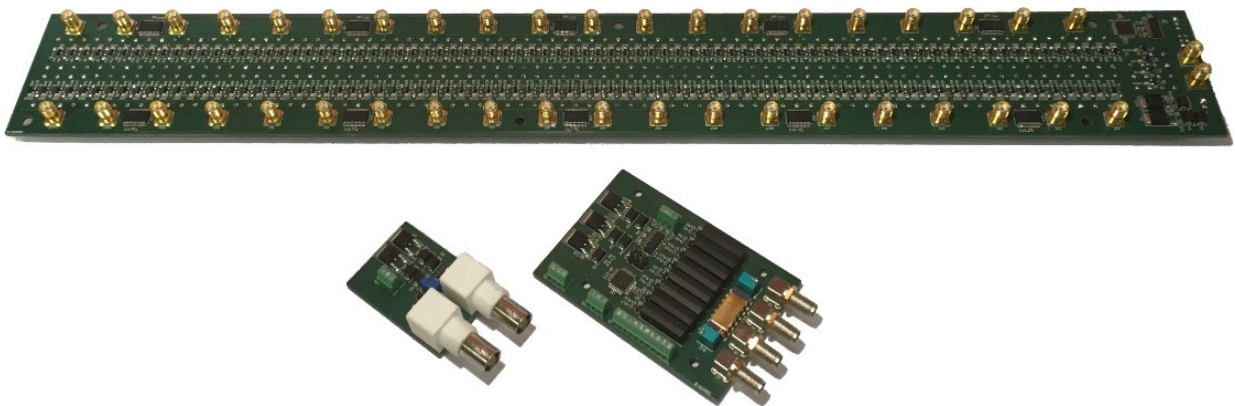

Figure 4.10. The unhoused devices developed. 1. Multiplexer, 2. Guard driver, 3. Amplifier.

relays are used to manipulate the gain of the device by altering the interconnection of the device's internal gain resistors. Gains between 1 and 1000 can be set by either a knob on the front of the device or by a serial interface. A full schematic is available in Appendix A.9.

The guard driver device can be thought of as two BNC connectors connected back-to-back, but where the shield of the second connector is driven to the potential of the signal connector. This is achieved by a THS4631D operating in unity gain configuration. A schematic is available in Appendix A.10.

4.3   Specimens and cells

The needle injections were carried out using a single injection setup and thus, there is non-marginal time between the first and the last specimen injected. Further, the specimens were stored before being put into the capsule. In order to be able to rule out, or confirm, any discrepancies in the results that stem from how the specimens were handled the details of the entire process from taking the specimens from the cable to sealing them in the capsules are given here.

The process of manufacturing a specimen begins by sawing a cross-section of the cable, using various tools with the last one being two parallel guillotine knives separated by slightly less than ten mm, a cuboid specimen with a total length of 17 mm and ~ 1 mm of semiconductor is the result. When finished, each specimen was wrapped in metallic foil. The specimens were handled using gloves. In total the time that they spent in air was less than one hour.

40 specimens were injected with a needle using a modified temperature curve, seen in Figure 4.11, as compared to the one seen in Figure 3.5. Specifically:

- The injection temperature was reduced from 130 to 120 degrees.
- The time spent waiting to allow the temperature of the cell and specimen to equalise before the needle starts to be lowered was reduced.
- Annealing time was changed to 15 minutes.
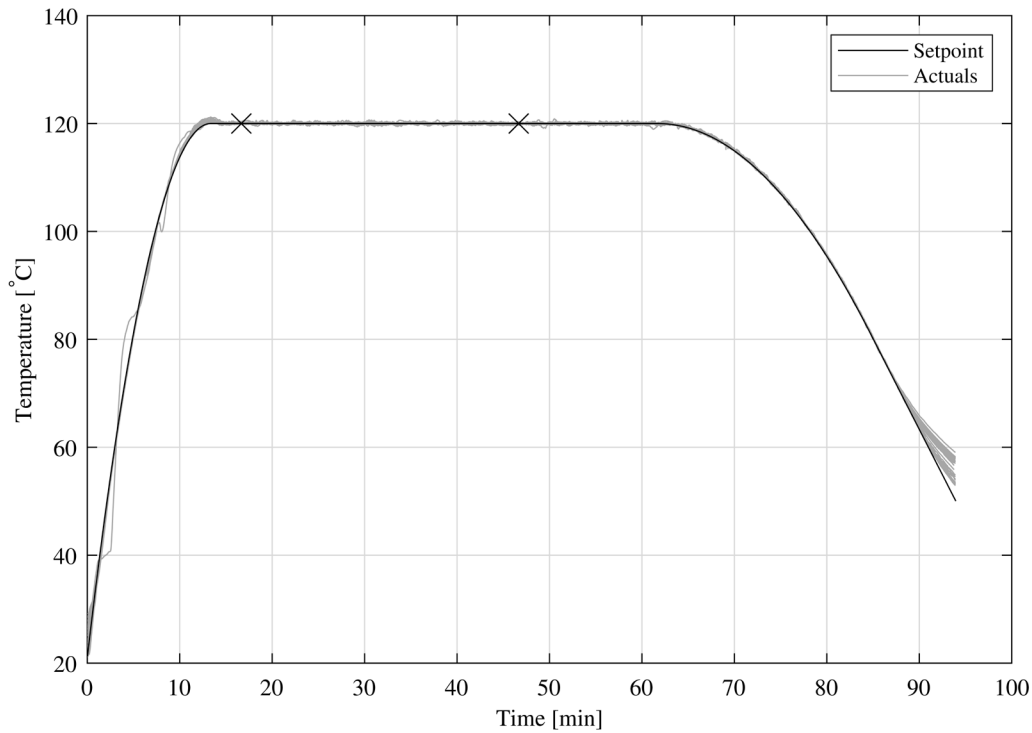- The needle insertion rate was 0.4 mm/min.

Figure 4.11. The injection cell temperature curve as well as the temperature curves from 40 injections. The first mark indicates when the needle enters the polymer, the second when it has reached its final depth.

The needles have a tip diameter of 5 ± 0.5 µm and are placed 4 mm from the semiconductor. Before insertion, they were ultrasonically cleaned in isopropanol and dried. After the injection process the specimens were packed in foil awaiting the final encapsulation.

Figure 4.12 shows the specimens during the assembly process and Figure 4.13 shows the finalised capsules. The figures show an updated version of the design from Figure 3.2 that occupies a smaller space and requires less material.
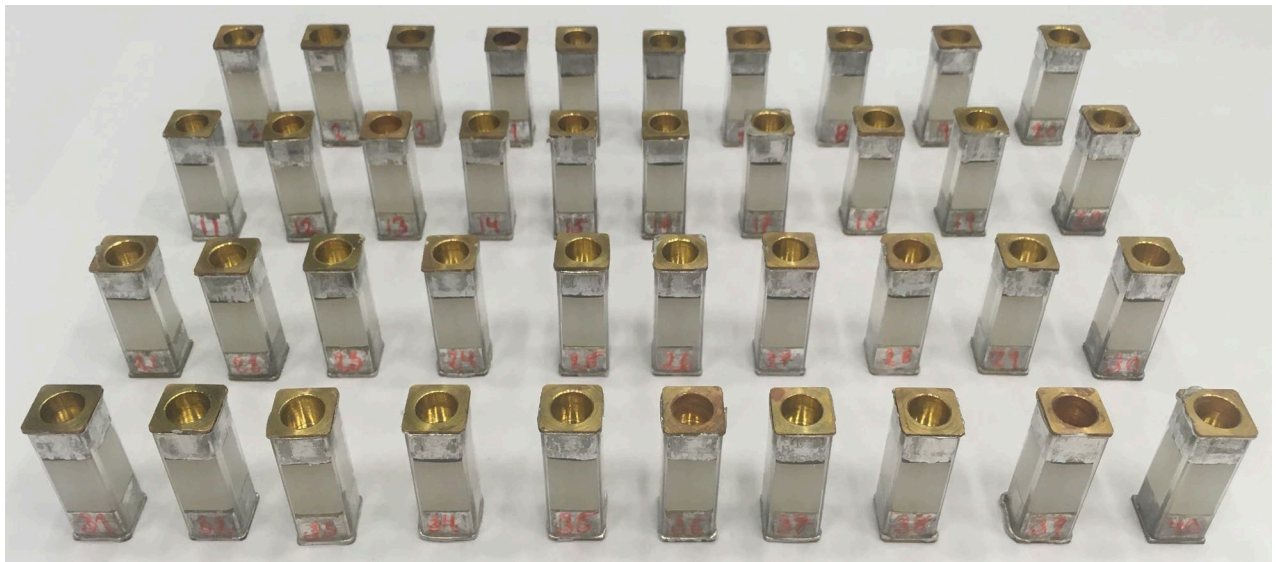
Figure 4.12. Specimens being assembled.

Figure 4.13. The finished specimens.

The cell received a minor iteration in its design in order to reduce the manufacturing time and to allow the electrical treeing experiments with a ramped sinusoidal voltage to be carried out without the use of oil. An exploded drawing of the modified cell and the specimen is seen in Figure 4.14. A transparent cross-section and the real view of the cell are shown in Figure 4.15 and Figure 4.16.
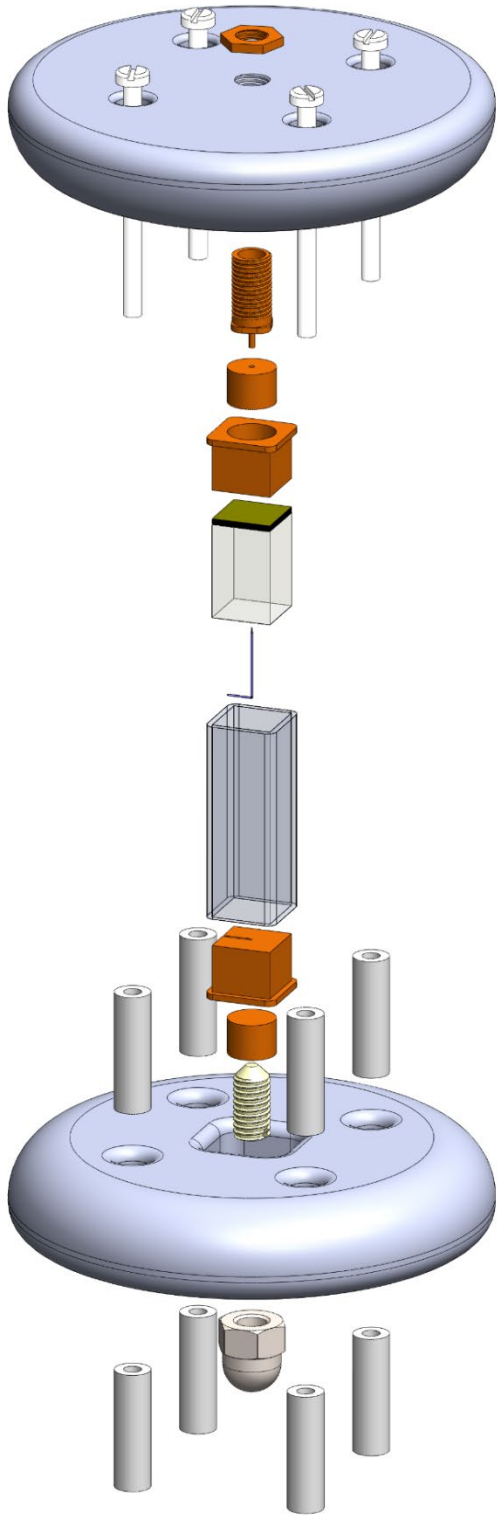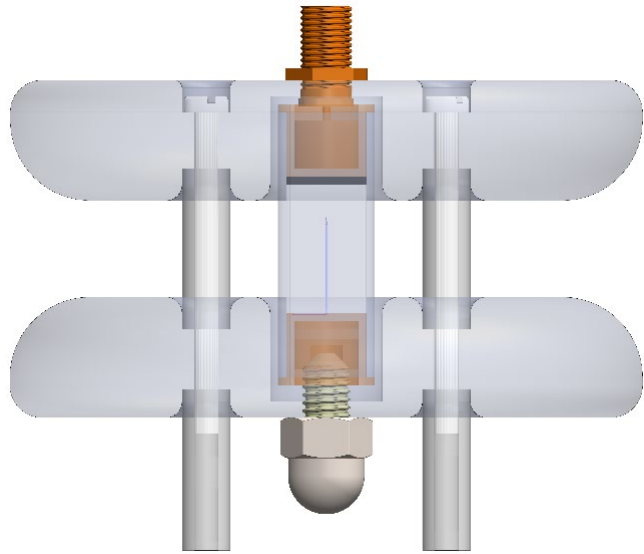
Figure 4.15 A transparent cross-section of the cell.

Figure 4.16 The actual cell.

Figure 4.14 Exploded view of the cell.
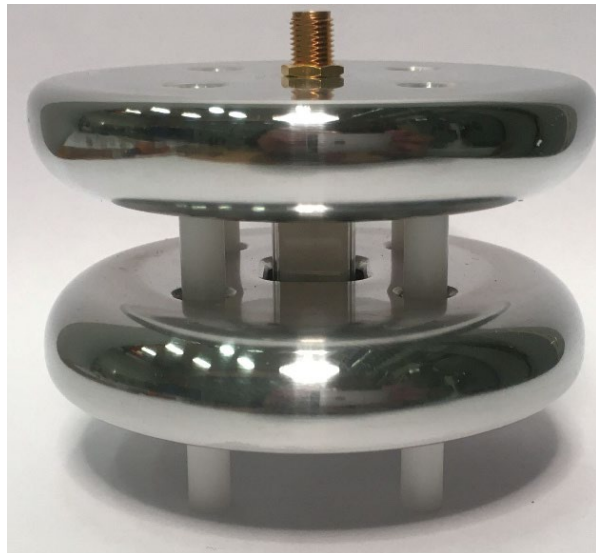
4.4 Parameters of the experiment

The DC-level of the experiment can be considered the most important parameter of this experiment. It decides the electric field distribution as well as the space charge concentration in between the needle tip and the planar electrode. The thought behind the choice of DC-voltage in this experiment is that it should give rise to an electric field magnitude around the tip of the needle that is comparable to the electric field magnitude surrounding an uncommon, but not impossible, defect in the cable. Other parameters are the temperature, the polarity of the defect, the total time and the amount of joint failure waveforms that the specimens are exposed to. This part goes through these parameters in the above order and presents the decisions that were made.

The DC-voltage

Given the range of available defects, a foreign contaminant in the form of a metallic inclusion is used as the template defect as it presents the worst-case scenario [23,24].

Investigations into actual XLPE insulated cables found that 10 % of contaminants are metallic. The shape of a natural inclusion is not well defined, but it can be systematically classified by curve fitting an ellipse onto the shape of the inclusion. By using the ellipse which fits best between the two sharpest points that are separated by the largest distance, the aspect ratio[1] of the inclusions are found to be between 0.07 and 0.7 [23]. Regarding the actual size of the inclusion, a commonly found value of the maximum allowable size of an inclusion for EHV cables is 70 μm [23,25].

The constant DC-level is found by calculating the voltage needed for the maximum Laplacian electric field strength around the tip of the needle to equal the maximum electric field strength around the template defect.

Given that the needle and defect are (i) on the same geometric scale and (ii) have similar work functions both the defect and the needle will inject a comparable amount of space charge and the resulting Poissonian electric field distribution will be of similar magnitude.

---

[1]The aspect ratio is defined as the tip radius divided by half of the length of the ellipse.

74

Calculating the maximum electric field using the method found in [23] with an aspect ratio of 0.07 and with a background field equal to that found around the inner conductor of the cable in question yields 264 kV/mm. An almost identical result is found in a simple Comsol simulation where the defect was modelled using a rotational symmetry in between two parallels separated by the distance in between the semiconductors of the actual cable. To worsen the case, the model was altered to have the defect in contact with one of the semiconductors and aligned in the direction of the electric field. This resulted in the electrical field strength increasing to 434 kV/mm. Solving the model for the needle instead finds that 3 kV is required to achieve the same electrical field strength.

Temperature

The experiment is conducted in room temperature, but the properties of XLPE has a temperature dependence that in turn stems from the temperature dependence of the cross-linking by-products stress relaxation effects [28].

In electrical treeing experiments where a static sinusoidal voltage is used, the inception time has been shown to decrease significantly when the temperature is raised from 25 to 90 °C. This effect decreases with higher excitation voltages [22].

In experiments where the excitation voltage is ramped, for defects in the range of 5 to 20 μm, the inception voltage for electrical trees is decreased by 15 – 30 % when the temperature is raised from 20 to 90 °C. For impulse voltages, the inception voltage is lowered by 66 % when the temperature is raised from 20 to 90 °C [29]. The maximum operating temperature of the cables in this study is 70 °C. In order to take this into account, the excitation voltage is rounded upwards to 5 kV.

Polarity

The polarity of the needle is negative. This is because a defect of negative polarity is more vulnerable to the inception of an electrical tree than a positive one [26, 27].

4.5   Results

The capacitance of the specimens should be measured using a sinusoidal voltage with a relatively small amplitude. From Figures 3.27a and 3.28a it is evident that the calculation methods used needs a substantial voltage before they converge. Magnitude wise, the voltage needed for these methods to converge is not suitable to use when measuring capacitance.

By using the jw-approach described in 3.6.2.1, with the addition that both the output from the voltage divider and the reference impedance fitted to the second order trigonometric Fourier series, the curve that is seen in Figure 4.17 was produced.
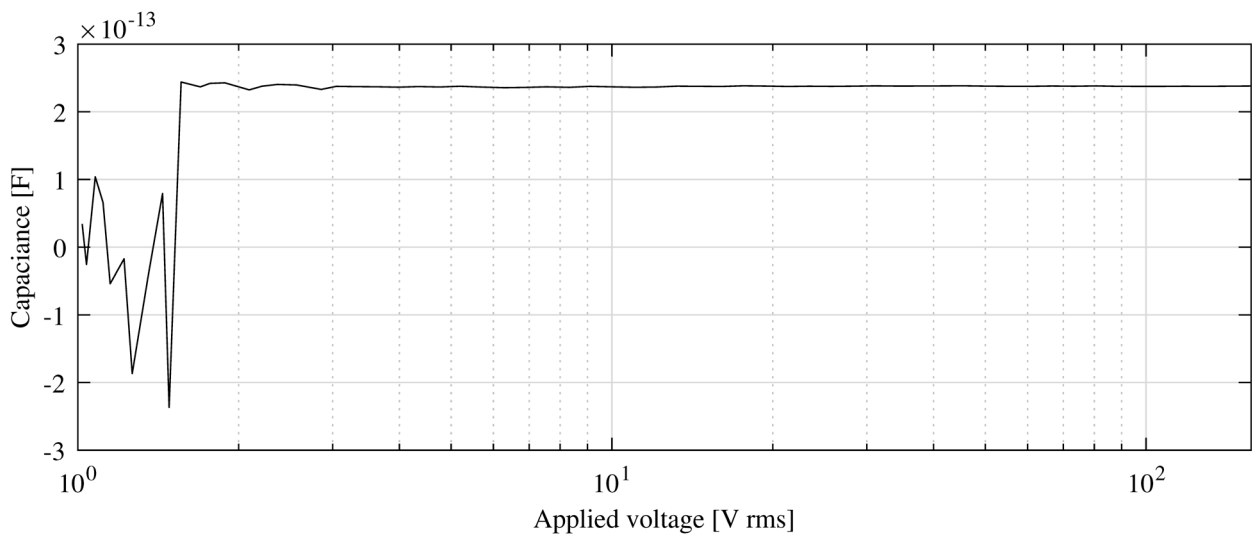

Figure 4.17. Voltage bias in the capacitance measurement.

Here, it is seen that the measurement system converges on a capacitance value for applied voltages above 2 V rms. It is worth noting that the signals measured are relatively small, the output from the reference impedance is in the range of single digit millivolts while they are in the range of tens of millivolts form the voltage divider. The trigonometric Fourier series fit of both helped to reduce noise.

The difference from the 'nofit' results in Figures 3.27a and 3.28b is that here, the specimen is modelled as an RC-parallel instead of a pure capacitance. The same behaviour could be reproduced by treating the specimen in the impedance calculations as a strictly capacitive.

All further capacitance measurements that are presented were done at 38 V rms, 51.2 Hz using 500 periods of data. An increased signal-to-noise ratio was the motivating factor behind using a much

76

larger voltage than 2 V rms as it produces more stable measurement values.

In order to check the stability of the entire setup, the capacitance of each specimen was measured 64 times over a 12-hour period. The results are seen in Figure 4.18. The maximum deviation was 6.5 fF, the minimum 0.25 fF and the average 0.57 fF.
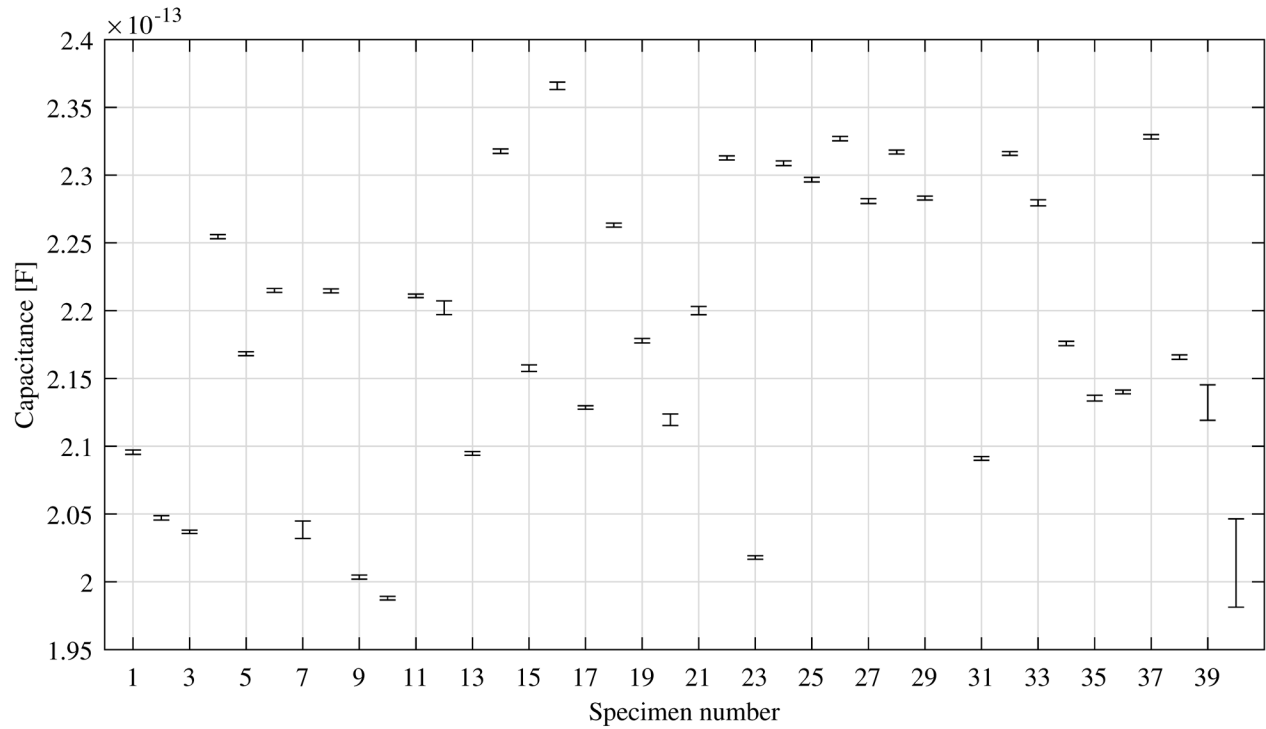

Figure 4.18. Capacitance variation of each specimen over a 12-hour period.

The setup was thereafter energised and specimens exposed to -5 kV DC for one hour. The capacitance values before the voltage was turned on and one hour afterwards is shown in Figure 4.19. If space charge injection from the needle takes place, any change that is observed in the sample capacitance should be of an increasing nature. Introducing additional charge to the dielectric means that there is now more to polarize than before. However, a clear change, be it decreased or increased, cannot be seen in the measured data. There is a vague tendency of a decrease, but most are within the error margin.
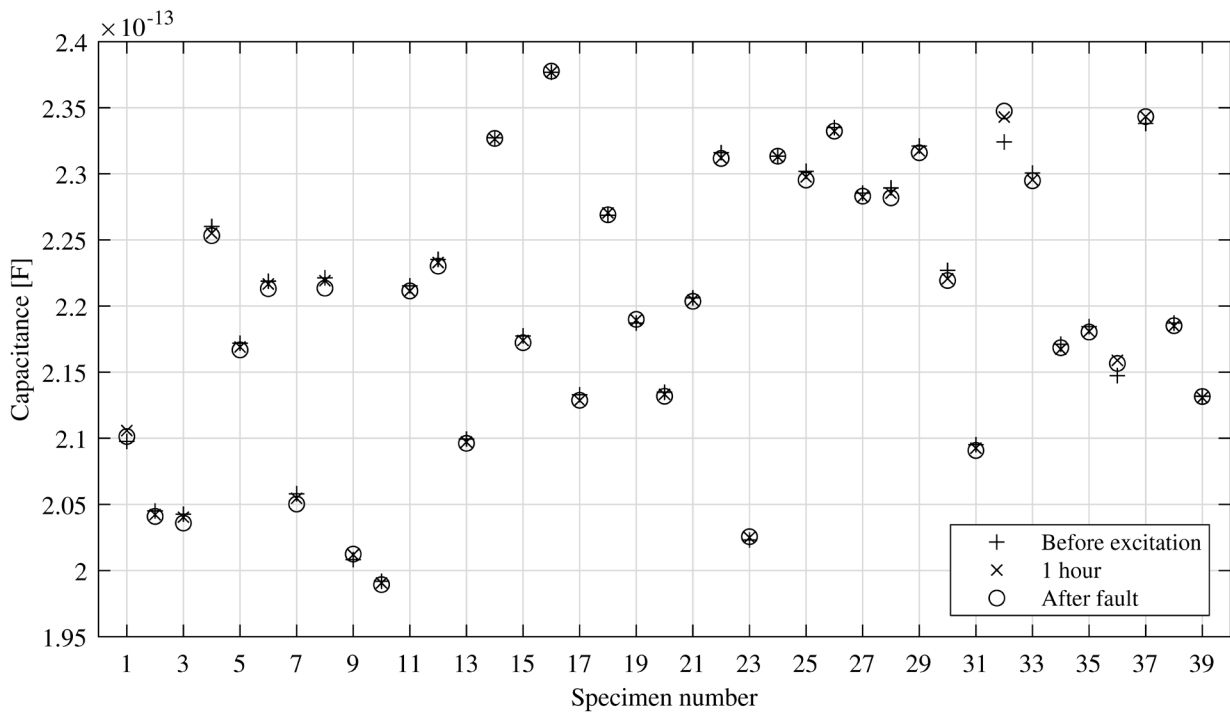
Figure 4.19. Capacitance before and after -5 kV excitation as well as after the fault.

At this point in time, specimens #1 – #20 were intended to be exposed to the short circuit waveforms. Instead, a fault in the high-voltage half-bridge caused the device to stop conducting. The main circuit of the oscillator was interrupted and the energy stored by the inductor was forced to dissipate elsewhere, causing an overvoltage. Figure 4.20 shows the erroneous waveform.
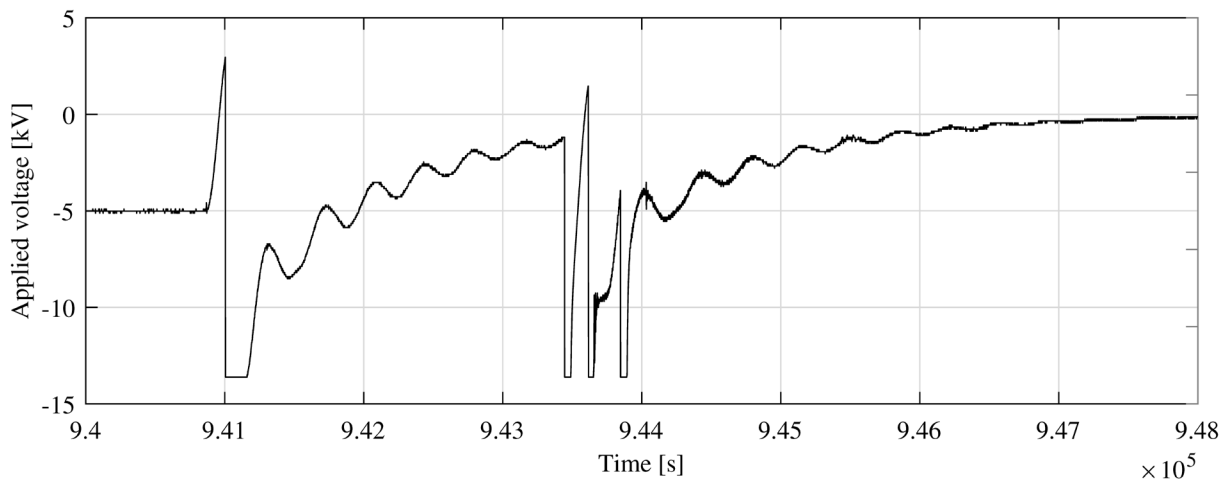

Figure 4.20. The waveform caused by the fault.

At the time of the fault, only specimen #1 was connected to the output of the oscillator. It remains a possibility that the 19 other relays connecting the specimens to the oscillator had an internal

78

flashover, but there is no evidence of this occurring and the devices are still functional. The capacitance of all the specimens was measured after the fault and the result is shown in Figure 4.19. No apparent change can also be discerned due to the fault.

In the following, the specimens were subjected to one hour of pre-stress at –5 kV DC and then 24 waveform exposures spread out over an hour. The excitation waveform is seen in Figure 4.21. and the capacitance of the specimens before and after the exposures is shown in Figure 4.22. In Figure 4.21 the specimen response is also seen.
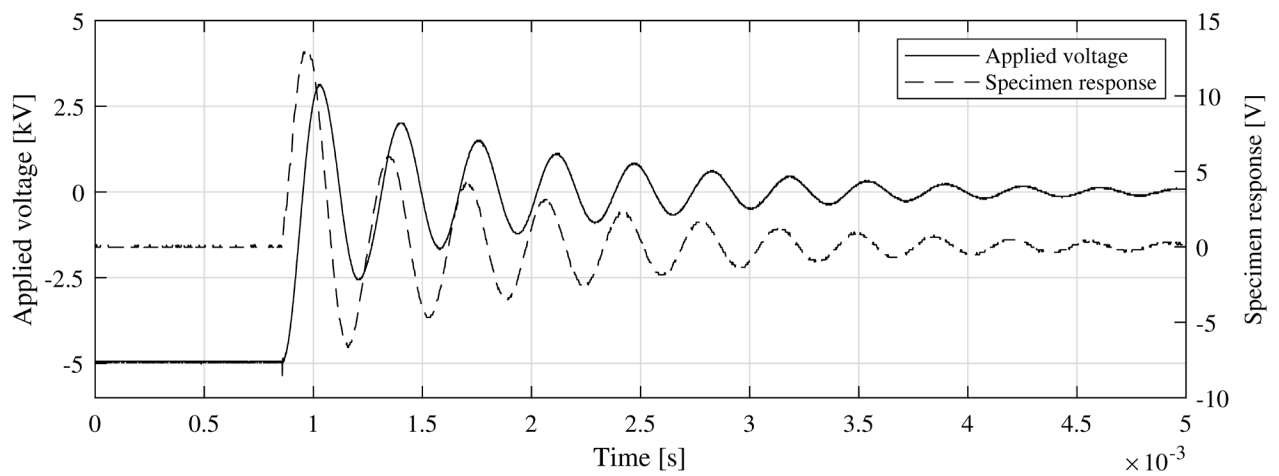

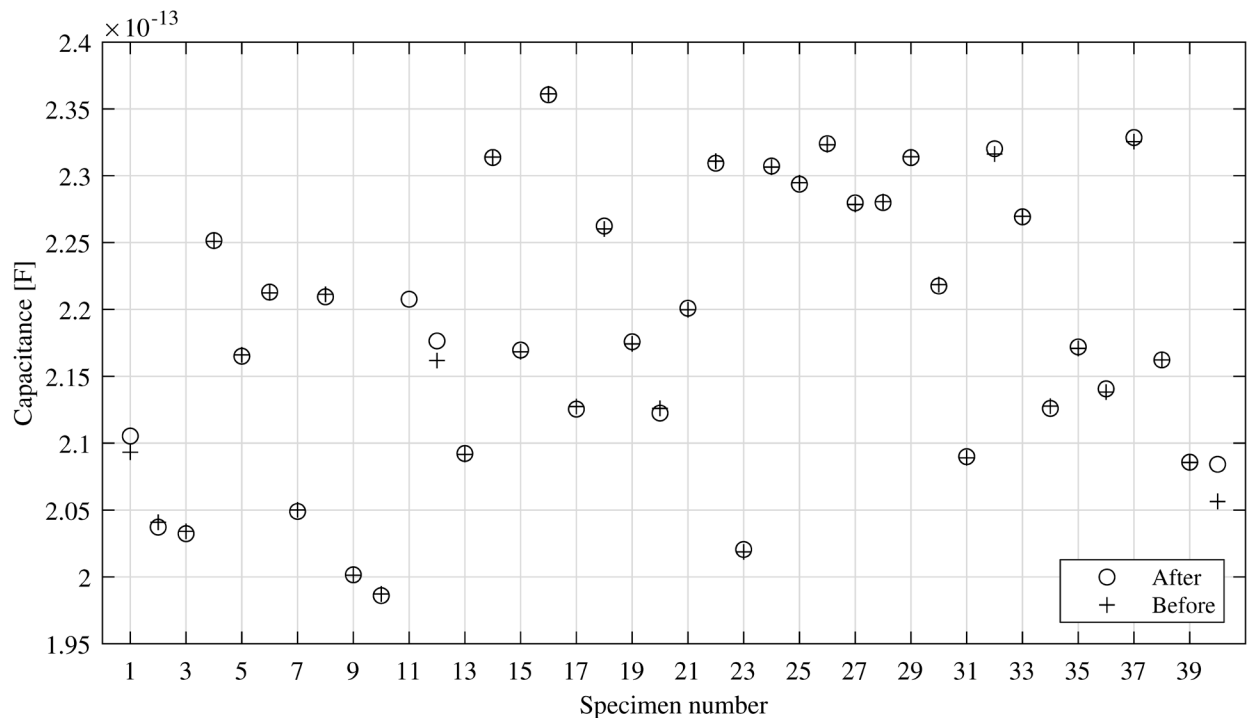Figure 4.21. The applied voltage to the specimen as well as its measured response.

Figure 4.22. Capacitance before and after exposure to 24 oscillations.

No clear trend is observable in the measured capacitance values that would indicate any degradation of the material due to the exposure to the fault waveforms.

Finally, the specimens were exposed to a ramped sinusoidal voltage until a visible tree was detected. The setup used was identical to the one described in 3.4, except that the external PD-circuit was not used due to it being redundant when the in series connected reference impedance and optical detection methods are used. The measurements were carried out in air at room temperature and the results are shown in Figure 4.23.
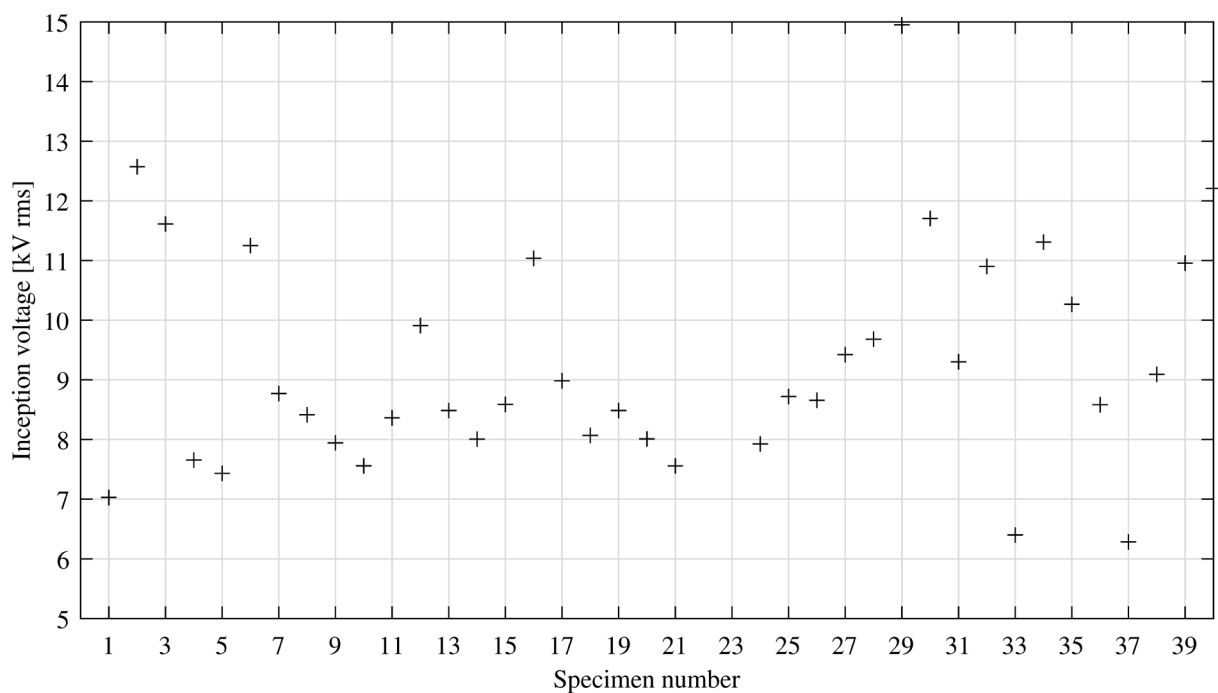

Figure 4.23. Results of the electrical tree inception voltage experiment.

The same results but viewed as a three parameter Weibull fit is seen in Figure 4.24. In Weibull probability, a parameter referred to as threshold indicates the x-axis intersect which corresponds to the lowest value where electrical tree inception can occur according to the model. That makes it apt to use as a statistical measure in this study.
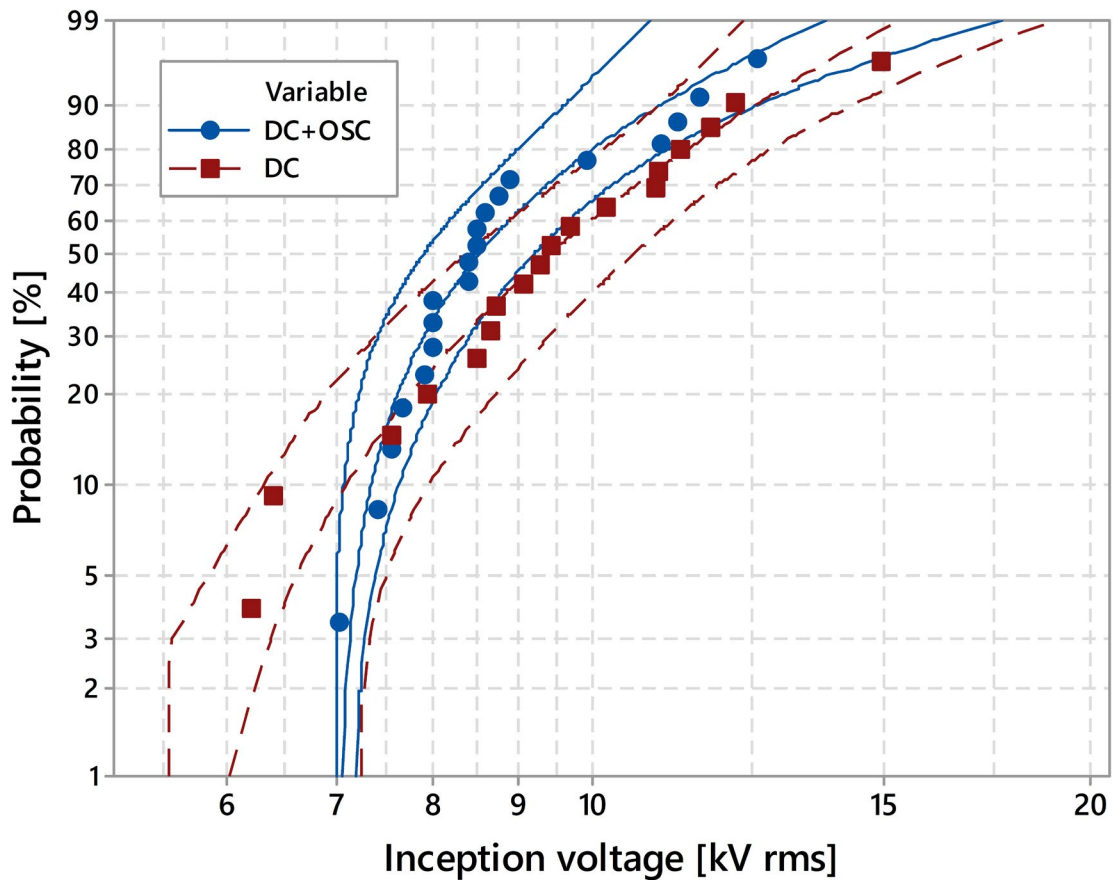
Figure 4.24. The results fitted to three-parameter Weibull probabilities with 95 % confidence intervals.

Examining the graph, it quickly becomes obvious that the results are awry. The reference group shows a large confidence interval at the threshold and consequently a smaller threshold value than the DC+osc group.

There are three statistical outliers in the dataset. Specimen #1, #33 and #37, all seen clearly in Figure 4.23. #1 was exposed to the waveform created by the interrupted inductor and exhibits the lowest inception of its group. The two latter suffered from defects in the specimen capsule. During manufacturing, some specimen capsules developed sprains in different sizes in the glass. The documentation of the specimen manufacture is not included in this thesis, but #32 and #37 are noted as very severe and severe respectively. By censoring these three data points Figure 4.25 was created.
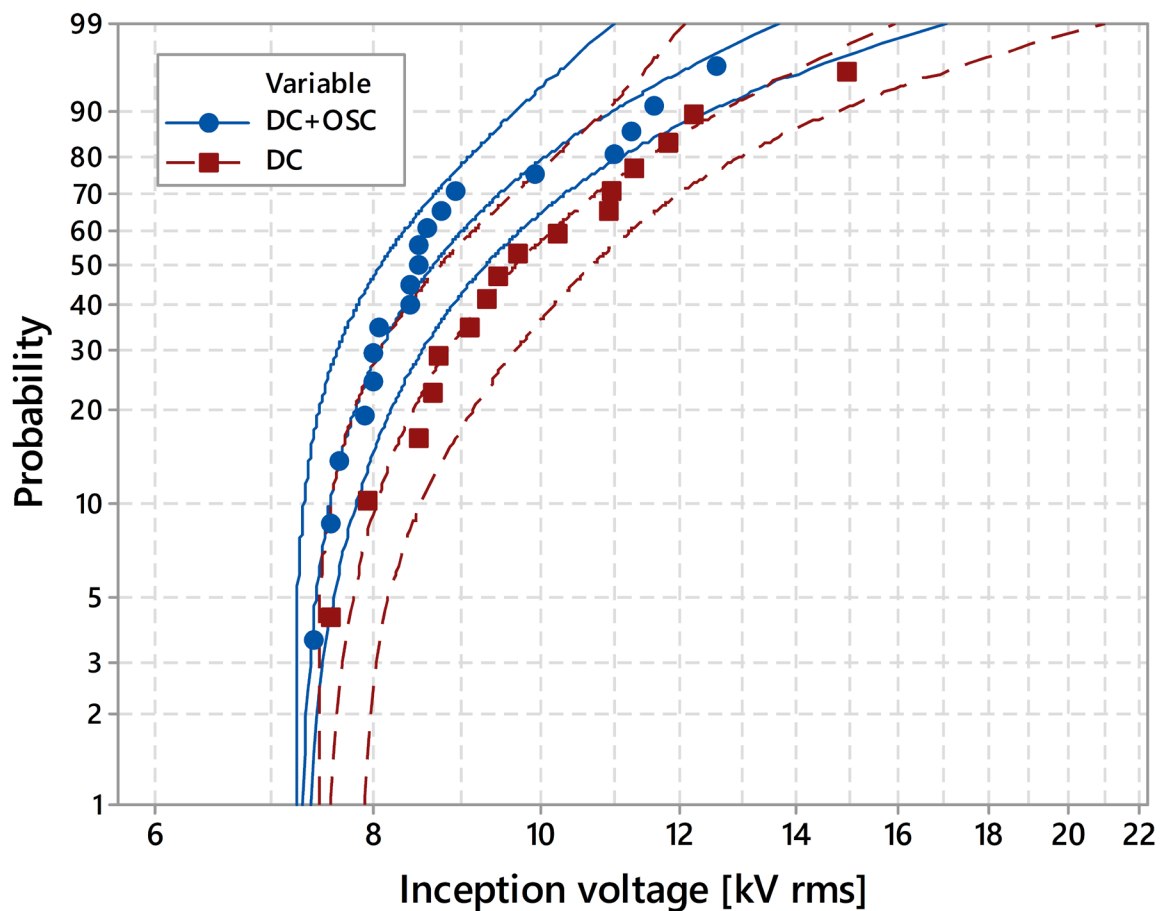
Figure 4.25. Weibull plot of the censored dataset.

Table 4.1. The Weibull parameters

Dataset	Shape	Scale	Threshold
DC+osc	1.25	1.91	7.23
DC	1.41	2.89	7.43

From the table, it can be surmised that there is a 2.7 % difference between the thresholds. Thus, it can be concluded that the insulation has only been marginally affected by the exposure to the 25 short circuit waveforms.

5. Summary and conclusions

This work has introduced methods for evaluating insulation materials that may degrade under service exposure. By locating specimens in an environment that mimics the conditions found in-service, usable results can be generated – independent of time frame. Anyone interested in measurements in sealed conditions is encouraged to take inspiration from this work to develop encapsulation strategies that generate valid data in their application. The concepts that are dealt with here are in no way exclusive to XLPE, they can be applied to any electrical measurement where the specimen needs to be separated from our ordinary environment.

The structure of this part is as follows. The fulfilment of the goals set up is summarised briefly, followed by a closer examination of the measurement techniques employed, the impact of the joint failure waveform, experiences related to the specimen encapsulation and comparability between the results. Possible improvements to the discharge free waveform and thus the impedance calculations are reviewed last.

Goals

Overall, the goals of this work can be summarised as:

- Locate the specimen in an environment that resembles an actual HVDC-cable
- Detect the inception voltage of an electrical tree during an experiment when an increasing sinusoidal voltage is applied
- Scale the methodologies to investigate the effects of a join failure waveform

The specimens were enclosed in a low-leakage container without using any excessive heat or chemicals. Measurement results indicate that every source of detection yielded an accurate value of the tree inception voltage and finally, the larger experimental series indicate that the techniques developed offer good repeatability and usable results. Thus, the goals can be considered to have been met overall.

5.1 Measuring the electrical tree inception

Out of the available detection sources, the signal from the reference impedance is arguably both the most practical and informative measure. It can be used to calculate the impedance of the specimen

in which the electrical inception voltage is easily detected as it manifests as a distinct rise of the capacitance. It also contains the base capacitance of the specimen as well as the capacitance change per time unit during tree growth. Both the latter quantities are useful for electrical treeing experiments. Finally, it provides access to the current in the circuit, which is by far the best quantity analyse for getting a quick overview of the outcome of an experiment.

The other inception sources each carries both advantages and disadvantages compared to the output from the reference impedance. While all remain basically equal in detecting the electrical tree inception voltage, they differ in the amount of information they yield and their practicality.

The external PD-circuit differs from the reference impedance in several ways:

- It is connected in parallel with the device under test giving it an advantage in terms of measurement system rigidity as a breakdown in the specimen will not present a hazard to it. An in series connected device used in this work and experiencing the same event would most likely be thoroughly destroyed.
- It has a short integration time, which means that it needs to be sampled at a high rate, in this case 10 MHz. A continuous recording of the output during a measurement results in a cumbersome amount of data.
- Its sensitivity is much less than that of the in series connected device. This can partly be explained by the fact that the coupling capacitor is not matched in value with the specimen capacitance.

The optical method of detecting the electrical tree inception voltage suffers the most in terms of design compromises in this implementation. The optical quality is diminished by the fact that the path from the microscope to the needle crosses five boundaries, the dominating of which is the surface of the polymer. Excellent optical quality can be achieved by heating the specimen inside of the capsule, moulding it to the glass wall and therefore eliminating the influence of the surface roughness of the specimen. Although this carries major risks in terms of specimen repeatability.

Neither the optical system nor the external PD-circuit were independently referenced to the excitation voltage, requiring them to be manually synchronized in time with a device with access to the

excitation voltage. Each of them also used own on-board clock. This introduces additional errors, (yet small in this work), in the measured electrical tree inception voltage. The DAQ-device operating with external PD-circuit could be used to also sample the output from the voltage divider, eliminating the need for synchronisation and thus also the error. Alternatively, it could be run off a shared clock source with the DAQ-device sampling the excitation voltage. Achieving a proper synchronization of the optical system would require a different strategy, as its output is currently layered through a commercial software.

5.2 Impact of the oscillatory waveform on the state of the insulation

Figure 4.25 shows that the difference in the electrical tree inception voltages between the two specimen groups is minor. Thus, it can be postulated that the insulation has not experienced any adverse effects due to the exposures. However, as this conclusion relies entirely upon the choice of the experimental parameters, a discussion regarding the results in conjunction with the parameters is necessary.

- From Figure 4.1 it is apparent that the waveform attenuates while travelling through the cable. This essentially means that every defect in the cable will experience a different voltage waveform. Further, it is unlikely that the fault occurs in the same location repeatedly, as that would require the joint and subsequent replacements to fail over and over. Thus, the same defect will experience different waveforms as different joints fail.

- The time it takes for the voltage to change polarity in the fault waveform is proportional to the distance from fault location to defect. The time needed for the voltage reversal and space charge build up to prevent a field enhancement and therefore, electrical tree initiation, is estimated for polyethylene at 25 °C as 30 – 80 µs [17].

- The first flank of the waveform that the artificial defects in the described experiment is exposed to is found at ~200 µs (see Figure 4.1). This places it well outside the critical region, meaning that the modelled metallic inclusion is located at a distance which is far enough away from the fault to limit the electric field around the tip. This is by intent and motivated by the fact that cables to which this experiment relates have experienced a limited number of faults and having all of their joints replaced before being taken out of service. In that

sense, it is not probable that a major defect, such as the one described in this work, is found in close vicinity to one of the failed joints.

Thus, given the assumption that the defect distribution in the cables is not unlikely, it can be concluded that the overall condition of the cable insulation has not experienced any adverse consequences due to the exposure.

5.3   Evaluating the specimen encapsulation

The specimens were housed in what can be referred to as a low-leakage environment. Some leakage was visible when the capsules were subjected to a bubble test at 100 mbar. Preferably, future experiments should be accompanied by a chemical analysis that shows for example by-products concentration before and after the study, thereby indicating whether the specimens properly represented the original material or not.

The method for securing the specimen capsule inside the cell was simplified for the short circuit waveform experiment. Some pressure must be applied in order to establish and maintain the electrical contact between the cell and the capsule. On the high voltage side this is accomplished with a stud, but on the other side it depends on the inner conductor of an SMA-contact. Vibrations, even rather small, could cause the specimen capsule to shift slightly inside the cell, leading to a change in the measured capacitance. This effect is evident when inspecting for example Figures 4.19 and 4.22. Specimen #16, for example, shows an indication of a distinct shift in capacitance while specimens #39 and #40 exhibit a large variance. Thus, the low voltage connection between the cell and the specimen capsule may need to be redesigned.

6.   Suggestions for future work

There are both technical as well as theoretical improvements possible to be made. While not strictly necessary for the main purpose of the work: to facilitate ageing and the detection of the inception voltage of an electrical tree, they would enhance the quality of the measurements as well as improve the impedance calculations.

Specimen containment wise this work presents the last iteration of a process in an attempt to create a way to place the test specimens in a service-like environment of a HVDC cable. More specifically, and in relation to the work already carried out, the data from the last 40 electrical treeing experiments should undergo the same comprehensive analysis as the data from the initial three experiments. Particularly interesting will be to compare how the tree initiates and progresses through the view of specimen capacitive changes.

Given that there are now thorough results of the impact of pure DC and DC plus oscillations exposures on the electrical tree inception voltage, an interesting compliment would be to measure the inception voltage in a group of specimens without any previous treatment. That would establish a base-line reference for the specimens and show whether the DC exposure alone may have an impact on the inception voltage.

There are also improvement opportunities to further explore the calculation of the discharge free waveform and impedance. Currently, both methods suffer from a slight overshoot in the waveform, though they could be improved by iterating the result. By subtracting the measured waveform with the calculated difference and then recalculating the discharge free waveform, the results will be more accurate as the exponential decays from the discharges would not be included in the fit.

The trigonometric Fourier series used the least square method to fit the discharge free waveform. It may be favourable to instead compute and use the Fourier coefficients of the measured waveform from the reference impedance for creating the fit. This method would inherently exclude the influence of discharge activity.

Finally, the author hopes that the experiences presented in this work regarding the creation of accurate laboratory representations of real service environments can be utilised to answer yet unknown insulation problems and as a compliment to the future development of new materials.

7. References

[1]   A. Smedberg, B. Gustafsson, and T. Hjertberg, "What is crosslinked polyethylene?" in IEEE International Conference on Solid Dielectrics, vol. 1, Jul. 2004, pp. 415–418 Vol.1.

[2]   G. Mazzanti and M. Marzinotto, Extruded cables for high-voltage direct-current transmission: Advances in research and development. University of Bologna: Wiley, 2013.

[3]   L. A. Dissado and J. C. Fothergill, Electrical degradation and breakdown in polymers, ser. IEE materials & devices series: 9. London : Peter Peregrinus, cop. 1992., 1992.

[4]   X. Qi and S. Boggs, "Thermal and mechanical properties of EPR and XLPE cable compounds," IEEE Electrical Insulation Magazine, vol. 22, no. 3, pp. 19–24, May 2006.

[5]   Y. Kao and P. Phillips, "Crystallinity in chemically crosslinked low density polyethylenes: 1. Structural and fusion studies," Polymer, vol. 27, no. 11, pp. 1669– 1678, 1986.

[6]   T. Andrews, R. N. Hampton, A. Smedberg, D. Wald, V. Waschk, and W. Weissenberg, "The role of degassing in XLPE power cable manufacture," IEEE Electrical Insulation Magazine, vol. 22, no. 6, pp. 5–16, Nov 2006.

[7]   L. Hill, M. Maringer, and A. Barlow, "Possible Mechanism of Microvoid Formation in Polyethlene Insulated High Voltage Cables," IEEE Transactions on Power Apparatus & Systems, vol. PAS-102, no. 7, p. 1921, 1983.

[8]   H. Herman, J. Thomas, and G. Stevens, "Spectroscopic and chemometrics analysis of cable condition in the Artemis program," in IEEE International Conference on Solid Dielectrics, vol. 2, Jul. 2004, pp. 623–627 Vol.2.

[9]   S. M. Gubanski, K. Karlsson, and U. Gedde, "Study of thermal oxidation in medium density polyethylene," in IEEE International Symposium on Electrical Insulation, Jun. 1992, pp. 161–164.

[10]   H. Li, J. Li, Y. Ma, Q. Yan, and B. Ouyang, "The role of thermo-oxidative aging at different temperatures on the crystal structure of crosslinked polyethylene," Journal of Materials Science: Materials in Electronics, vol. 29, no. 5, pp. 3696–3703, Mar 2018.

[11]   J. Paul, E. W. Hansen, and J. Roots, "Probing the molecular dynamics in XLPE aged at different temperatures by 1H NMR relaxation time measurements," Polymer Degradation and Stability, vol. 97, pp. 2403 – 2411, 2012.

[12]   G. C. Montanari and A. Motori, "Thermal endurance evaluation of XLPE insulated cables," Journal of Physics D: Applied Physics, vol. 24, no. 7, pp. 1172–1181, 1991.

[13]   B. Garros, "Ageing and reliability testing and monitoring of power cables: diagnosis for insulation systems: the ARTEMIS program," IEEE Electrical Insulation Magazine, vol. 15, no. 4, pp. 10–12, Jul. 1999.

[14]   J. C. Fothergill, "Ageing, Space Charge and Nanodielectrics: Ten Things We Don't Know About Dielectrics," in IEEE International Conference on Solid Dielectrics, Jul. 2007, pp. 1–10.

[15]   J. C. Fothergill, "The coming of age of HVDC extruded power cables," in IEEE Electrical Insulation Conference, Jun. 2014, pp. 124–137.

[16]   A. Tzimas, S. Rowland, L. A. Dissado, M. Fu, and U. H. Nilsson, "Effect of longtime electrical and thermal stresses upon the endurance capability of cable insulation material," IEEE Transactions on Dielectrics and Electrical Insulation, vol. 16, no. 5, pp. 1436–1443, Oct. 2009.

[17]   F. Nota, N. Yoshimura, and T. Oota, "Tree initiation in polyethylene by application of dc and impulse voltage," in IEEE International Conference on Electrical Insulation, Jun. 1976, pp. 205–208.

[18]   G. C. Montanari, G. Mazzanti, F. Palmieri, G. Perego, and S. Serra, "Dependence of space-charge trapping threshold on temperature in polymeric DC cables," in IEEE 7th International Conference on Solid Dielectrics, 2001, pp. 81–84.

[19]   S. Rasikawan and N. Shimizu, "Effect of additives on treeing initiation as a function of oxygen concentration in polyethylene," in *IEEE Transactions on Electrical Insulation*, vol. 27, no. 6, pp. 1089-1094, Dec. 1992.

[20]   Y. Mecheri, M. Nedjar, A. Lamure, M. Aufray and C. Drouet, "Influence of moisture on the electrical properties of XLPE insulation," 2010 Annual Report Conference on Electrical Insulation and Dielectic Phenomena, West Lafayette, IN, 2010, pp. 1-4, doi: 10.1109/CEIDP.2010.5724017.

[21]   C. Shinoda, T. Hashizume, T. Tani, Y. Tanaka and T. Takada, "A consideration of mechanism of DC leakage current peak in XLPE cables," Proceedings of 5th International Conference on Properties and Applications of Dielectric Materials, Seoul, South Korea, 1997, pp. 402-405 vol.1, doi: 10.1109/ICPADM.1997.617621.

[22]   R. J. Densley, "An Investigation into the Growth of Electrical Trees in XLPE Cable Insulation," in IEEE Transactions on Electrical Insulation, vol. EI-14, no. 3, pp. 148-158, June 1979, doi: 10.1109/TEI.1979.298215.

90

[23] J. -. Bostrom, E. Marsden, R. N. Hampton and U. Nilsson, "Electrical stress enhancement of contaminants in XLPE insulation used for power cables," in IEEE Electrical Insulation Magazine, vol. 19, no. 4, pp. 6-12, July-Aug. 2003.

[24] Zhong Zheng and S. Boggs, "Defect tolerance of solid dielectric transmission class cable," in IEEE Electrical Insulation Magazine, vol. 21, no. 1, pp. 34-41, Jan.-Feb. 2005.

[25] Hampton, Nigel and H. Lennartsson. "Long-life Xlpe Insulated Power Cable." (2007).

[26] Y. Wang, F. Guo, J. Wu and Y. Yin, "Effect of DC Prestressing on Periodic Grounded DC Tree in Cross-Linked Polyethylene at Different Temperatures," in IEEE Access, vol. 5, pp. 25876-25884, 2017.

[27] M. Selsjord and E. Ildstad, "Electrical treeing caused by rapid DC-voltage grounding of XLPE cable insulation," Conference Record of the 2006 IEEE International Symposium on Electrical Insulation, Toronto, Ont., 2006, pp. 502-505.

[28] A. Ishibashi *et al*., "A study of treeing phenomena in the development of insulation for 500 kV XLPE cables," in IEEE Transactions on Dielectrics and Electrical Insulation, vol. 5, no. 5, pp. 695-706, Oct. 1998.

[29] Malik, N.H., Al-Abdullah, A.A., Al-Arainy, A.A. and Qureshi, M.I. (2006), Factors influencing electrical treeing in XLPE insulation. Euro. Trans. Electr. Power, 16: 205-218.

Appendix

Schematics
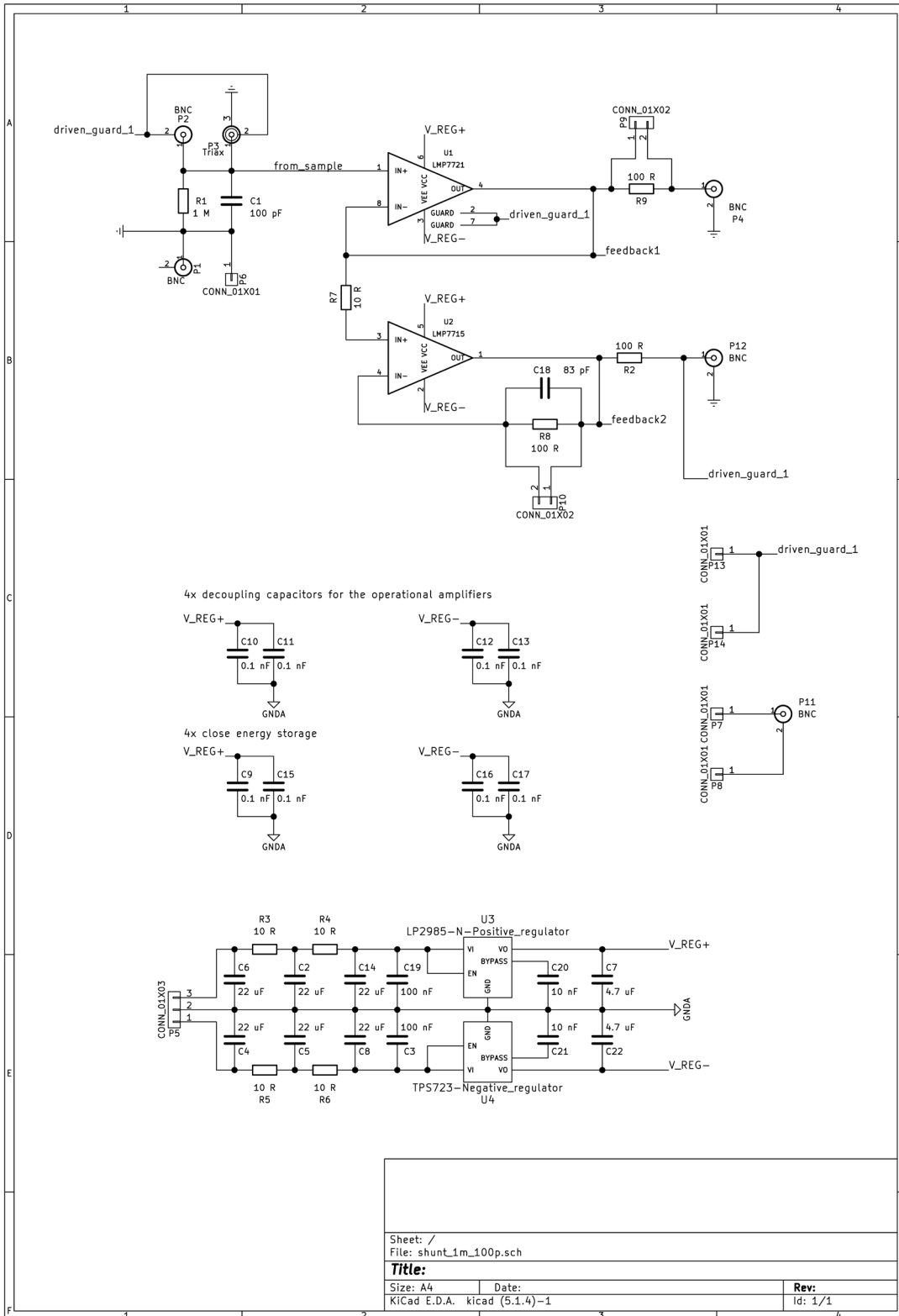
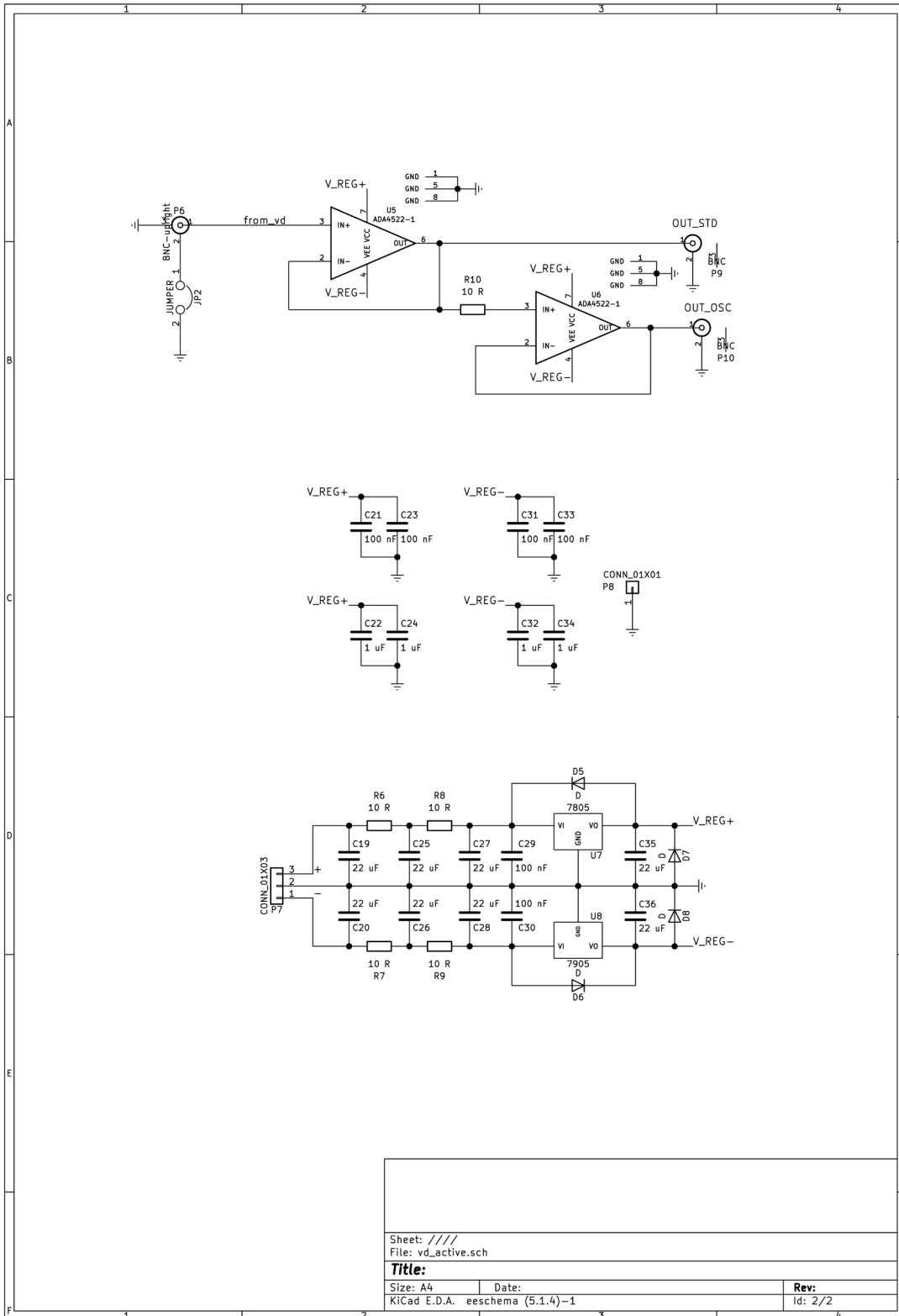Figure A.1: Schematic of the reference impedance.

Figure A.2: Schematic showing the operational amplifiers for the voltage divider.
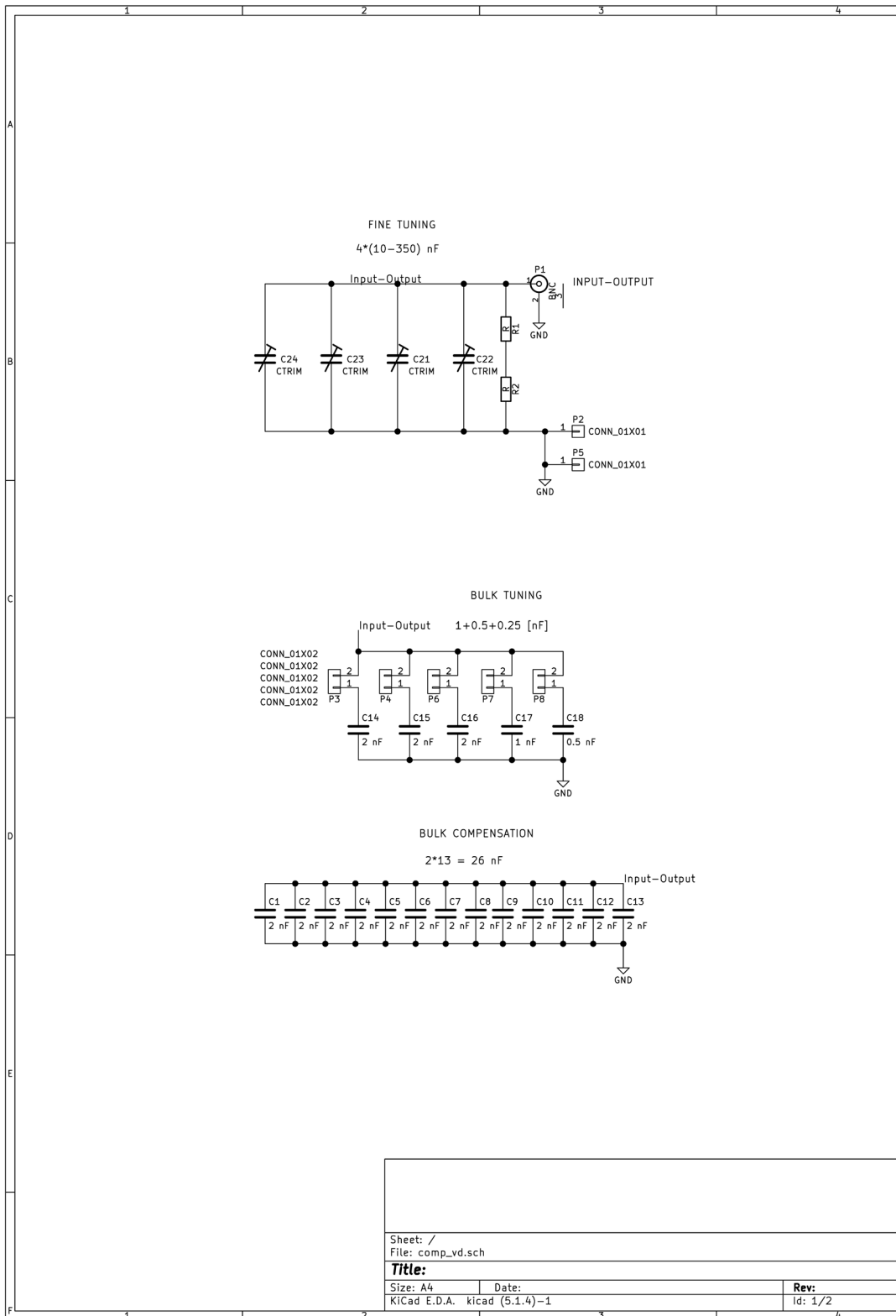
Figure A.3: Schematic showing the passive components in the LV-arm of the voltage divider.
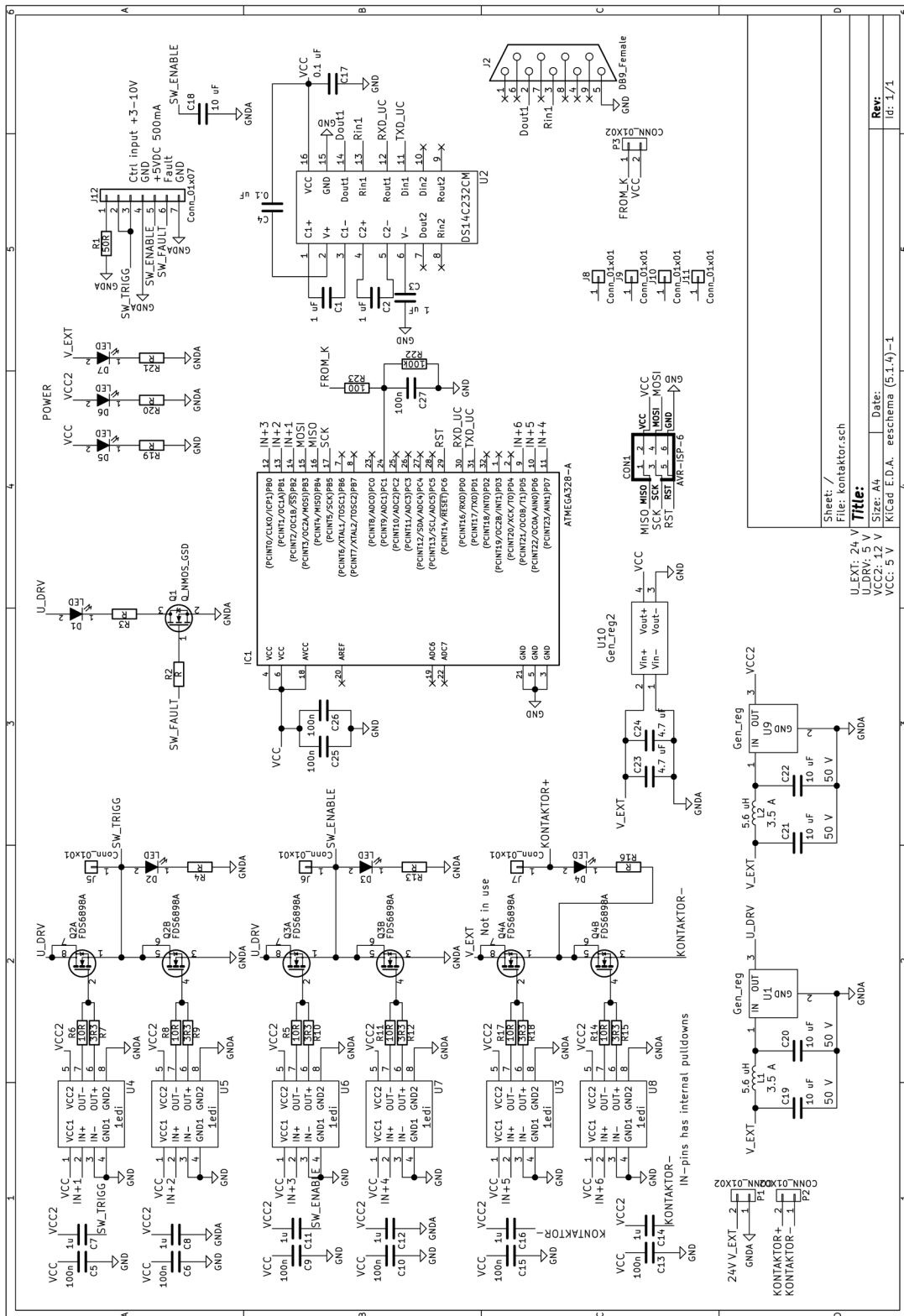
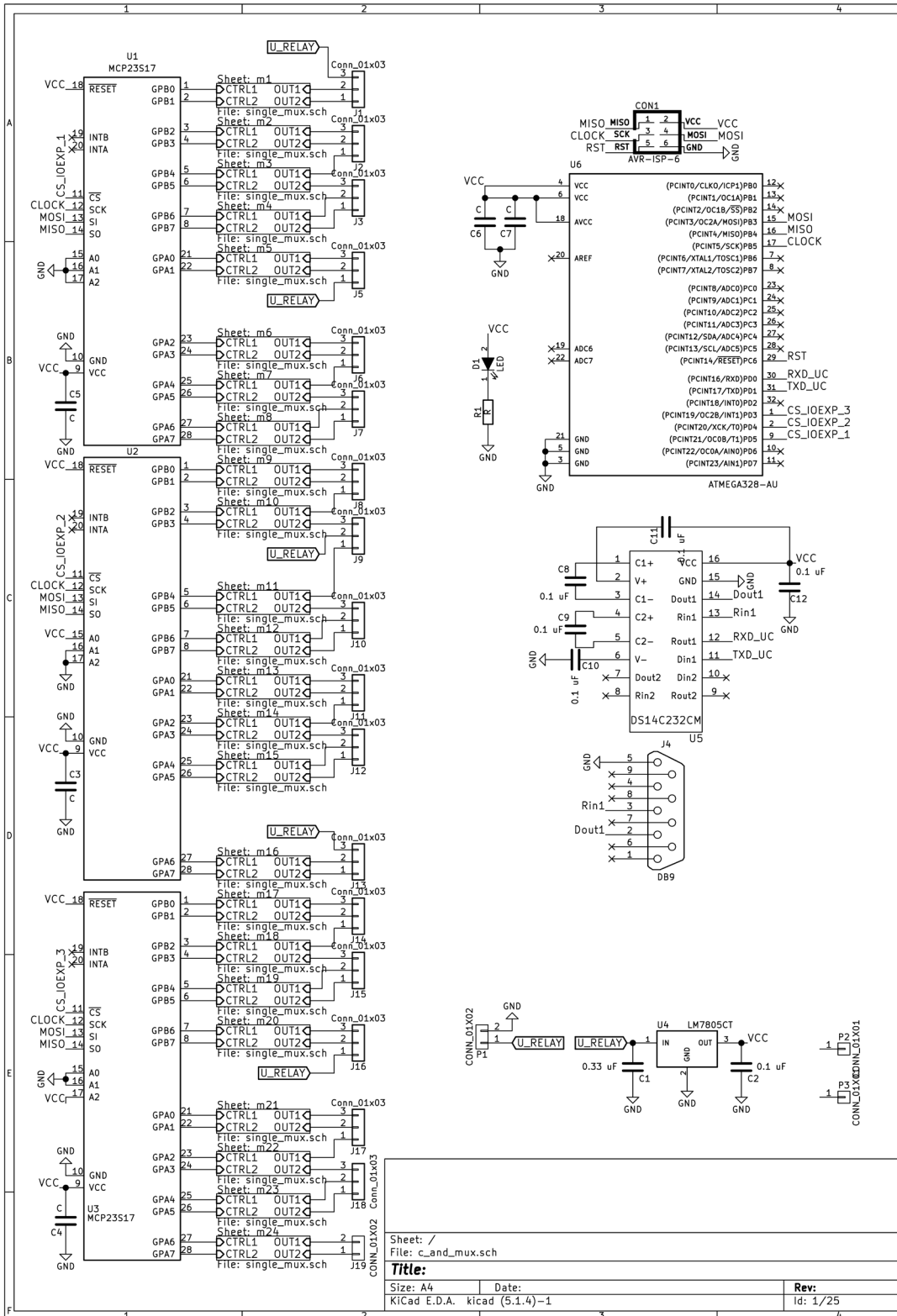Figure A.4: Schematic illustrating the switch controller.
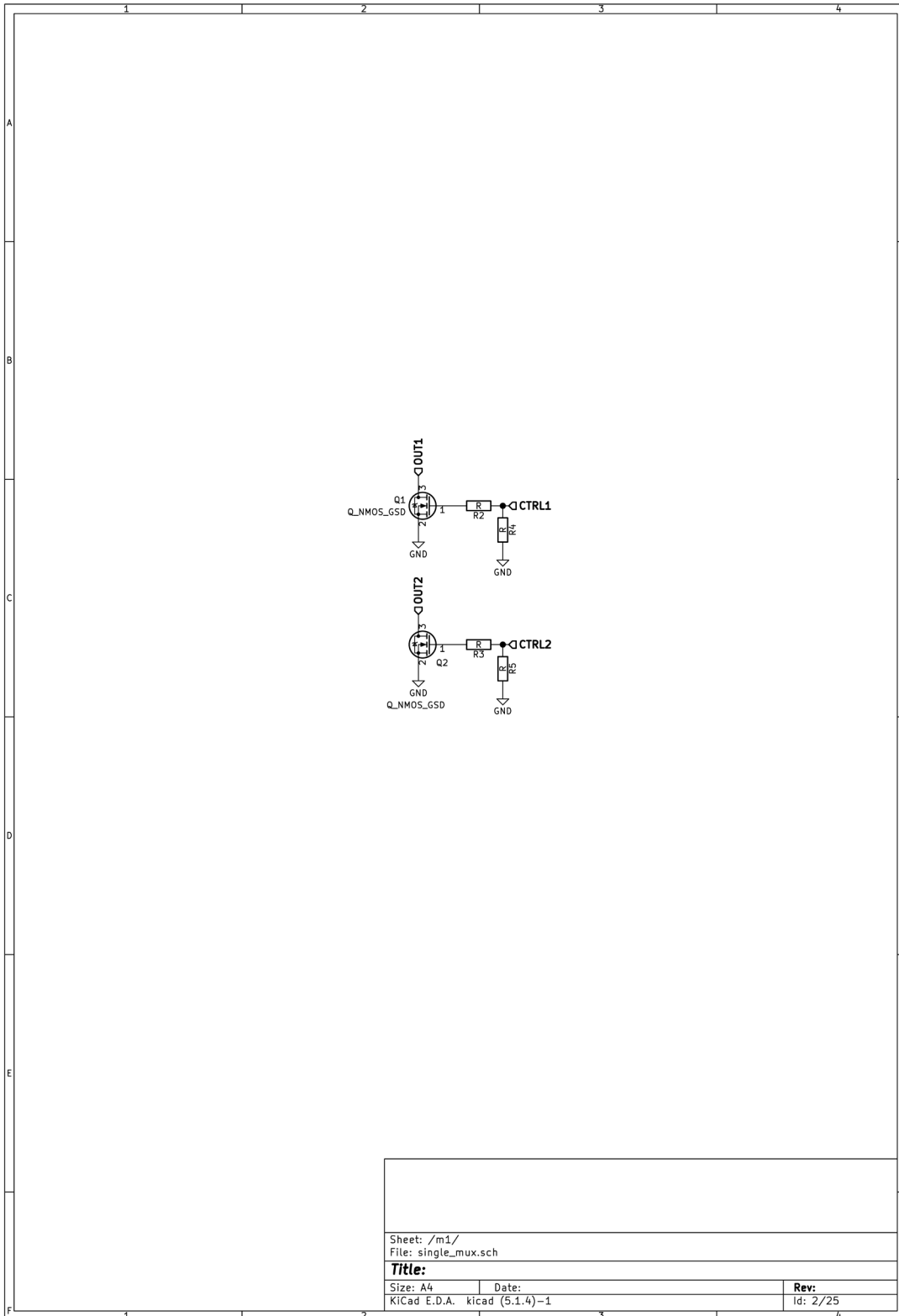
Figure A.5: Schematic showing relay controller.

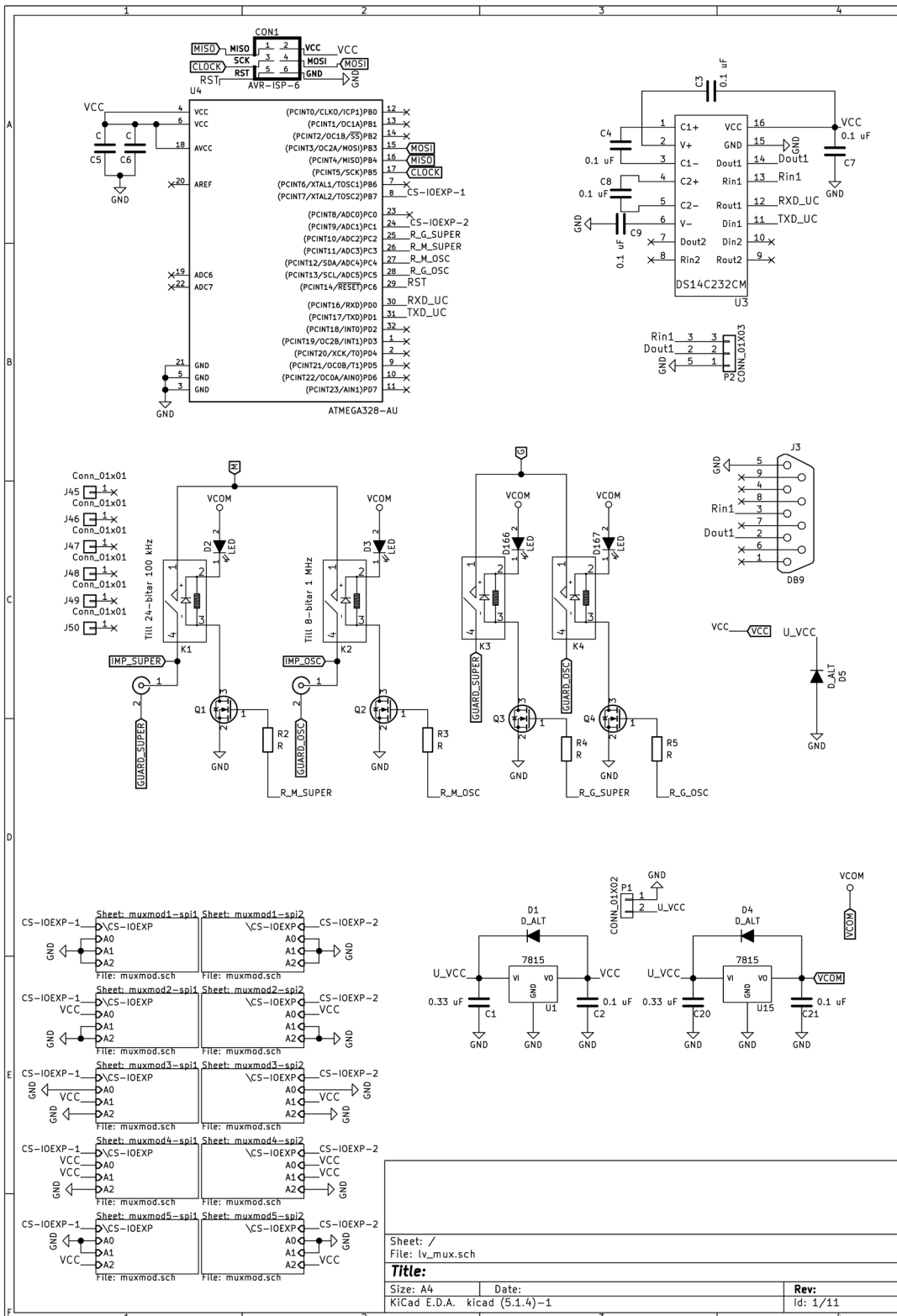Figure A.6: The sub-schematic of the relay controller.
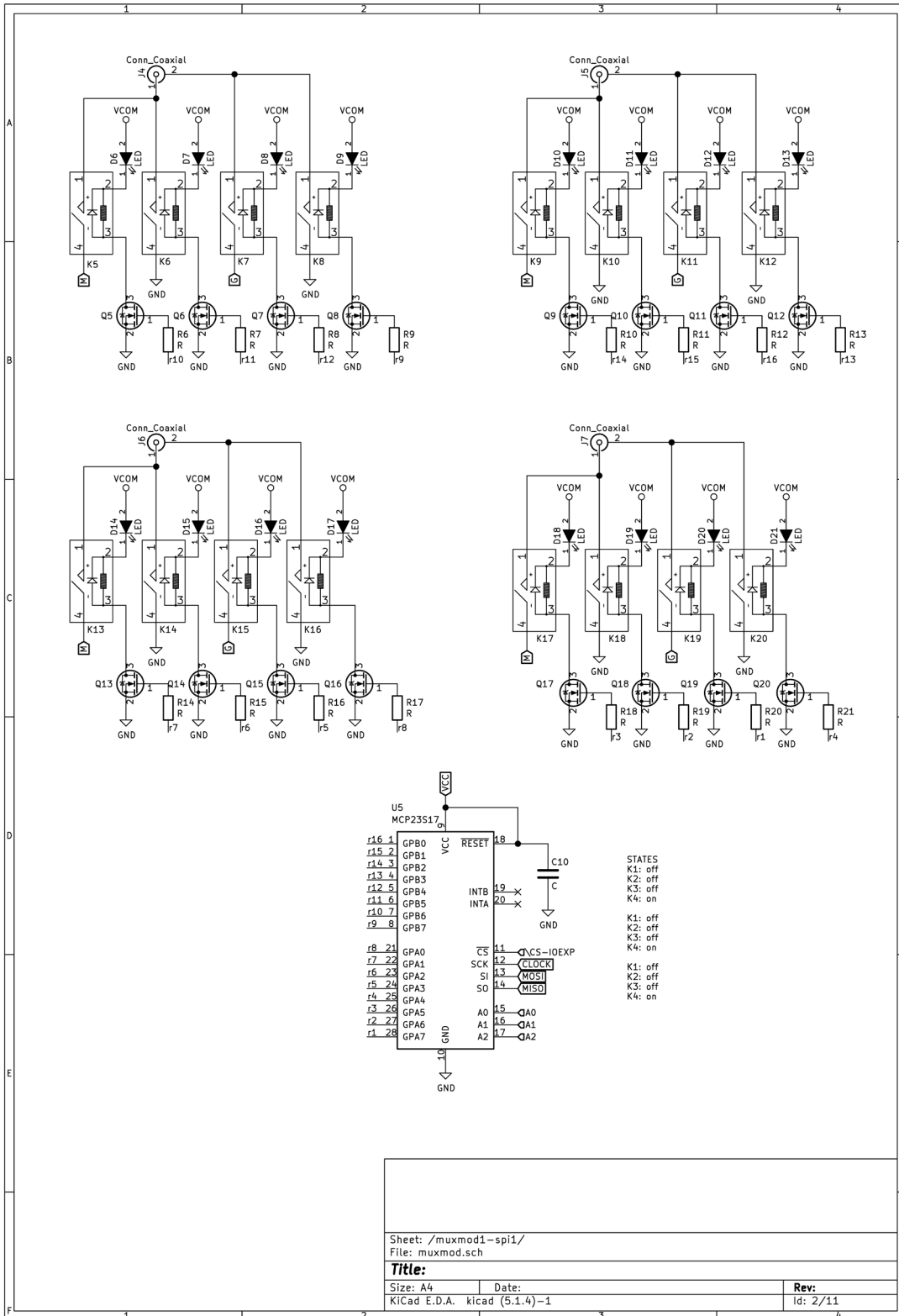
Figure A.7: Schematic showing multiplexer.

Figure A.8: The sub-schematic of the multiplexer the LV-arm of the voltage divider.
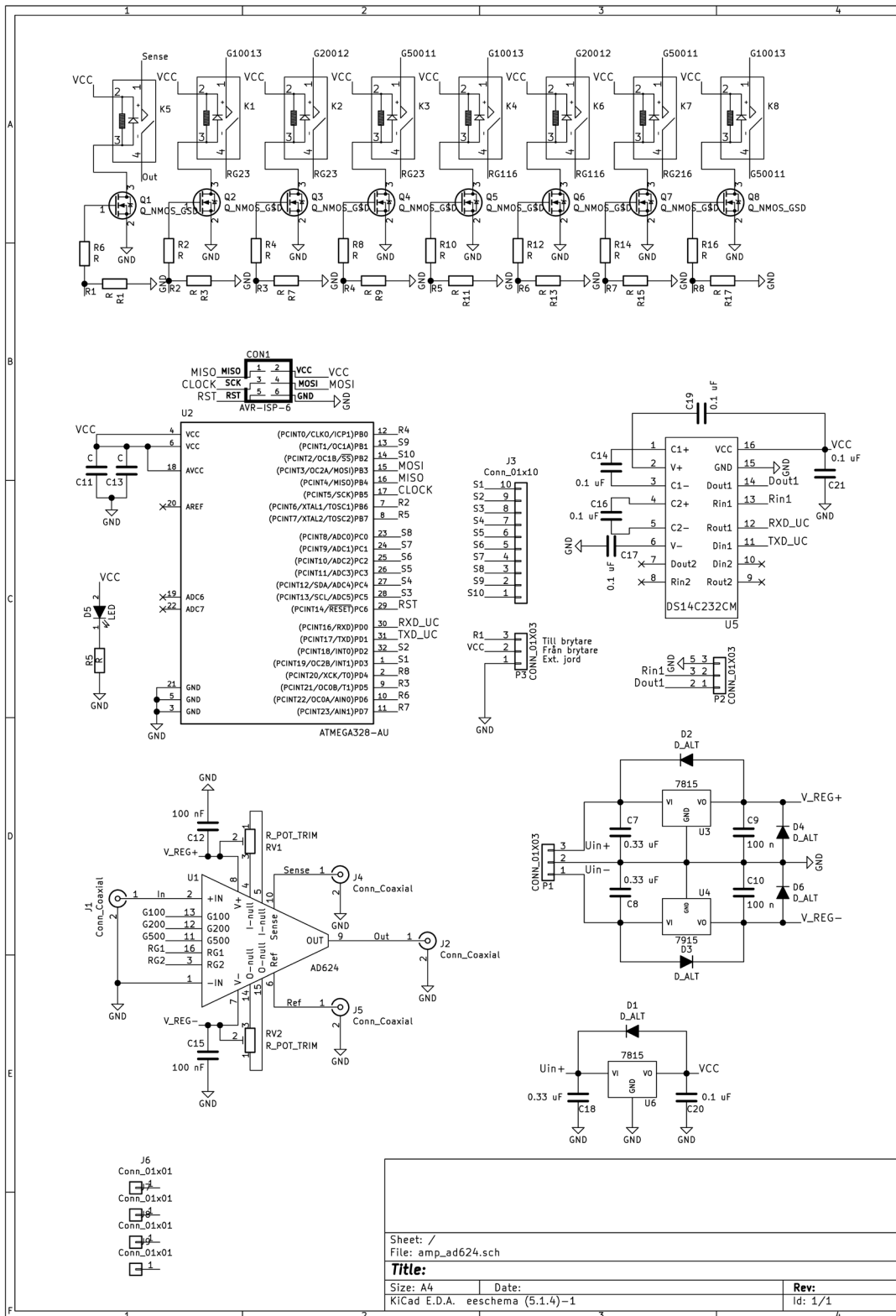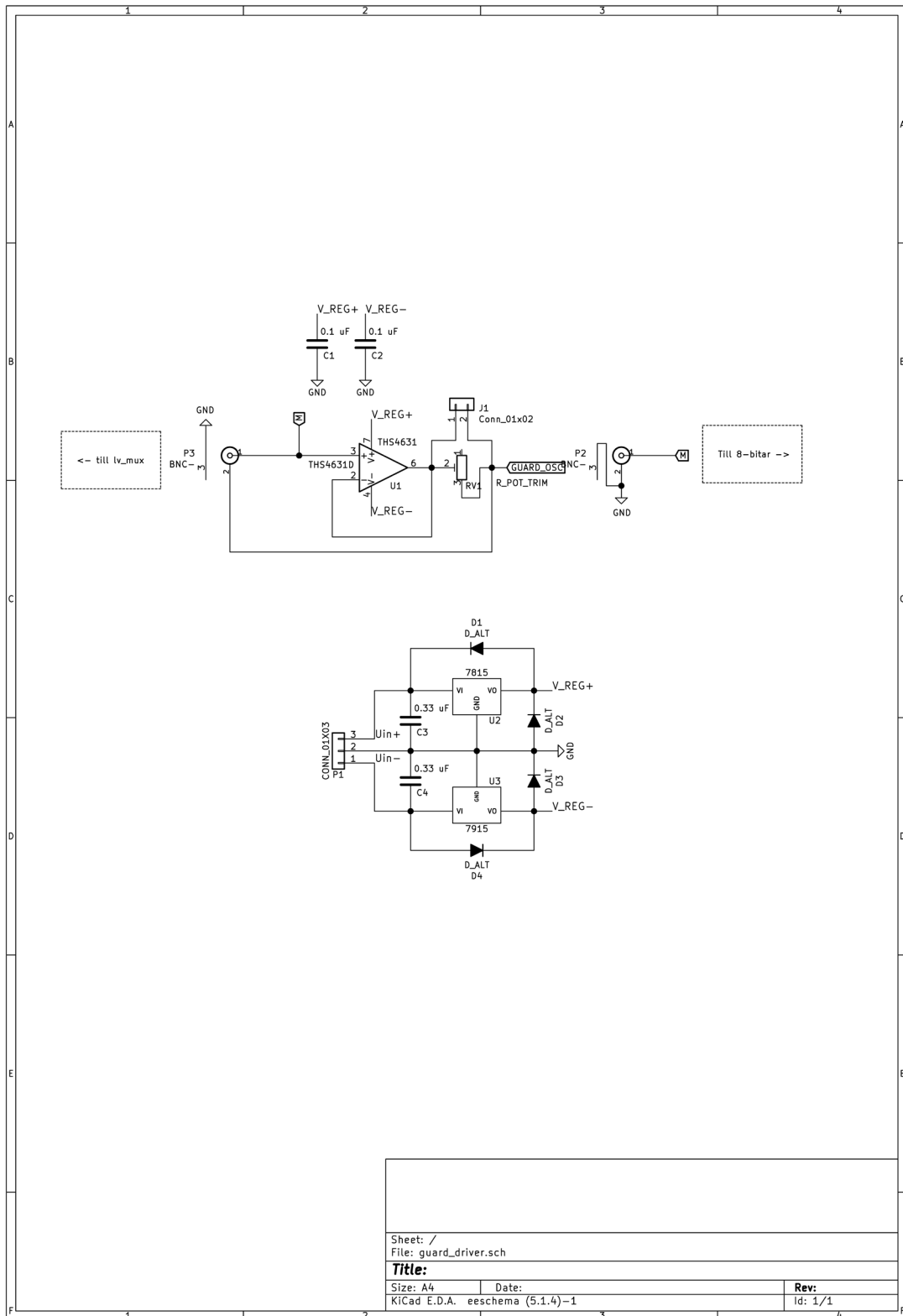
Figure A.9: Schematic of the amplifier.

Figure A.10: Schematic showing the guard driver.